DEVELOPMENT AND VALIDATION OF HIGH-RESOLUTION CARDIOVASCULAR PHENOTYPING STRATEGIES IN ZEBRAFISH REVEALS THE CLINICAL RELEVANCE OF *ROBO4* TO CONGENITAL HEART DEFECTS

by
Courtney Woods

A dissertation submitted to Johns Hopkins University in conformity with the requirements for the degree of Doctor of Philosophy

Baltimore, Maryland
July, 2017

Abstract

Bicuspid aortic valve (BAV) is a congenital heart defect, affecting 1-2% of the general population. Approximately 30% of individuals with BAV develop ascending aortic aneurysm (AscAA). Although the etiology of BAV/AscAA is unknown, previous family-based studies suggest that BAV is highly heritable. Using whole-exome sequencing, we have systematically screened nine patient families, 286 probands, and 193 unrelated controls to identify causative variants. *ROBO4* is a gene in which we have detected multiple independent predicted deleterious alleles showing appropriate familial segregation. Targeted sequencing of an additional 441 unrelated probands and 183 controls detected six additional rare alleles predicted deleterious. Using zebrafish, we have established a robust pipeline to functionally evaluate the biological relevance of genes/variants implicated in BAV/AscAA. It provides an unprecedented capacity to interrogate the cardiovascular structural and functional correlates of BAV/AscAA in genetically defined developing and adult zebrafish. First, we establish mutant fish lines for selected genes using CRISPR/Cas9 or identify functionally equivalent mutants in public resources. For *robo4*, we generated a 7 base pair deletion in exon six of 19. As predicted, this mutation results in nonsense mediated mRNA decay, significantly reducing mRNA levels as quantified by qRT-PCR. In order to measure complete cardiac function in adult zebrafish, we have optimized two different methods – echocardiography and electrocardiography (ECG). We have completed a longitudinal study of wild-type zebrafish, establishing normative values for three to eleven months of age for both echocardiography and ECG – a critical resource to document genetic predisposition and

progression of disease. These data enabled development of a linear model, adjusting for the influence of specific parameters such as age, sex, and body size on cardiovascular measurements in zebrafish. Furthermore, we were able to apply the newly developed echocardiography and ECG methods as well as this linear model to two well-characterized zebrafish models of arrhythmia as proof-of-principle. Echocardiography of *robo4* mutants at approximately four to six months reveals extreme outflow turbulence and regurgitation (11/41), compared to wild-type fish (4/45). Importantly, our echocardiograms from mice homozygous for a *Robo4* loss-of-function mutation display a similar phenotype. These data establish *ROBO4* as a gene critical for the normal development and homeostasis of the left ventricular outflow tract and launch a vigorous pipeline and protocols for functional validation of other candidate genes of BAV/AscAA.

Advisor: Andrew S. McCallion, Ph.D.

Reader: Kirby Smith, Ph.D.

Preface

First I would like to thank my PhD advisor. My PhD would have been impossible without Dr. Andrew McCallion. Without Andy's immense patience and guidance, I would never have been able to survive, let alone succeed, the last five years. I have learned so much about the scientific process, presenting for small and large audiences, communicating with collaborators, how to travel and present abroad, and most importantly, the significance of a strong and team-based work environment. Thank you, Andy, for letting me be part of the McCallion lab family.

I would like to thank Dr. Jennifer Armstrong of the Keck Science Department at Claremont McKenna College. It was Dr. Armstrong's strong mentorship starting my sophomore year that led me to pursue my interest in science, lab work, and eventually graduate school. Dr. Armstrong's encouragement also led me to apply to medical school. With that, I would also like to thank Dr. Emily Wiley of the Keck Science Department at Claremont McKenna College, whose Molecular Biology course really jumpstarted my interest in molecular biology. Dr. Wiley's support was also instrumental in my medical school application process.

I would like to thank my "career" mentor, Dr. Hans Björnsson. Hans interviewed me for the program six years ago and has believed in me since then. Not only did I rotate in Hans' lab, where I became much more familiar with Kabuki Syndrome on a molecular level, but I have shadowed in Hans' Epigenetics and Chromatin Clinic where I met so many extraordinary patient families. In the clinic, my passion for patient care blossomed

and it was Hans' unwavering commitment to helping me get into medical school to become a physician that made it happen.

I would like to thank Dr. David Valle, Dr. Kirby Smith, Sandy Muscelli and the entire training program committee for giving me the amazing opportunity to learn in this caring and supportive community-based environment. So many faculty members from the program have supported me including Dr. Jill Fahrner, Dr. Joann Bodurtha, Dr. Hilary Vernon, Dr. Julie Hoover-Fong, and Dr. Nara Sobriera. With their help, I feel entirely prepared to go to medical school and share genetics with the world.

I would like to thank my thesis committee: Dr. Hal Dietz, Dr. Mike Parsons, Dr. Kathy Gabrielson, and Dr. Hans Björnsson for helping me develop my project, especially Kathy, taking it upon herself to help me get the echocardiography up and running.

To my amazing lab mates, thank you so much for putting up with me and making the lab so much more fun even on the hardest of days. Samantha Maragh first convinced me to try out the McCallion lab, with fascinating disease-based cardiac projects. She mentored me and taught me everything in the lab from *in situs* to injecting embryos to how to take over her lab chore. Dave Gorkin and Xylena Reed made the lab a home. Dave, Sam, and Xy were truly inspirations and set the bar for my own research and PhD training. Paul, thank you for always being in the lab, first as a technician literally optimizing CRISPR for me or as a graduate student to bounce ideas off of. I will miss sitting behind you, sometimes. Sarah, you are a remarkable lab mate and friend. Thank you for correcting my math, checking my qPCR experiments, analyzing all of my data in R, editing my presentations, and helping me maintain confidence despite it all. I will sorely miss our late night meals (sometimes at Nando's) and phone chat sessions. Becca,

I could not have done it without you. Your help with all of the fish work was so vital, but most importantly, our friendship outside of lab and traveling to Wake Forest, Penn State, etcetera definitely made it enjoyable. I am so happy that Nicole joined the lab two years ago. Nicole, you have added a perfect combination of sass and cats to the lab. Joey, I am so glad you joined us on team zebrafish #ClutchGoals. Bill, it has been great adding you to the group and I hope you to continue to enjoy it (and finish Game of Thrones soon). To the newest technicians in the lab, I am so excited to see where Eric Waite and Sam Kearns end up. I have the utmost confidence in their successes.

Finally, I would like to thank my friends and family. To all of my lab and lab-related friends including Genay Pilarowski, Hannah Edelman, Ryan Longchamps, Julie Jurgens, Allison Miller, and Tim Kelly thank you for always being there to help me with data, practice presenations, vent, chat, and laugh together in and out of the lab. To the lovely ladies of the Leducq MIBAVA consortium, Nicole Wilson, Nikhita Bolar, and Ilse Luyckx, I cherish the memories our fun international adventures and appreciate the extra fun support system you provided. To Michele Barnhill, Jessica Mao, and Elica Sharifnia, thank you for your friendship over the last five years. It is so funny to me that we all ended up in graduate school. To Carolyn Lehman, you are a remarkable best friend and I am so lucky to have you. To Nicole Eckart, Foram Ashar, and Shannon Ellis, thank you so much for helping me in countless ways. From checking my R code, to writing my R code, to sending inspirational postcards, to making me dinner, to taking me out to dinner, to going to get ice cream for any and every reason, thank you for letting me into your friend group. You have provided an unbelievable sisterhood.

To my extended family including Uncle Dennis and Auntie Gretchen, thank you for all of your letters and calls of encouragement. Emily and Elise, I am so proud of both of you and love you so much. I thank you for always keeping me grounded and reminding me that life goes on outside of the zebrafish facility. And finally, to my parents, thank you for your immeasurable support. For my entire life, if I ever wanted to try something or do something, you simply asked what could you do and provide me to help me get there. For that incredible support and care, I thank you.

Table of Contents

List of Tables

List of Figures

Chapter 1: Introduction

1.1 Zebrafish as a model organism

Zebrafish (*Danio rerio*) are a valuable model system for the study of cardiovascular development and function. Their external fertilization and transparency as embryos means development of the zebrafish heart is readily studied, even at the cellular level (Stainier & Fishman, 1994). Zebrafish can overcome cardiovascular insults in early life, deriving sufficient oxygen exchange via passive diffusion across their small body surface to sustain life (Pelster & Burggren, 1996). This allows for the analysis of mutations that would be lethal in other organisms. Most importantly, zebrafish cardiac electrophysiology closely resembles that of human, despite the fish having a two-chambered heart rather than a four-chambered heart (Sedmera et al., 2003). Specifically, the heart rate of humans and zebrafish are similar (in both development and adulthood) (Kopp, Schwerte, & Pelster, 2005; Milan, Jones, Ellinor, & Macrae, 2006). By comparison, the heart rate of the adult mouse is about four times faster than that of humans' (Babij, Askew, Nieuwenhuijsen, & Su, 1998; M. P. Lee et al., 2000; Nerbonne, 2004; Salama & London, 2007).

These facts, together with the existence of many mutant lines that have already been generated and studied, support the development of zebrafish as a model for human cardiac function. Initially, forward genetic screens, using chemical (most commonly ENU) mutagenesis to introduce point mutations throughout the genome were performed to great success. Dozens of studies have produced a wealth of mutant lines, which elucidate the requirement of many genes and pathways in cardiac development

(Alexander, Stainier, & Yelon, 1998; Beis et al., 2005; Chen et al., 1996; Chi et al., 2008; Stainier et al., 1996; Warren, Wu, Pinet, & Fishman, 2000). The advent of genome engineering has further enhanced the power of the zebrafish model, significantly reducing the technical challenge of targeted genome manipulation. Many of the studies of the resulting mutant zebrafish, however, have focused on the embryonic and larval stages. Until very recently, the paucity of high resolution imaging techniques for use in live adult zebrafish has precluded more complete studies of their heart anatomy and evaluation of cardiovascular function beyond larval stages. In my thesis, I aim to advance and optimize the technologies to study the adult zebrafish heart – establishing the use of zebrafish as a model organism to examine structural and electrophysiological defects in humans.

1.2 Challenges of studying adult zebrafish

Although technologies such as echocardiography and electrocardiography (ECG) have been previously implemented in adult zebrafish, their utility has been hampered by limited resolution of available apparatus (Milan et al., 2006; L. Sun, Lien, Xu, Shung, et al., 2008). For echocardiography, studies have endeavored to document normal and mutant adult cardiovascular function using a range of commercially available or custom-made echocardiography transducers (Kang et al., 2014; J. Lee et al., 2014; Scheid et al., 2016). Other studies have investigated age-related changes in the heart, recovery of the heart after cryo-injury, and cardiac responses to temperature changes via echocardiography (Hein et al., 2015a; L. Lee et al., 2016; Y. Sun, Fang, Xu, Lu, & Chen, 2015). Previous electrocardiography studies on adult fish, although capturing consistent ECG traces, require perfusion and the fish is sacrificed, preventing longitudinal studies

(Milan et al., 2006). Most of these studies, however, predate the availability of contemporary high-frequency probes, ECG machines, and advanced equipment for analysis. Further, previous analyses failed to fully account for principal components of inter-fish variation - physical parameters such as age, sex, body length, body width, and body weight. My work optimizes echocardiography and ECG for use with zebrafish of different ages, sizes and phenotypes, while determining the factors that need to be adjusted for to develop the most biologically accurate models for future analysis.

1.3 Adult zebrafish cardiac anatomy and electrophysiology

Historically, zebrafish have been utilized as a model for embryonic development. Recently, studies have focused on adult zebrafish where understanding the adult zebrafish heart anatomy and physiology is key. Unlike mammalian hearts, the adult zebrafish heart consists of two heart chambers, an atrium and a ventricle, and a structure analogous to the aorta -- the bulbus arteriosus (Hu, Joseph Yost, & Clark, 2001) (Figure 1-1). The sinus venosus, similar to the mammalian vena cava, collects deoxygenated blood that flows into the atrium, through the atrioventricular valve, and then into the ventricle (Figure 1-1). The atrium has a very thin muscular wall and thin trabeculae within the lumen. Interestingly, the atrium has a significant pumping function, playing a much larger role in pumping than in humans. In fact, in zebrafish, the atrium provides a strong atrial kick to move blood into the ventricle rather than relying on a pressure gradient, as in humans. The ventricle is thicker than the atrium and has numerous trabeculae. Blood flows from the ventricle through the bulboventricular valve into the bulbus arteriosus. The bulbus arteriosus works as a capacitor to maintain blood through the fish. Similar to the human

aorta, the bulbus arteriosus is made up of three tissue layers: the endothelial (intima), media, and externa (Hu et al., 2001). Importantly, the media is made up of smooth muscle cells and an intricate network of collagen and elastin fibers. The cell-makeup of the zebrafish heart and bulbus arteriosus is similar to the human heart and aorta, suggesting the disease pathogenesis of interest in humans could be modeled in the zebrafish. Finally, blood flows from the bulbus arteriosus into the ventral aorta and then to the gills for oxygenation. Echocardiography allows us to visualize each chamber of the heart and the bulbus arteriosus as well as blood flow patterns and velocities. Measurements of the chambers are the same as the measurements of the human heart chambers. The blood flow patterns in zebrafish are almost identical to the human blood flow patterns through the mitral valve and the aortic valve, while keeping in mind the strength of the zebrafish atrium compared to the ventricle.

The electrophysiology of zebrafish and humans are also remarkably similar (Sedmera et al., 2003). The propagation of action potentials (AP) in zebrafish, like humans, starts with the sinoatrial node between the sinus venosus and atrium. It travels to the atrium and then slows down before reaching the atrioventricuar node. At the ventricle, contraction occurs from the apex to the base. This AP can be visualized in a diagram with four phases, where electrical charge (mV) on the y-axis and time on the x-axis. The AP begins with a resting membrane potential of -90 mV and then rapidly depolarizes (phase 0). The membrane potential quickly spikes to +20 mV. Next, there is a slight repolarization during phase 1. From there the AP is lengthened and the AP plateaus at around +15mV. In the third phase, there is rapid repolarization to -90 mV. Finally, the resting membrane potential is restored and this is maintained until the next AP. This

action potential results in the contraction of the heart and can be monitored using electrocardiography (ECG). Finally, the human heart rate is around 60 to 100 beats per minute with an ECG cycle of around 1 second (I. U S Leong, Skinner, Shelling, & Love, 2010).

To model disease, mice have typically been used due to the fact that they are small, fast breeding mammals with a high fecundity. When studying cardiac function, however, mice are less than optimal. Mice have a heart rate around 310 to 480 beats per minute. The ECG cycle for mice is around 0.1 second and most importantly, mice have a different action potential and a very different electrocardiogram compared to humans (Figure 1-2). Zebrafish as a model organism for cardiac diseases, comparatively, have a heart rate of about 100 to 130 beats per minute depending on age with an ECG cycle of around 0.4 seconds (Figure 1-3). And finally, the zebrafish action potential is almost identical to human with a sharp depolarization followed by a large plateau, before repolarization (I. U S Leong et al., 2010). This leads to an almost identical ECG trace between zebrafish and humans (Figure 1-3). The similarities between zebrafish and human heart biology, particularly in comparison with mice heart biology, leads us to believe zebrafish is a great model organism to not only use for embryonic studies, but also adult studies.

1.4 Development of tools to study adult zebrafish hearts

In this investigation we undertake a longitudinal echocardiographic and ECG studies of adult zebrafish. Using a high frequency (70 MHz) transducer, we capture high-resolution, real-time documentation of the structural integrity of the two-chambered heart

and the bulbus arteriosus. It also allows evaluation of functional integrity via analyses of heart rate (HR), blood flow velocity through the atrioventricular (AV) and bulboventricular (BV) valves, isovolumetric relaxation and contraction times (IVRT and IVCT), velocity time integral (VTI) through the AV and BV valves, ventricular ejection time (VET), and a variety of other anatomical and physiological measurements for analysis. Concurrent with these echocardiographic analyses, we document the cardiac conductance characteristics of zebrafish. ECG analysis was performed with the iWorx Zebrafish ECG Recording and Analysis System, designed specifically for zebrafish, to capture accurate electrical activity of the adult zebrafish heart.

We followed two groups of fish over a three-month period measuring echocardiography and ECG measurements in all fish in both groups for three consecutive months. The early-life adult (ELA) zebrafish were measured at ages three, four, and five months, and mid-life adult (MLA) zebrafish were measured at months nine, ten, and eleven. We next determined which measurements and parameters are correlated amongst the echocardiographic and ECG measurements. These measurements and parameters should be adjusted for in order to properly analyze all echocardiography and ECG data. From these correlation analyses, we determined a linear model to account for multiple measurements from each fish and adjust for appropriate covariates to accurately correct for the effect of age, sex, and body size parameters on our cardiovascular measures of interest as well as the random effects due to date of acquisition for both echocardiography and ECG. We demonstrate that failure to properly account for physical parameters as covariates can lead to erroneous identification of differences between zebrafish cohorts. This analysis of wild-type fish provides a guide for how to properly perform

echocardiography and ECG on zebrafish, and also establishes normal values for wild-type fish of ages that are commonly used in the laboratory setting. It should be noted that due to the high genetic diversity in zebrafish (an outbred model organism), each laboratory must conduct their own studies with their in-house zebrafish to establish baseline measurements for their facility. Taken together our data establish a robust strategy for non-terminal echocardiography and ECG in zebrafish, which I then applied to various mutant lines.

1.5 Application of echocardiography and ECG techniques

To validate the utility of these techniques and the value of adjustments for body size, we evaluated previously described models of arrhythmias and long QT syndrome in zebrafish, resulting from mutations in the *kcnh6a* gene (R Arnaout et al., 2007; Langheinrich, Vacun, & Wagner, 2003). *kcnh6a* encodes a voltage-gated potassium channel that is required for normal repolarization of ventricular action potentials. The human orthologous gene for *kcnh6a* is KCNH6, as determined by conserved genome location (synteny) and amino acid sequence comparison (Ivone Un San Leong, Skinner, Shelling, & Love, 2010). Although little is known about defects in the human *KCNH6*, mutations in the paralogous and structurally highly related human *KCNH2* cause around 45% of cases of autosomal dominant long QT syndrome (Sehnert & Stainier, 2002; Splawski et al., 2000). Adult heterozygote *kcnh6a*^{s290} zebrafish have delayed ventricular repolarization and the reported QT interval detected by terminal ECG is significantly longer than in wild-type fish. Homozygosity for this allele is lethal (R Arnaout et al., 2007). Evaluation of adult heterozygote *kcnh6a*^{s290} zebrafish in our pipeline confirms a

clear arrhythmia by ECG with longer PR, QRS, and QT intervals. By echocardiography, heterozygote *kcnh6a*^{s290} mutants demonstrate significantly decreased velocity time integrals (VTI) through the AV valve. Another mutant allele, *kcnh6a*^{tb218}, has been previously characterized with a 2:1 AV block embryonically and with long QT as adults (Kopp et al., 2005; Meder et al., 2011). In our evaluation of adult *kcnh6a*^{tb218} homozygotes we detect no significant electrophysiological differences compared to wild-type zebrafish. By echocardiography, they also do not show any structural or flow differences. These studies demonstrated the pipeline was working and ready for analysis of candidate genes for diseases of interest.

1.6 Bicuspid aortic valve with and without ascending aortic aneurysm

Bicuspid aortic valve (BAV) is the most common congenital heart defect, affecting 1-2% of the population. These individuals, instead of having an aortic valve with 3 leaflets, have only 2 leaflets. BAV is associated with ascending aortic aneurysm (AscAA) and dissections of the aorta (Braverman et al., 2005). BAV does not cause aneurysm of the aorta. For example, patients with BAV can undergo valve replacement surgery and still develop aneurysm of the aorta (Braverman et al., 2005). Furthermore, members of patient families often demonstrate variations of isolated BAV, BAV with AscAA, and AscAA (Loscalzo et al., 2007). Overall, patients with BAV have a 9x risk of a dilated aorta (Larson & Edwards, 1984). This risk begins at a younger age than in individuals without BAV and increases with age (Larson & Edwards, 1984). Unlike Marfan syndrome (MFS), which also presents with thoracic aortic aneurysm, aortic dilatation in patients with BAV presents in the ascending aorta rather than the sinuses of

Valsalva (aortic root), more similar to what is seen in patients with Loeys-Dietz syndrome (LDS) (Dore, Brochu, Baril, Guertin, & Mercier, 2003). Patients with LDS, however, rarely present with isolated dilatation of the ascending aorta (without bicuspid aortic valve).

Studies have shown that BAV is highly heritable (heritability of 89%) (Cripe, Andelfinger, Martin, Shooner, & Benson, 2004). It is an autosomal dominant disorder, with a 3:1 male predominance and incomplete penetrance (Loscalzo et al., 2007). Interestingly, similarly to both MFS and LDS, reduced fibrillin-1 and increased TGF-β signaling have been determined in patients with BAV with and without AscAA. Other genes/pathways implicated in BAV with and without AscAA from numerous human studies include *NOTCH1* (Garg et al., 2005; McKellar et al., 2007), *SMAD6* (Tan et al., 2012), *ACTA2* (Guo et al., 2007), *MYH11* (L. Wang et al., 2010), and mouse studies including *GATA5* (Laforest et al., 2011) and *eNOS* (T. C. Lee, Zhao, Courtman, & Stewart, 2000). Despite the similarly seeming disease pathogenesis with other diseases of aneurysm and the various studies on BAV, the genetic etiology and disease mechanism underlying BAV and associated aneurysm is still unknown. Likely obstacles to studying BAV and aneurysm include extreme locus heterogeneity (Martin et al., 2007), variable expressivity (Loscalzo et al., 2007), and the confounding influence of incomplete penetrance, sex bias, and environmental and/or genetic modification of disease onset and severity. The McCallion lab is in a larger consortium that is working to determine some causes of BAV and associated aneurysm. Specifically, we have used zebrafish as a cost-effective model organism with which to study potential candidate genes for BAV with and without aneurysm.

1.7 Roundabout 4 (ROBO4)

With the consortium I examined multiple candidate genes in zebrafish, *ROBO4* is the most complete story. In 2002, Huminiecki et al. found a new member of the roundabout family (ROBO) called magic roundabout or ROBO4 (Huminiecki, Gorn, Suchting, Poulsom, & Bicknell, 2002). *ROBO4* was determined to be expressed in endothelial tissue and to encode a 107 kD protein. The protein, unlike other members of the roundabout family, contains only 3 immunoglobulin and 2 fibronectin domains in its extracellular region. This is compared to five immunoglobulin and 3 fibronectin domains in both ROBO1 and ROBO2. ROBO3 is similar to ROBO4 in that it also uniquely differs structurally from the other members of the ROBO family. Other relevant regions of the ROBO4 protein include an N-terminal signal peptide, four N-glycosylation sites within the extracellular domain, a transmembrane region, and a proline-rich region within its intracellular domain.

Members of the roundabout family have typically been associated with Slit-Robo signaling, which is involved with axon repulsion in the developing nervous system. However, ROBO4 has consistently been shown to be involved with angiogenesis and the development of blood vessels, specifically in endothelial tissue. In 2005, Bedell et al. demonstrated, in zebrafish embryos, that *robo4* is expressed in the endothelial tissue, the dorsal aorta, posterior cardinal vein, and intersomitic vessels (Bedell et al., 2005). Morpholino knockdown studies showed the loss of intersomitic vessels in morphant zebrafish. The loss of robo4 was compensated for when human *ROBO4* coding sequence was injecting alongside the morpholino, suggesting evolutionary conservation. In vitro

studies by Jones et al. showed that ROBO4 is vital for blood vessel permeability and loss of ROBO4 leads to increased vascular leakage and decreased cell barrier integrity (Jones et al., 2008). ROBO4 function is still under debate, specifically its role in Slit signaling. There has been numerous studies suggesting that ROBO4 binds to Slits (Enomoto et al., 2016; Fritz et al., 2015; Jones et al., 2008; Yu et al., 2014), but there is also data against this, suggesting ROBO4 binds to UNC5B (Koch et al., 2011). Regardless, Mommersteeg et al. recently showed valve defects in knockout mice for *Robo1* and *Robo2* or *Slit3*. No studies looked at *ROBO4*. Although the exact mechanism of ROBO4 is still being explored, from this literature, *ROBO4* seemed to be a good candidate to move forward with for studies of BAV with and without AscAA.

1.8 Figures

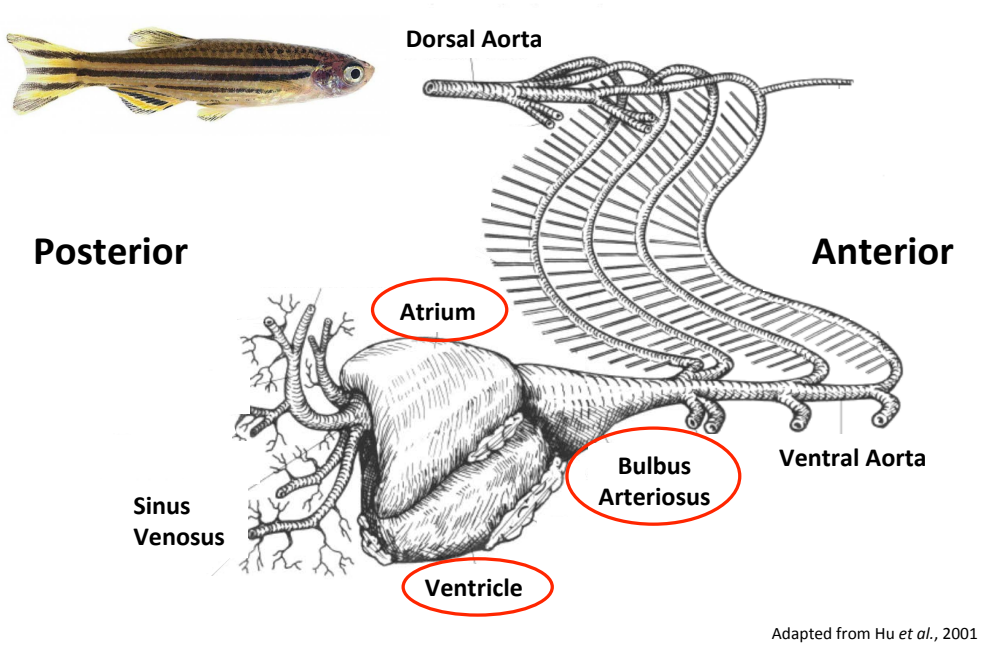

Figure 1-1. Zebrafish have a two-chambered heart. The zebrafish heart is made up the sinus venosus (inflow tract), atrium, ventricle, and bulbus arteriosus (outflow tract).

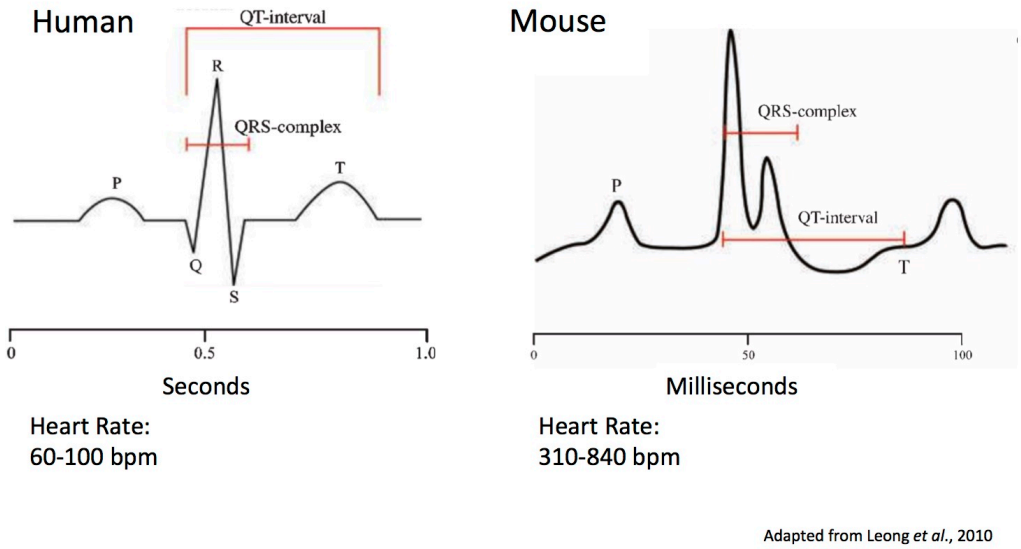

Figure 1-2. Mouse cardiac electrophysiology exhibit major differences to human cardiac electrophysiology. The action potential and ECG cycle between mice and humans are quite different causing difficulties in studying cardiac biology in mice.

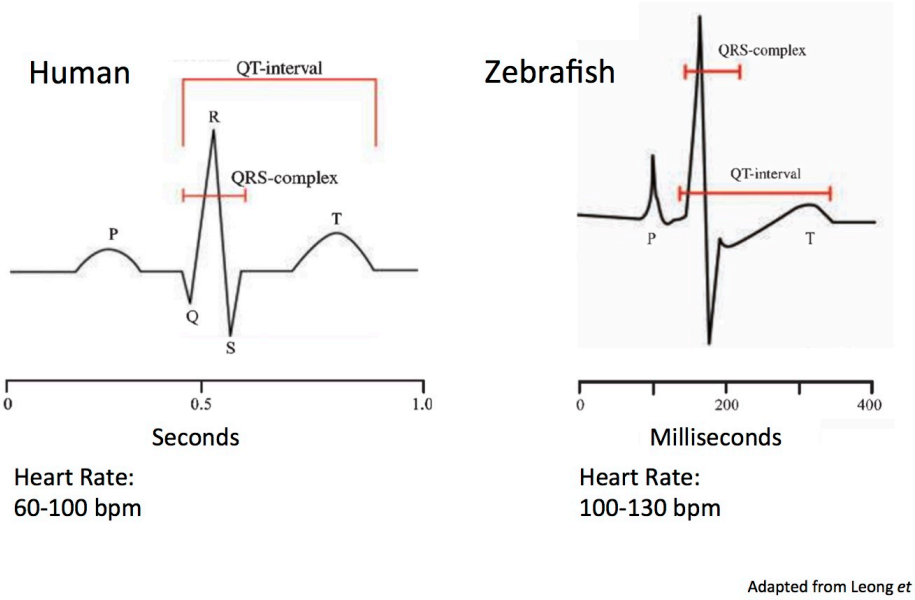

Figure 1-3. Zebrafish cardiac electrophysiology is similar to human cardiac electrophysiology. The action potential and ECG cycle between zebrafish and humans are quite similar making zebrafish a good model organism with which to study cardiac diseases.

Chapter 2: Development of echocardiography for adult zebrafish

2.1 Introduction

Although the adult zebrafish heart should have great potential as a tool for studies of cardiovascular development, structure and function, the utility of this model system has been limited by the small size of its heart, approximately one millimeter in length (Hu et al., 2001). It has therefore been challenging to image adult zebrafish heart structure and function in vivo at high resolution. To address this challenge, we set out to capture high-quality images of the small adult zebrafish heart, using high frequency ultrasound at 70 MHz. In this chapter, I optimize the procedure. For each aspect of the procedure, a standard operating procedure was written. First, the anesthetic was decided. Commonly in zebrafish studies, tricaine (MS-222) is used as a general anesthesia for genotyping. In ECG studies, a paralytic is used to minimize gill movement. In order to provide the most biologically relevant data, without disrupting the normal breathing patterns of the zebrafish, tricaine was used. A paralytic was used during optimization, but the fish did not survive the procedure (data not shown). Position of the transducer on the fish, duration of the echocardiography session, and finally orientation of fish in the trough were all optimized to capture all heart chambers and blood flow between chambers. Due to the goal of our studies (specifically the outflow tract), positioning was adjusted to focus on the bulbus arteriosus and the ventricle rather than the atrium. Finally, to maximize both resolution and viability of each assayed fish, the amount of gel on the fish was optimized. Only a half-centimeter deep of gel is placed on the transducer, which is then lightly placed onto the fish. This provides the highest resolution of images. We also

tried placing the fish in a conical of water and placing gel on the conical, but the resolution was quite poor (data not shown).

After the echocardiography protocol was improved, we captured echocardiography measurements on 20 wild-type (AB) fish total for two different three-month longitudinal studies. Of the 20 fish, two different groups were studied (ten in each group). The two groups were broken up by age – young adult and mid-life adults, encompassing most time points commonly used in the laboratory setting. Using measurements from this study (60 echocardiographic studies total), we were able to determine the best method by which to model the data accurately. This includes which parameters to incorporate as covariates and random effects. Currently zebrafish groups working on echocardiography are not adjusting or controlling for size of the fish when measuring the heart (Hein et al., 2015b; Kang et al., 2014; J. Lee et al., 2014; L. Lee et al., 2016; Scheid et al., 2016; L. Sun, Lien, Xu, & Shung, 2008; Y. Sun et al., 2015; L. W. Wang et al., 2017). In this chapter, I explain that specific measurements and parameters must be adjusted for in order to model the data most accurately.

2.2 Results

2.2.1 *Establishing a protocol for echocardiography*

We designed a clay mold to hold individual fish, which was sized to each fish. The mold with the fish was placed inside a larger trough, filled with zebrafish facility water containing the anesthetic MS-222 (Figure 2-1a). The zebrafish are placed in the trough, dorsal side down (ventral surface upwards). The fish is submerged in the anesthetic solution in order to maintain oxygen circulation, leaving its ventral surface exposed. A thin layer of ultrasound gel is placed on the transducer. The gel increases image quality immensely and, used sparingly, showed no negative effects on the fish.

In our hands, the highest quality imaging of the atrium, ventricle, and bulbus arteriosus in a single plane was obtained from sagittal long axis views (LAX) using B-Mode imaging (Figure 2-1b). The probe is placed directly onto the ventral side of the fish. In this way, we were able to capture measurements pertaining to the ventricle and the bulbus arteriosus. Atrial measurements were not captured due to the difficulty in visualizing the chamber (Figure 2-1b). Due to the highly trabeculated nature of the ventricle, the epicardial surface of the ventricle was traced for measurements rather than the endocardial edge as done in clinical studies. In systole and diastole, we calculated ventricular diastolic and systolic areas and volumes (Figure 2-1c, d). From these measurements, stroke volume (SV), ejection fraction (EF), and fractional shortening (FS) were calculated. The diameter of the bulbus arteriosus was measured using the aortic arch function while in ventricular systole (Figure 2-1d). The diameter is measured at the widest section of the bulbus arteriosus while still remaining parallel with the ventricle. After B-Mode imaging was concluded, color Doppler mode was used to determine

location and direction of blood flow through the heart. The red flow is towards the ultrasound transducer and blue is flow away. Flow from the atrium into the ventricle is away from the probe and can be seen in red (Figure 2-1e). Blood flow from the ventricle into the bulbus arteriosus is toward the probe and can be seen in blue (Figure 2-1f). While in LAX and color Doppler mode, PW Doppler was used to display the sample volume overlay on the color Doppler mode image. The sample volume wireframe was moved in order to acquire blood velocity measurements from the AV valve, over the red flow in color Doppler mode (Figure 2-1e). Cine loops were captured and used to calculate early (E) and late (A) atrial diastolic filling velocities, velocity time integral through the AV valve (AV VTI), isovolumetric contraction time (IVCT), and isovolumetric relaxation time (IVRT) (Figure 2-1g). It should be noted that in zebrafish the A peak is taller than the E peak. This is opposite of what is seen in humans for flow across the mitral valve. This is because of the strong pumping power of the atrium during ventricle filling in zebrafish.

Next, the wireframe was moved to acquire blood velocity measurements through the BV valve and the ventricular outflow tract (VOT), which should appear blue in color Doppler mode (Figure 2-1h). The captured trace was then used to calculate the heart rate (HR), mean and peak outflow velocities through the VOT, velocity time integral (VTI), and ventricular ejection time (VET) (Figure 2-1h). For optimal fish anesthetic recovery, imaging sessions lasted no longer than 10 minutes. The E/A ratio was determined by using the E and A velocities to determine diastolic function. The Tei index (myocardial performance index) was calculated from (IVCT+IVRT)/(VET). The cardiac output was calculated as the product of SV and HR.

2.2.2 *Determining biological covariates for echocardiography data*

Despite the technological advances in the capacity to record echocardiography, we are very aware that analyses of cohorts of fish may be impeded by first, noise that results from genetic variation within a population, second, covariates in age, sex, body size/volume/mass parameters much like the human population and finally, from technical variation arising. We set out to collect data from two cohorts of zebrafish representing two age intervals: early-life adult (ELA) and mid-life adult (MLA) fish. For the ELA cohort, measurements were taken once a month at three months, four months, and finally, five months of age (Table 2-1). Thus, this longitudinal study included measurements acquired at three time points for each ELA zebrafish. Similarly, for the MLA cohort, we took measurements at nine, ten, and 11 months of age (Table 2-2). These time points were chosen because these are commonly used for laboratory fish. It should be noted that the ELA and MLA cohorts are two different sets of fish and not the same fish. For each set of measurements, individual fish underwent echocardiography, and were returned to a tank for recovery. Fish were maintained in individual tanks to avoid the risk of "sample switching" and to control for food intake. Food intake can greatly affect the size of the individual fish and by keeping the fish by itself the competition for food is removed. Once these data were collected, we then evaluated how best to analyze these age data with respect to the working hypothesis that the size of the fish could affect the size of the heart and this must be adjusted for in analysis of the heart.

2.2.3 *Age and sex affect the size of zebrafish*

Next, we determined the effect of one of the major variations between fish – size. Common observation shows that the older the fish, the bigger the fish and that female fish are larger than male fish, but no groups have published these data plainly. This observation is compounded by the fact that the fish community says that overcrowded tanks of zebrafish results in smaller fish overall, but also a skewed proportion of male fish to female fish in the tank. Looking at body weight in grams as a measure of body size at three time points (three, four, and five months of age), we see that individual fish get larger over time (**$P < 0.01$, Figure 2-2). In order to best control for the growth of individual fish, particularly between studies, fish should be maintained in individual tanks starting at maturity. Under these conditions and using body weight as a measure of size, we determined that female fish are consistently larger in size compared to male fish (Figure 2-3, *$P < 0.05$). This is logical since female fish are often gravid with eggs, making them larger. Even non-gravid female fish are often larger than males. Both gravid and non-gravid fish were used in this study. From these two tests, we determined that age and sex of zebrafish matter in size of the fish and are two covariates that must be adjusted for in analysis.

2.2.4 *Body size parameters affect echocardiography measurements*

Next, to determine more covariates that affect the data, we generated a correlation plot for all echocardiographic data. This plot describes the relationship between anthropometric parameters and all measured traits. To generate this plot and analysis, each parameter and echocardiographic measurement was plotted against all other traits and itself (Figure 2-4). For each trait-trait pair, a correlation relationship was determined

and shown visually by a colored dot (either blue or red for direct or anti-correlation, respectively). The stronger the correlation, the dot for each trait-trait pair is darker in color and the larger in size. As seen in Figure 2-4, sex was not included in the analysis since our previous analysis showed that sex affects size (Figure 2-2 and Figure 2-3).

For measurements determined via echocardiography, the correlation plot reveals that body size parameters including body length, width and body weight are each highly correlated with the majority of measurements (Figure 2-4). In particular, anatomical measurements such as the diameter of the bulbus arteriosus, the area and volume of the ventricle in both systole and diastole, and measurements such as SV, cardiac output, and blood flow velocity through the BV valve (mean and peak) were directly correlated with these parameters. Early filling velocity (E) was highly anti-correlated. Body length, width, and body weight were all highly correlated with one another, as expected. As illustrated by this plot, body size parameters are clearly correlated with most of the echocardiographic measurements. These parameters become very important when comparing measurements between groups of individuals by echocardiography.

2.2.5 *Failure to adjust for body size parameters results in inaccurate results*

This importance can be clearly seen when we look at the diameter of the bulbus arteriosus during systole, as an example of the effect of size on analysis, results, and conclusions. The diameter of the bulbus arteriosus is a simply determined by measuring across the bulbus ateriosus, from one side to the next. Since this bulbus arteriosus is conical this measurement is a diameter. The diameter of the bulbus arteriosus is strongly positive correlated with body size parameters (body weight, length, and width) as

determined by the correlation plot analysis (Figure 2-4). As seen in the top panel of Figure 2-5, the measurement of the diameter of the bulbus arteriosus (y-axis) increases with the size of the fish, shown here by body weight in grams. We can see this relationship by a regression analysis, with an R^2 value of 0.32. This means that around 32% of the variance in the diameter of the bulbus arteriosus is predicted by the size of the individual fish. This proportion shows a clear relationship between diameter of the bulbus arteriosus and body size. Thus, the data needs to be adjusted for size. When the residuals of the measurements of the diameter of the bulbus arteriosus are regressed against body size, the R^2 value decreases to 0.018 (bottom panel, Figure 2-5). This means that if body size is adjusted for, the proportion of the variance in the diameter that is predicted by the size of the fish decreases from 32% to 1.8%. From this regression analysis it is clear that body size parameters need to be adjusted for because failure to adjust for size could lead to inaccurate conclusions. For example, if we have two fish: a wild-type fish and a mutant fish and the mutant fish are larger than the wild-type fish, comparison of the two values for diameter of the bulbus arterious will indicate that the mutant fish has a larger diameter. This could lead incorrectly to the conclusion that the mutant fish have aneurysm in comparison to wild-type fish. Furthermore, adjusting for size provides the most accurate data set for the most accurate analysis. Although this a specific example, the correlation plot from Figure 2-4 shows that most of the echocardiographic measurements must be adjusted for size.

2.2.6 *Adjusting for body size parameters removes correlations*

The strong effect of size on the diameter of the bulbus arteriosus can be observed in a majority of echocardiographic measurements (Figure 2-4). The strongest positive correlations with body size are echocardiographic traits that are measurements of the heart chambers (ventricle area and volume in systole and diastole), stroke volume (which is dependent on size of the ventricle), and cardiac output (which is calculated from stroke volume). Figure 2-4 shows velocity through the outflow tract and the A peak inflow velocity is positively correlated with size as well, but to a lesser extent. The strongest anti-correlation with body size parameters is the E peak velocity. These correlations need to be removed and body size needs to be adjusted for. We re-determined the correlations between all echocardiographic traits and measurements, adjusting for body size parameters, by performing correlation analysis on the residuals of the measurements (Figure 2-5). Correlations seen previously without adjustment are now corrected. The circles that mark correlations between, for example, diameter of the bulbus arteriosus and the body size parameters are now gone. The adjustment for body size parameters now allow us to see true correlations in the data such as the diameter of the bulbus arteriosus and outflow tract velocity.

As mentioned earlier, sex and body size are related. Sex was not included in the correlation analysis because it is a binary trait and the effects of sex on size are included in the correlation analysis. We did perform correlation analysis, including adjustment for body size, on females alone (Figure 2-6) and males alone (Figure 2-7). These plots show the correlations between different echocardiographic measurements in both females and males. These differences in correlations between echocardiographic measurements in

females and males are not unexpected, but show that male and female fish should be studied individually or sex should be adjusted for in future studies.

2.3 Discussion

In light of our conclusions from the data correlation analyses, we proceeded to establish a linear mixed effects model to adjust for the traits and parameters shown to affect echocardiographic measurements – age, sex and body size parameters. A linear regression model is a statistical analysis often used for data that is grouped in a hierarchical structure. In the echocardiography data, ages, time points, sex were considered groups within the data. Furthermore, from the correlation analysis, we needed to adjust for specific parameters or covariates. Each covariate added systematically into the final model and each model was compared using ANOVA, confirming the covariate changed the model in statistically significant manner. The final covariates included were group (which will be genotype in future studies), type (mutant line or AB lines for future studies), age, sex, and body size parameters (body weight, body length, and body width). These covariates are all fixed effects. The final covariate is date of echocardiography, as a random effect. Due to the nature of the protocol for echocardiography, the transducer set-up differs for each session of echocardiography. This change can affect the readings and cause batch effects. To control for this, date of echocardiography was included as a random effect. The protocol for reading the echocardiograms (taking the measurements) is not set-up dependent and therefore was not included in the final model. The final model for all future analysis is: lmer(trait) ~ group + type + body weight + body length + body width + age + sex + (1 | date of echo).

2.4 Methods

2.4.1 ***Zebrafish maintenance*****.** All adult (three months and older) wild-type (AB) zebrafish lines were maintained in system water according to standard methods[28]. Animal upkeep and experimental procedures were in accordance with the ethical permits set by the Johns Hopkins Institutional Animal Care and Use Committee.

2.4.2 ***Echocardiography*****.** To capture high-resolution images, the Vevo 2100 Imaging System equipped with a 70 MHz ultrasound transducer was used (VisualSonics®, Toronto, ON, Canada). The following settings were used for all reported zebrafish echocardiography sessions: imaging frequency, 50 MHz for B-Mode, 40 MHz for Pulsed-Wave (PW) Doppler and color Doppler, 10-20 Hz pulse repetition frequency, adjusted as necessary, 30-35 Db Doppler gain, 200 frames per second in B-mode, and 7 mm image depth. The zebrafish (n=10 per group) were anesthetized by placing the fish into a plastic cup filled with 100 ml of 168 μg/ml MS-222 (tricaine methane sulfonate). Stage 3-anesthesia (loss of equilibrium, decreased opercular movement rate, no voluntary locomotion, non-responsive to stimuli) was obtained prior to imaging and maintained throughout the period of data recording. Fish were weighed and measured for width and length and then stabilized in the clay mold within the plastic trough filled with MS-222, leaving only the most ventral surface of the ventrum exposed. A thin layer of Parker Aquatic 100 ultrasound gel was then applied to the transducer array (2-3 mm) using a cotton swab. *n.b.* Excessive amounts of ultrasound gel may result in suffocation of the fish.

The transducer probe was positioned in a vertically within the manipulator with the notch facing caudally, meaning the transducer surface lies longitudinally over the ventrum of the fish along the anterior-posterior axis. Thus, the ultrasound beam is thus perpendicular to the long axis of the fish. The transducer was lowered towards the fish until it makes contact with the gel and the heart is visualized in B-Mode. Touching the transducer to the surface of the fish will distort the signal. Two-dimensional B-Mode imaging was used to obtain videos of the heart, including ventricle, atrium, and bulbus arteriosus, in long axis view. These 100 frame cine loops were then analyzed using the Vevo Lab Software cardiac package.

The left ventricular trace function was used to trace the epicardial surface of the ventricle in systole and diastole, calculating ventricular systolic and diastolic areas and volumes, stroke volume (SV), ejection fraction (EF), and fractional shortening (FS). The diameter of the bulbus arteriosus was measured using the aortic arch function while in ventricular systole. Color Doppler mode was used to determine location, direction, and velocity of blood flow through the heart. While in long axis view and color Doppler mode, PW Doppler mode was used to display the sample volume overlay on the color Doppler mode image. The sample volume wireframe was moved in order to acquire velocity measurements from the ventricular outflow tract (VOT), which should appear blue in color Doppler mode. The Doppler angle was adjusted to align the yellow gate as parallel as possible to blood flow through the VOT. Cine loops were captured as desired and analyzed to calculate the heart rate (HR), mean and peak outflow velocities through the VOT, velocity time integral (VTI), and ventricular ejection time (VET). Next, the wireframe was moved to acquire velocity measurements through the atrioventricular

(AV) valve, which should appear red in color Doppler mode. Cine loops were captured and used to calculate early (E) and late (A) diastolic filling velocities, AV VTI, isovolumetric contraction time (IVCT), and isovolumetric relaxation time (IVRT). The Doppler angle was adjusted to align the yellow gate as parallel as possible to the flow of blood through the AV valve and cine loops were captured. The Tei index, also known as the myocardial performance index, was calculated from (IVCT+IVRT)/(VET). The cardiac output was calculated from SV multiplied by HR. The fish were removed from the imaging trough and placed in a cup of fresh room temperature aquarium water to facilitate recovery from anesthesia. To ensure optimal recovery, imaging sessions lasted no longer than 10 minutes. Evaluated zebrafish were then returned to individual tanks to recover.

2.4.3 ***Statistical Analysis.*** For experiments including multiple comparisons, *P* values refer to one-way ANOVA. For experiments including only one comparison, *P* values refer to unpaired two-tailed Student's *t*-test or two-tailed Welch's *t*-test. Means with ranges are shown. *P* values less than 0.05 were considered significant. Correlation plots were generated using the corrplot() package in R version 3.2.3. A linear mixed effects regression model estimated the effect of group on mutation status. Age, sex, body size parameters, and type were included as covariates with date of echocardiography as a random effect: lmer(trait) ~ group + type + body weight + body length + body width + age + sex + (1 | date of echo). All statistical analyses were implemented in R version 3.2.3.

2.5 Tables

Parameters and Measurements	Mean (range) ELA 1	Mean (range) ELA 2	Mean (range) ELA 3
AV Measurements			
Early (E) Diastolic Filling (mm/s)	21.48 (10.94-28.17)	15.37 (10.94-21.88)	21.45 (14.29-27.34)
Late (A) Diastolic Filling (mm/s)	92.07 (49.22-135.6)	129.6 (57.42-218.6)	136.2 (39.59-275.6)
E/A	0.2687 (0.1053-0.4545)	0.1353 (0.07353-0.2857)	0.2258 (0.06349-0.6154)
Velocity Time Integral (mm)	8.095 (5.093-11.74)	8.396 (5.592-11.96)	10.8 (5.642-25.95)
IVCT (ms)	28 (15-45)	26.5 (20-40)	29.5 (25-40)
IVRT (ms)	74.13 (35-105)	58.58 (35-95)	60.1 (23.3-137.5)
BV Measurements			
Heart Rate (bpm)	70.9 (50-90)	68.4 (37-101)	77 (58-96)
BV Mean Velocity (mm/s)	51.54 (21.37-102.2)	75.95 (58.2-107.2)	53.72 (28.86-101.8)
BV Peak Velocity (mm/s)	88.65 (33.56-177)	131.5 (97.45-184.1)	95.15 (49.98-194.9)
Velocity Time Integral (mm)	10.07 (4.578-21.35)	14.29 (8.662-21.55)	10.59 (4.565-22.06)
Ventricular Ejection Time (ms)	172.5 (155-195)	154 (90-185)	157.5 (130-185)
Ventricular and BA Measurements			
Systolic Area (mm^2)	0.6872 (0.226-1.282)	0.8644 (0.665-1.41)	0.9077 (0.667-1.157)
Diastolic Area (mm^2)	1.054 (0.336-1.766)	1.349 (0.923-1.93)	1.31 (0.874-1.744)
Systolic Volume (mm^3)	0.4769 (0.179-0.938)	0.5868 (0.359-1.087)	0.6058 (0.351-0.819)
Diastolic Volume (mm^3)	0.7748 (0.14-1.617)	1.108 (0.583-1.762)	1.05 (0.52-1.514)
BA Diameter (mm)	0.5698 (0.437-0.738)	0.7868 (0.503-0.991)	0.665 (0.507-0.923)
Stroke Volume (mm^3)	0.3706 (0.06-0.679)	0.5145 (0.225-0.812)	0.4444 (0.169-0.698)
Ejection Fraction	46.81 (36.14-59.82)	46.09 (38.29-58.17)	41.69 (32.51-51.28)
Fractional Shortening	19.8 (7.273-33.69)	22.16 (10.28-30.53)	17.3 (9.664-31.22)
Tei Index	0.5892 (0.4194-0.7297)	0.575 (0.3692-0.9811)	0.5414 (0.2353-1.155)
Cardiac Output (mm^3/min)	25.38 (5.34-52.65)	34.32 (18.45-69.83)	33.85 (14.2-66.31)

Table 2-1. Means and ranges for echocardiographic measurements of early-life adult (ELA) zebrafish. The means and ranges for all echocardiographic measurements of ELA fish at the three time points (1, 2, and 3) which correspond to three months, four months, and five months, respectively.

Parameters and Measurements	Mean (range) MLA 1	Mean (range) MLA 2	Mean (range) MLA 3
AV Measurements			
Early (E) Diastolic Filling (mm/s)	15.67 (8.202-32.81)	18.95 (8.919-30.08)	18.7 (10.94-30.08)
Late (A) Diastolic Filling (mm/s)	103.5 (46.48-227)	113.6 (54.69-169.6)	113.1 (51.96-158.1)
E/A	0.1865 (0.06378-0.4444)	0.2078 (0.07408-0.4231)	0.1869 (0.09434-0.4211)
Velocity Time Integral (mm)	7.374 (2.263-10.75)	7.458 (4.751-11.13)	7.877 (3.507-13.26)
IVCT (ms)	35.62 (15-45)	35 (30-45)	33.75 (20-65)
IVRT (ms)	62.91 (51.6-81.7)	68.75 (41.6-103)	69.79 (9-121)
BV Measurements			
Heart Rate (bpm)	74.2 (56-104)	88.4 (51-127)	80.25 (63-100)
BV Mean Velocity (mm/s)	49.76 (26.56-78.07)	46.51 (25.19-78.87)	57.4 (32.24-95.42)
BV Peak Velocity (mm/s)	84.92 (43.75-141.3)	78.65 (38.91-137.1)	100.7 (54.12-172)
Velocity Time Integral (mm)	9.954 (4.382-18.44)	8.466 (4.545-14.66)	11.45 (6.747-22.24)
Ventricular Ejection Time (ms)	152 (120-190)	149 (120-180)	161.9 (140-185)
Ventricular and BA Measurements			
Systolic Area (mm^2)	0.8763 (0.554-1.458)	0.9234 (0.452-1.608)	0.9005 (0.562-1.41)
Diastolic Area (mm^2)	1.322 (1.041-2.039)	1.405 (0.724-2.202)	1.395 (0.832-2.106)
Systolic Volume (mm^3)	0.6051 (0.323-1.234)	0.6315 (0.199-1.401)	0.6281 (0.313-1.112)
Diastolic Volume (mm^3)	1.084 (0.768-2.035)	1.198 (0.433-2.331)	1.178 (0.541-2.031)
BA Diameter (mm)	0.6968 (0.335-0.949)	0.6847 (0.488-0.955)	0.8146 (0.62-0.988)
Stroke Volume (mm^3)	0.4844 (0.296-0.801)	0.566 (0.234-0.929)	0.5501 (0.229-0.919)
Ejection Fraction	44.7 (37.28-57.95)	48.49 (39.88-55.84)	46.16 (40.53-56.74)
Fractional Shortening	21.4 (6.292-32.38)	17.82 (9.649-26.28)	20.77 (11.12-30.84)
Tei Index	0.6412 (0.5089-0.8174)	0.6954 (0.5628-0.8331)	0.6313 (0.1871-0.8432)
Cardiac Output (mm^3/min)	35.55 (16.58-47.37)	49.31 (21.11-69.78)	43.69 (15.57-67.78)

Table 2-2. Means and ranges for echocardiographic measurements of mid-life adult (MLA) zebrafish. The means and ranges for all echocardiographic measurements of ELA fish at the three time points (1, 2, and 3) which correspond to nine months, ten months, and eleven months, respectively.

2.6 Figures

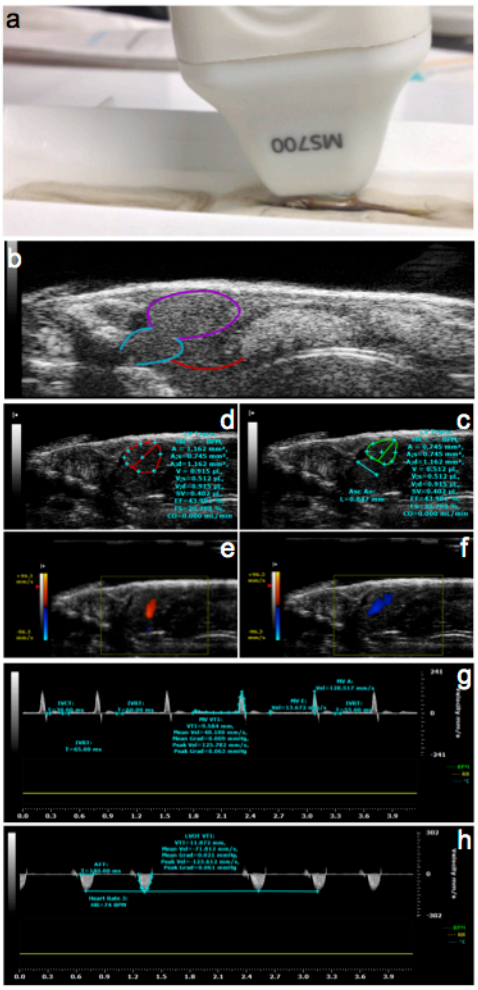

Figure 2-1. Acquiring echocardiography measurements for adult zebrafish. (a) The adult zebrafish is placed dorsal-side down (ventral side up) in a custom-made clay mold (fit to the size of the fish), inside a larger trough with water and anesthetic. Gel is placed on the VisualSonics 70MHz ultrasound transducer probe and is lowered onto the fish so an interface is established between the water and the gel. It is imperative the probe is directly parallel the fish. (b) During B-mode lateral imaging, the atrium (red), ventricle (purple), and the bulbus arteriosus (blue) are clearly visible. (c) To calculate anatomical

measurements for the ventricle, the epicardium is traced using the Visual Sonics program while in diastole (red) and labeled Ld. (d) Next, the ventricle in systole is measured (green). This can be marked Ls. The diameter of the bulbus arteriosus can also be measured. Measurements calculated from both traces include: area (systole and diastole), volume (systole and diastole), EF, and FS. (e) Color Doppler is used to image blood flow directionality. In this color Doppler echocardiogram, blood is flowing away from the atrium into the ventricle (inflow, red). (f) The blue flow represents outflow from the ventricle into the bulbus arteriosus. (g) During lateral imaging of the adult zebrafish, PW Doppler is used to capture blood flow through the AV valve. Measurements determined include: early (E) diastoltic flow and late diastolic atrial (A) velocities, velocity time integral (VTI), ventricular ejection time (VET), isovolumetric contraction time (IVCT), and isovolumetric relaxation time (IVRT). (h) PW Doppler is also used to capture blood flow through the BV valve. From this, the HR, mean and peak velocities are calculated.

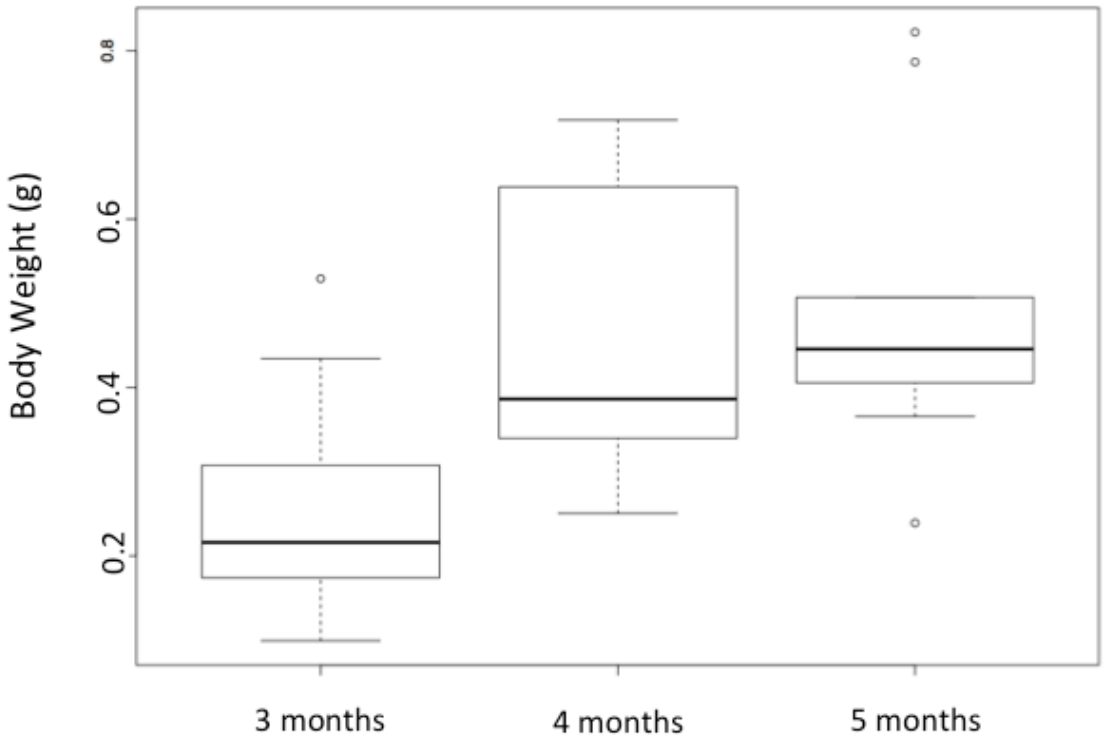

Figure 2-2. Size of adult zebrafish by age. Age (3 months, 4 months and 5 months) is on the x-axis. Body weight is in grams is on the y-axis. The size of the fish varies significantly with age (n = 10 fish at each time point, P = 0.008 by ANOVA, means with ranges).

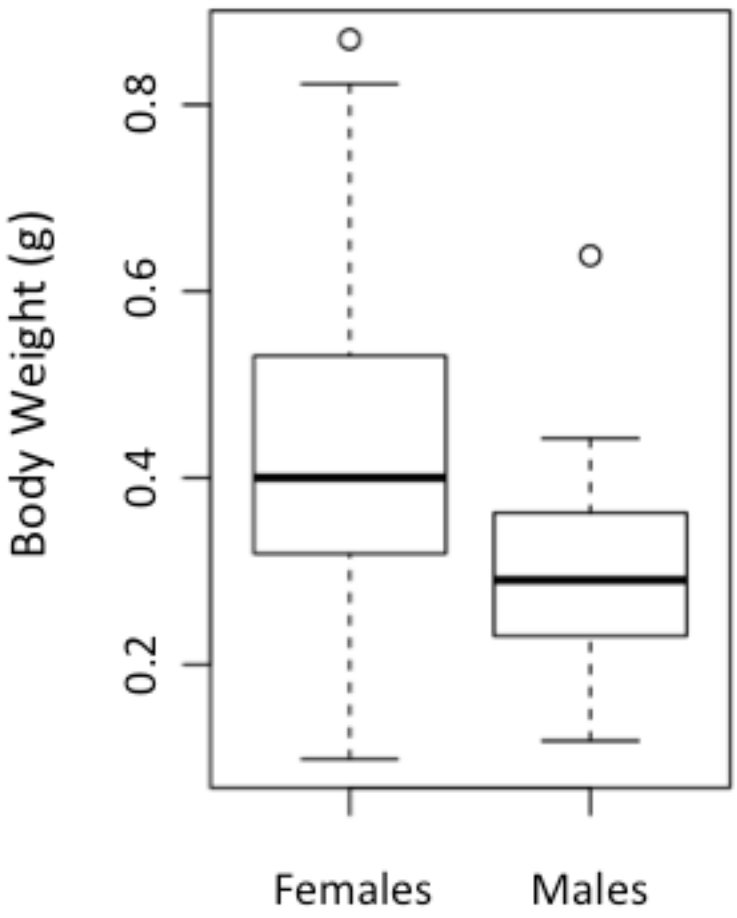

Figure 2-3. Sizes of zebrafish differ between female and male fish. Female fish are statistically significantly larger compared to male fish as determined by weight (P = 0.00231; Welsh two sample t-test, *P < 0.05, means with ranges).

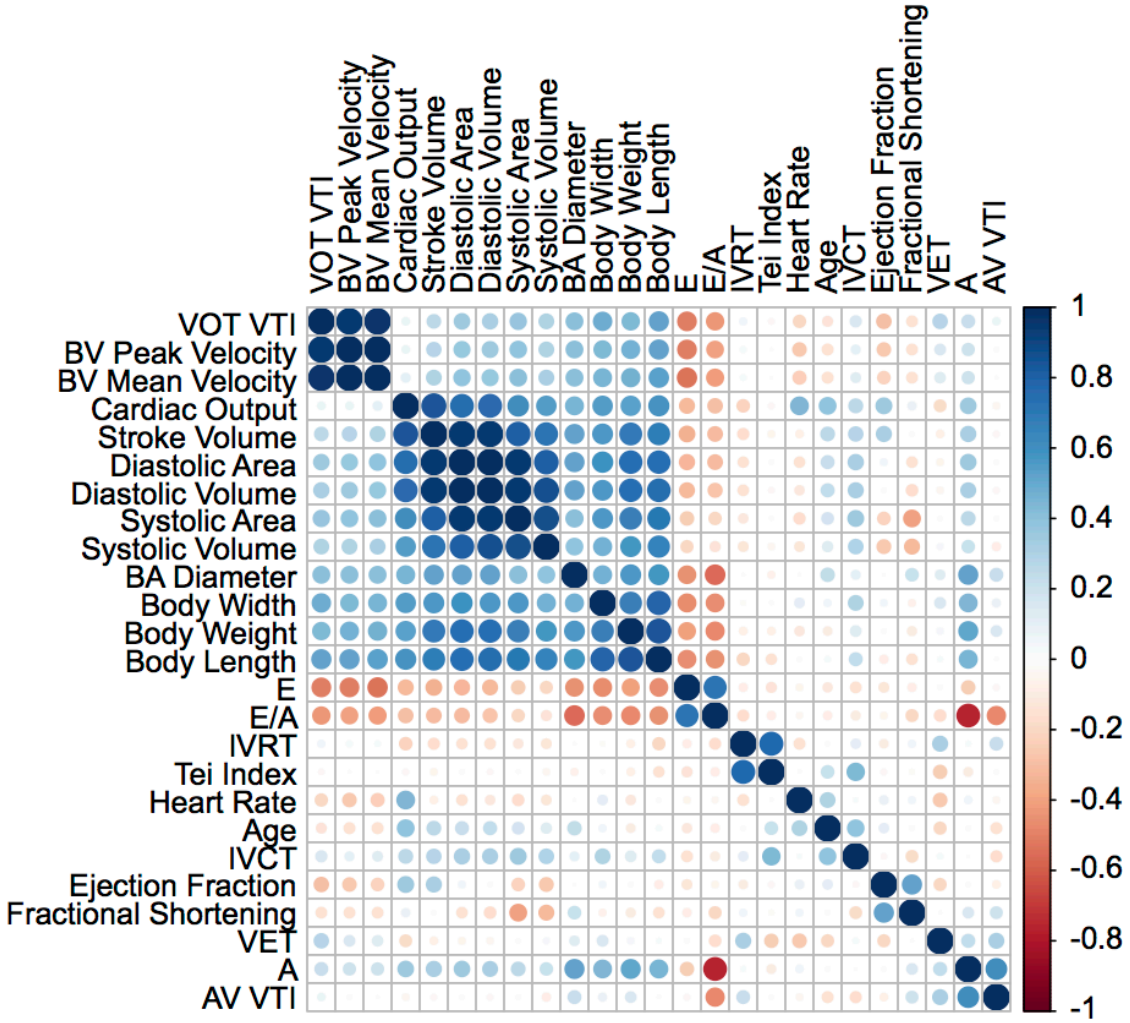

Figure 2-4: Correlation plot between traits, measurements, and parameters determined by echocardiography. Measurements and parameters captured by ECG were plotted by correlation analysis. A blue circle shows a direct correlation whereas a red circle shows an anti-correlation. The size and shade of color shows the strength of correlation (direct or anti-) where 1 and -1 are the strongest direct and anti- correlation, respectively.

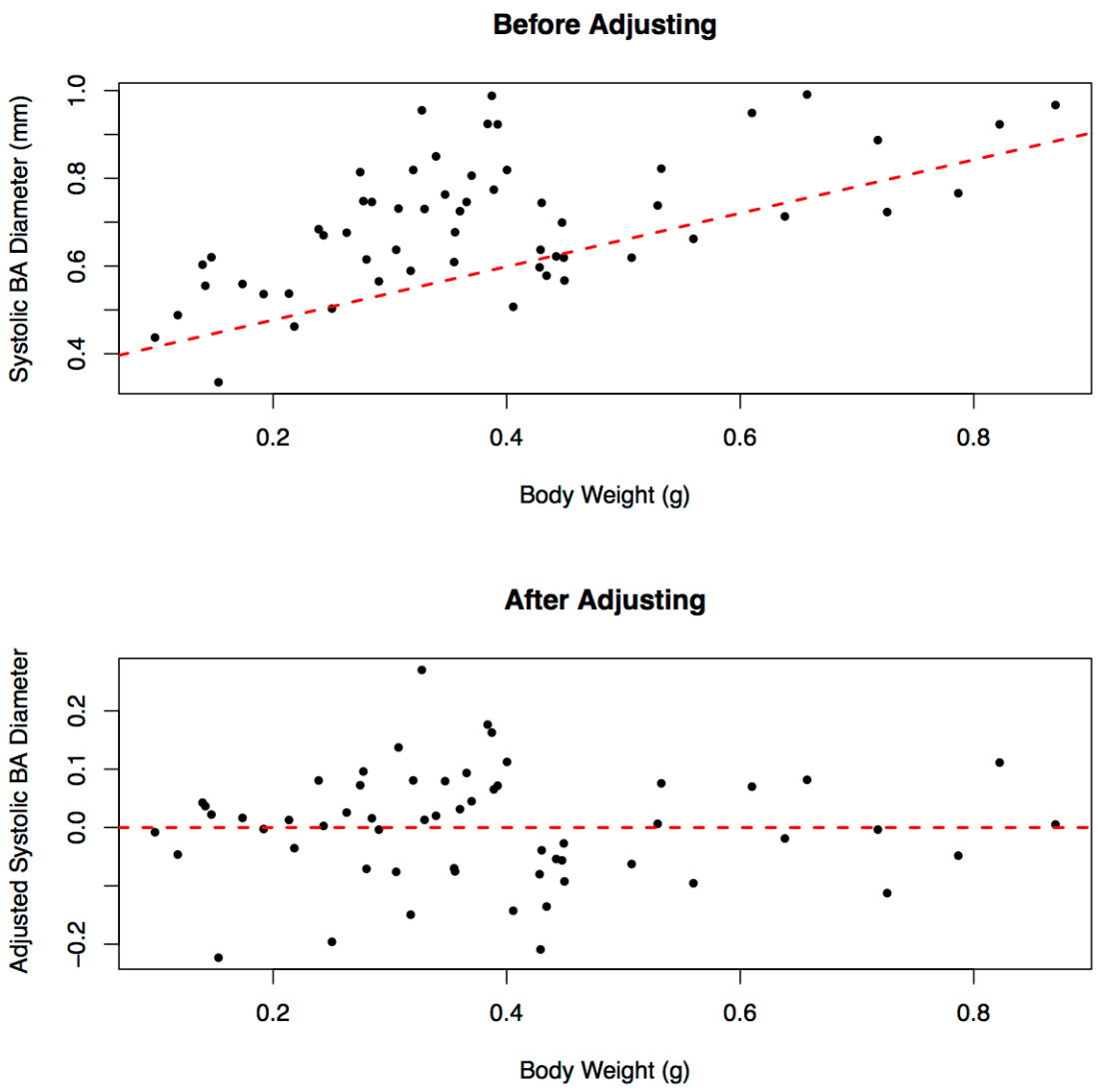

Figure 2-5. Systolic diameter of the bulbus arteriosus (BA) needs to be adjusted for body weight. The top plot shows raw diameter measurements of the bulbus arteriosus (y-axis) as a function of body weight (x-axis) of the same fish for wild-type fish. Regression analysis determines $R^2 = 0.32$. The bottom plot shows residuals for the diameter of the bulbus arteriosus in systole (y-axis) regressed against body weight of the same fish (x-axis). Regression analysis determined $R^2 = 0.018$.

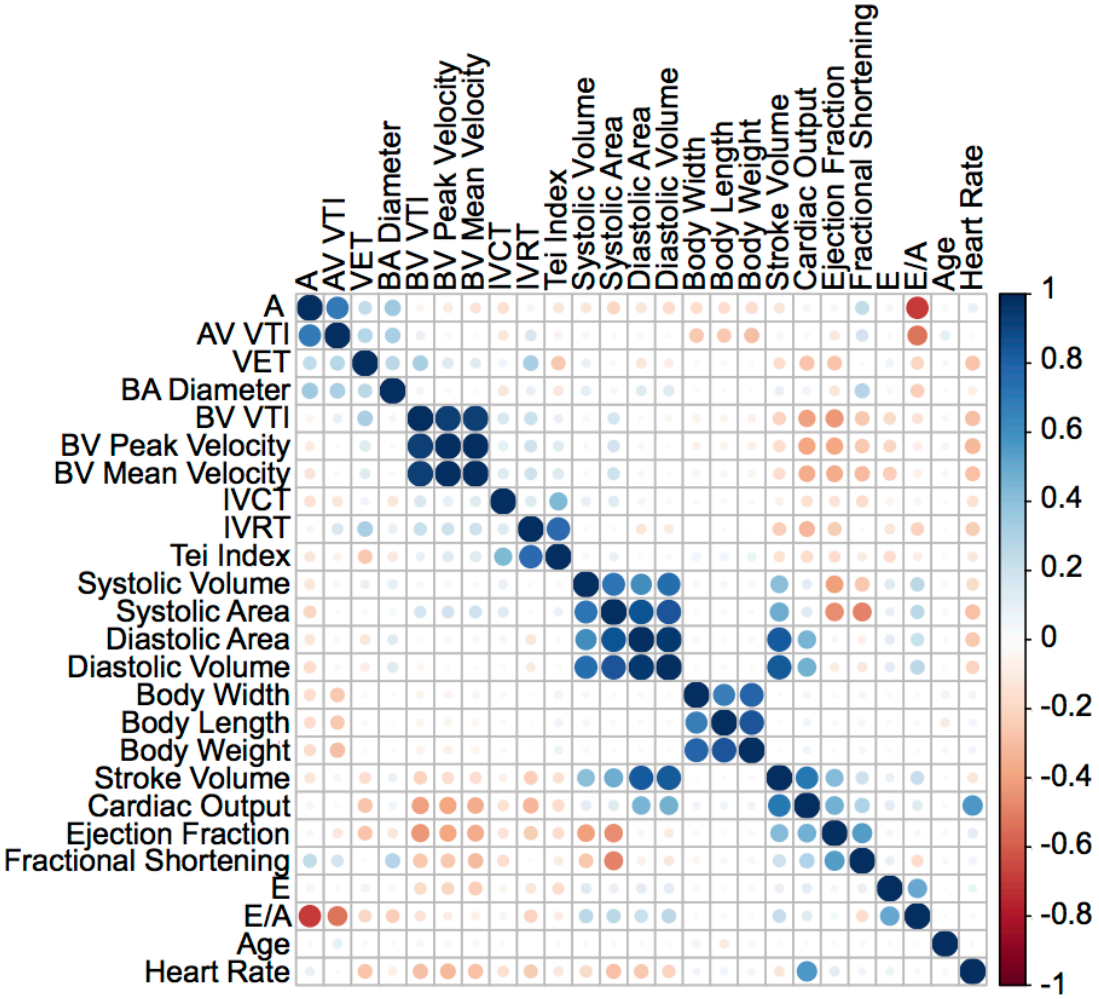

Figure 2-6. Correlation plot between residuals of measurements and parameters determined by echocardiography. The same correlation analysis was performed as in Figure 2-4, but residuals of the measurements and parameters were plotted rather than raw measurements. A blue circle shows a direct correlation whereas a red circle shows an anti-correlation. The size and shade of color shows the strength of correlation (direct or anti-) where 1 and -1 are the strongest direct and anti- correlation, respectively.

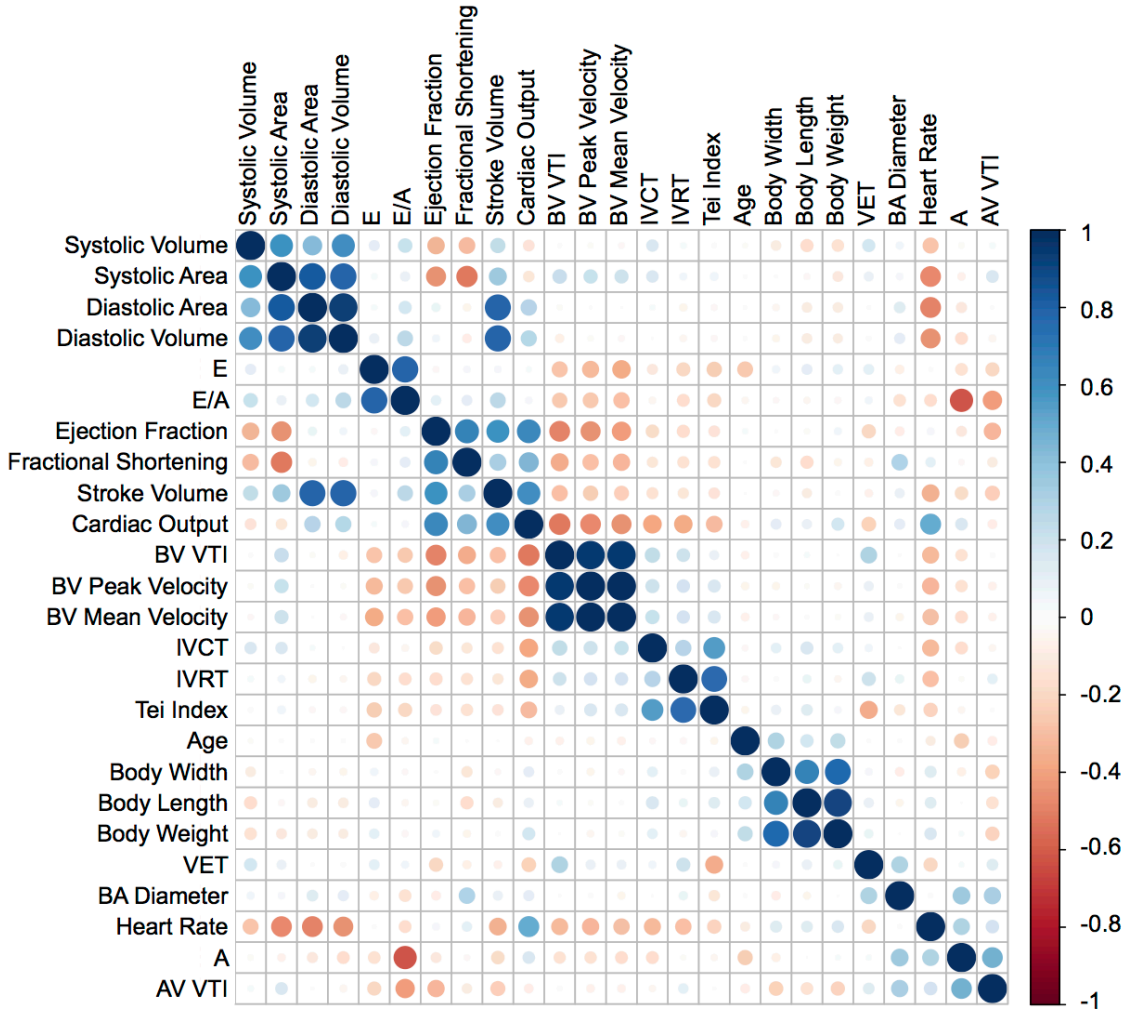

Figure 2-7. Correlation plot between residuals of measurements and parameters determined by echocardiography for female fish only. Residuals of the measurements and parameters for female wild-type fish were plotted by correlation analysis. A blue circle shows a direct correlation whereas a red circle shows an anti-correlation. The size and shade of color shows the strength of correlation (direct or anti-) where 1 and -1 are the strongest direct and anti- correlation, respectively.

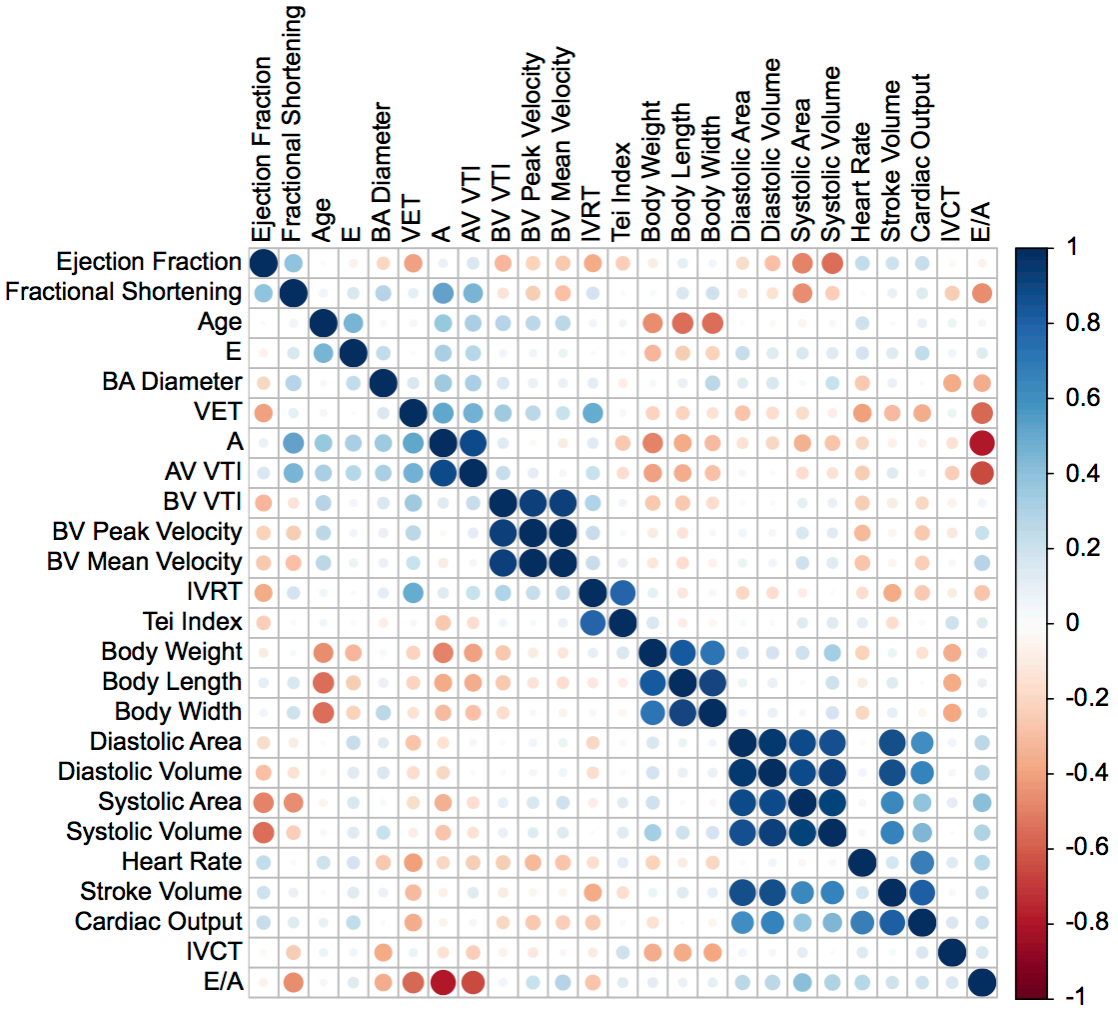

Figure 2-8. Correlation plot between residuals of measurements and parameters determined by echocardiography for male fish only. Residuals of the measurements and parameters for male wild-type fish were plotted by correlation analysis. A blue circle shows a direct correlation whereas a red circle shows an anti-correlation. The size and shade of color shows the strength of correlation (direct or anti-) where 1 and -1 are the strongest direct and anti- correlation, respectively.

Chapter 3: Development of electrocardiography for adult zebrafish

3.1 Introduction

Electrocardiographic (ECG) measurements of adult zebrafish performed previously demonstrate clear P waves, QRS complexes and T waves as seen in human ECG traces (Milan et al., 2006). Although these studies helped define ECG measurements in zebrafish, most analyses were terminal. They required perfusion and the invasive placement of a needle electrode in the heart tissue. Further, it has not been used in longitudinal analyses and a limited number of groups have performed it in tandem with echocardiography (Y. Sun et al., 2015). Here we set out to complete a comprehensive pipeline, facilitating genesis of longitudinal echocardiographic and ECG data, collected in parallel. This chapter establishes the ECG standard operating procedure, collecting ECG measurements on two sets of wild-type fish in a longitudinal study (early-life adults and mid-life adult fish), and finally, determines covariates and random effects that must be taken into account for future ECG studies, similar to the echocardiography data (See Chapter 2).

3.2 Results

3.2.1 *Establishing a protocol for ECG*

Using the iWorx Zebrafish ECG Recording and Analysis System, we are able to capture high-quality ECG traces with unprecedented simultaneous analysis of all traits typically examined in a clinical setting including, but not limited to HR, PR interval, QRS complex, and QT interval. The fish are anesthetized using a solution of 2-phenoxyethanol, almost completely extinguishing gill movement, which can affect traces captured by the machine. Once appropriately anesthetized, the zebrafish are removed from anesthesia and placed dorsal side down on the apparatus (Figure 3-1a). Gel is then placed on the Ag/Ag-Cl electrodes, which are lowered until they make light contact with the surface of the ventrum. The electrodes are positioned such that the most cranial electrode sits immediately at the edge of the gills, along the midline of the fish (Figure 3-1a). It is imperative that the electrodes sit on the skin versus the fins. Once the fish is properly positioned, the ECG trace of the fish\ is recorded for five minutes using the iWorx Zebrafish ECG Recording and Analysis System software. In our analysis pipeline, we first select an interval of the captured ECG trace as being representative of the overall wave pattern (Figure 3-1b). This time window typically contains one QRS complexes (n~1) and must begin prior to the initiation of a new electrical waveform i.e. including a P wave and end after a completed T wave. Once the representative trace is selected, it is applied to define waveforms throughout the entirety of the data recording for that individual fish. Traces are plotted to include the R amplitude of each interval. In this way, outliers can be readily identified and removed (Figure 3-1c). Finally, the average

waveform trace for each fish is labeled manually to denote the P, Q, R, S, and T waves for each electrophysiological wave (Figure 3-1d).

3.2.2 *Determining biological covariates for electrocardiography data*

Unlike the echocardiography study, few groups have performed ECG analysis on zebrafish and no group has published ECG data using this surface ECG machine. We therefore set out to establish wild-type ECG measurements and determine any covariates in age, sex, body size/volume/mass parameters that must be adjusted for, similar to the echocardiography data. To establish a more complete picture of zebrafish heart metrics over time, we acquired ECG data corresponding to each time point for the early-life adult (ELA) and mid-life adult (MLA) cohorts (the same fish used in the echocardiography study, see Chapter 2). For the ELA cohort, measurements were taken once a month at three months, four months, and five months of age and as close to the date of echocardiography as possible. Similarly, for the MLA cohort, we took measurements at nine, ten, and 11 months of age and performed ECG as close to the date of echocardiography as well. This was done to get a complete analysis and complete phenotype for each fish heart at a single point in time – both anatomical and physiological. For each set of measurements, individual fish underwent ECG analysis for five minutes (to capture the ECG recording) and were returned to a tank for recovery. Fish were maintained in individual tanks to avoid the risk of "sample switching" and to control for food intake. Food intake can greatly affect the size of the individual fish and by keeping the fish by itself the competition for food is removed. Once these data on the two groups of fish were collected, we then evaluated how best to analyze these ECG data

with respect to the working hypothesis that the size of the fish could affect the capturing the most accurate ECG or the electrophysiology of the fish and then must be adjusted for in analysis of the electrophysiology.

3.2.3 Body size affects ECG measurements

We then performed a correlation analysis against all ECG measurements and body size parameters of the fish including body weight, length, and width. The correlation plot describes the relationship between anthropometric parameters and all measured ECG traits. To generate this plot and analysis, each parameter and ECG measurement was plotted against all other traits and itself (Figure 3-2). For each trait-trait pair, a correlation relationship was determined and shown visually by a colored dot (either blue or red for direct or anti-correlation, respectively). The stronger the correlation, the dot for each trait-trait pair is darker in color and the larger in size. As seen in Figure 3-2, sex was not included in the analysis since our previous analysis showed that sex affects size (Figure 2-2). As seen in Figure 3-2, the correlation plot revealed that body length, width and body weight are each correlated with a majority of measurements. Length and weight are more correlated, directly or inversely, with the ECG measurements than body width. Heart rate and QT interval are most correlated with the body size parameters. PR interval is slightly less correlated and QRS is least correlated with body size parameters. This correlation plot shows, for ECG, like echocardiography, body size parameters are critical for evaluation.

3.2.4 Adjustment for body size removes correlation between measurements

These correlations derived from analysis of raw measurements are seen in Figure 3-2. The correlations need to be removed and body size parameters need to be adjusted for. We re-determined the correlations between all echocardiographic traits and measurements, adjusting for body size parameters, by performing correlation analysis on the residuals of the measurements rather than the raw measurements themselves (Figure 3-3). Correlations seen previously without adjustment are now corrected. The circles that mark correlations between, for example, QT interval or heart rate and the body size parameters are now gone. The adjustment for body size parameters now allows us to see any true correlations in the data, such as in the echocardiography data set. As seen in Figure 3-3, few correlations between the ECG measurements remain after the adjustment. These correlations are between heart rate and PR interval and QRS interval with QT interval. Interestingly, our data does not show a correlation between QT interval and heart rate. This is not expected since in humans, QT interval and heart rate are correlated and, biologically, related.

3.3 Discussion

After investigation into echocardiography analysis, we proceeded to perform the same correlation analyses on electrocardiography data to determine factors that needed to be adjusted to establish the most accurate way to model the data. We determined this model would be a linear mixed effects model to adjust for the traits and parameters shown to correlate with ECG measurements, including body weight, body length, and body width. Since these body size parameters were shown earlier (Figure 2-2 and Figure 2-3) to be affected by age and sex of the fish, these were also included as covariates. Again, as with the echocardiography model, each covariate was added systematically into the final model and each model was compared using ANOVA, confirming the covariate changed the model in statistically significant manner. The final covariates for the ECG model were group (which will be genotype in future studies), type (mutant line or AB lines for future studies), age, sex, and body size parameters (body weight, body length, and body width). These covariates are all fixed effects. The final covariate is date of ECG, as a random effect. Due to the nature of the protocol for ECG, each fish is placed under the electrodes individually. We try to keep this as standardized as possible, but unfortunately, day of ECG does have an effect. These small changes can affect the readings and cause batch effects. To control for this, date of ECG was included as a random effect. The protocol for reading the ECG measurements (taking the measurements) is not set-up dependent and typically all ECG measurements are read for a single study in one day, and therefore was not included in the final model. The final model for all future analysis is: lmer(trait) ~ group + type + body weight + body length + body width + age + sex + (1 | date of ECG).

3.4 Methods

3.4.1 ***Zebrafish maintenance*****.** All adult (three months and older) wild type (AB) zebrafish lines were maintained in system water according to standard methods (Westerfield, 2007). Animal upkeep and experimental procedures were in accordance with the ethical permits set by the Johns Hopkins Institutional Animal Care and Use Committee.

3.4.2 ***Electrocardiography.*** ELA and MLA zebrafish cohorts were evaluated by ECG using the iWorx Zebrafish ECG Recording and Analysis System. To facilitate recording, all zebrafish were individually anesthetized using a solution of 2-phenoxyethanol (Fluka Analytical 77699-250ML) diluted 1:1000 in aquarium water. Each fish is placed into the solution for two to three minutes (or until there is minimal gill) movement. Body weight and length measurements for each fish were recorded prior to ECG. The fish is placed dorsal side down (ventral side up) on the provided pedestal and the electrodes are positioned such that the most anterior electrode is sits immediately at the caudal edge of the gills, along the midline of the fish (Figure 2a). Data is recorded for five minutes using the iWorx Zebrafish ECG Recording and Analysis System software before the fish is put into a recovery tank full of clean system water. The Labscribe3 software (iWorx) was used to analyze ECG data and calculate measures of cardiac electrophysiology. To limit the potential for noise introduced into the recordings by electrostatic or electromagnetic interference, the apparatus is maintained within a Faraday cage.

3.4.3 ***Statistical Analysis*****.** Correlation plots were generated using the corrplot() package in R version 3.2.3. A linear mixed model estimated the effect of group on mutation status. Age, sex, body size parameters, and type were included as covariates with date of echocardiography as a random effect: lmer(trait) ~ group + type + body weight + body length + body width + age + sex + (1 | date of ECG) All statistical analyses were implemented in R version 3.2.3.

3.5 Figures

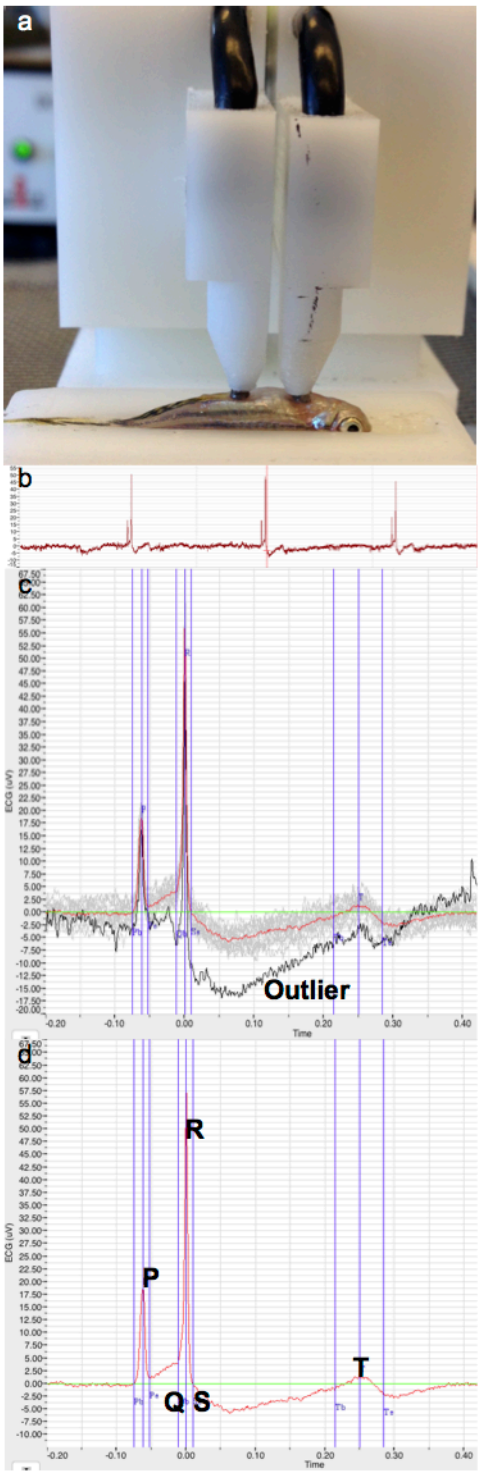

Figure 3-1. Acquiring electrocardiography measurements for adult zebrafish. (a) To capture electrocardiography measurements, the adult zebrafish is placed dorsal side down on the pedestal. (b) Using the iWorx Zebrafish ECG Recording and Analysis System, first, a single complex of the captured ECG trace is chosen to determine the overall wave pattern for the larger, five minute trace. Individual rhythm strips for each fish are identified for artifacts and outliers. (c) Any additional outlier strips not captured by the software are manually removed (black outlined trace is identified as an outlier in comparison to the gray traces). (d) The average rhythm strip for each fish (red) is appropriately labeled for each electrophysiological wave.

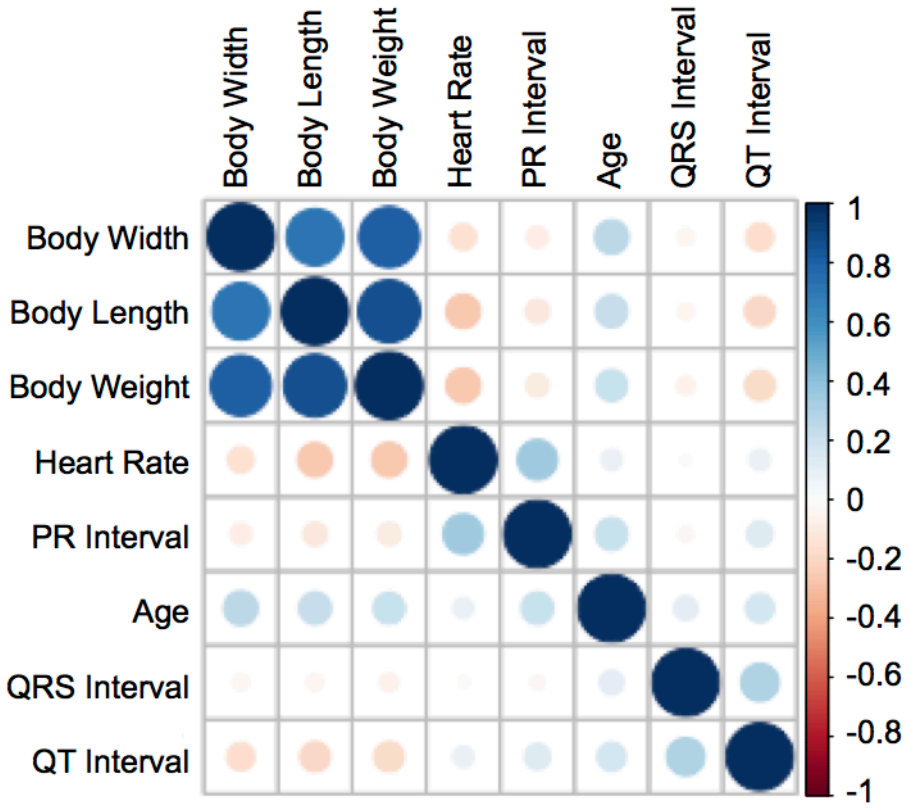

Figure 3-2. Correlation plot between traits, measurements, and parameters determined by electrocardiography. Measurements and parameters captured by ECG were plotted by correlation analysis. A blue circle shows a direct correlation whereas a red circle shows an anti-correlation. The size and shade of color shows the strength of correlation (direct or anti-) where 1 and -1 are the strongest direct and anti- correlation, respectively.

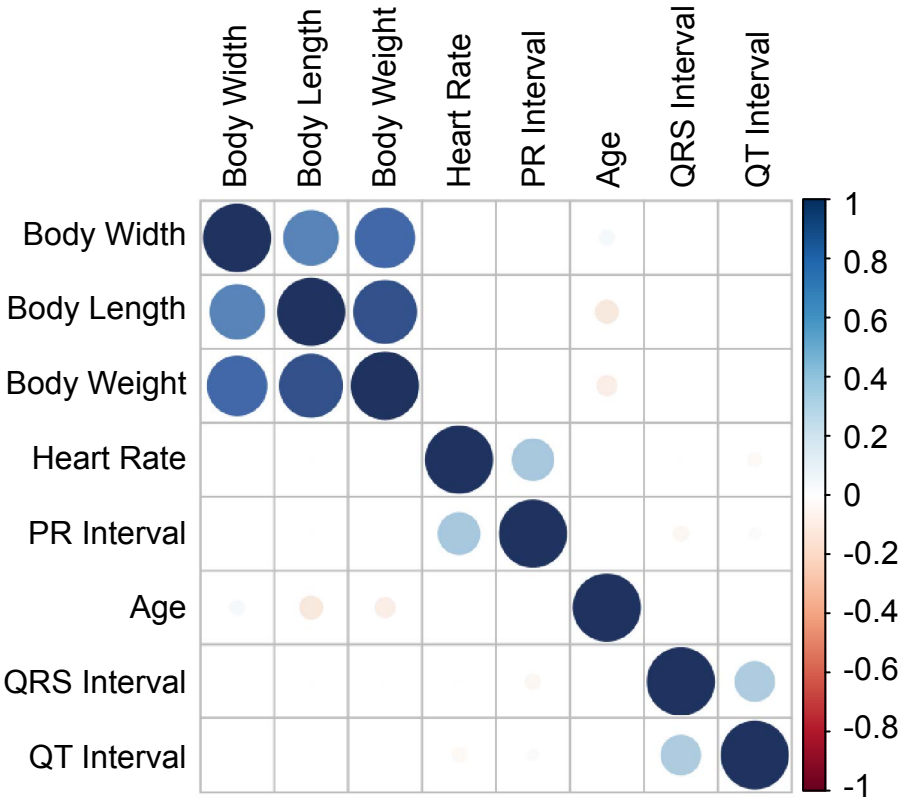

Figure 3-3. Correlation plot between residuals of measurements and parameters determined by electrocardiography. The same correlation analysis was performed as in Figure 3-2, but residuals of the measurements and parameters were plotted rather than raw measurements. A blue circle shows a direct correlation whereas a red circle shows an anti-correlation. The size and shade of color shows the strength of correlation (direct or anti-) where 1 and -1 are the strongest direct and anti- correlation, respectively.

Chapter 4: Validation of echocardiography and electrocardiography

4.1 Introduction

After establishing baseline measurements via echocardiography and electrocardiography for wild-type fish of ages commonly used in laboratory settings, we applied these methods to two well-characterized mutant lines. First, the mutant line of the gene, *kcnh6a*, *kcnh6a*^{tb218} has been previously described with an embryonic phenotype of 2:1 AV block. This means there is a defect in the electrical signal reaching the atrioventricular node and results in the atrium contracting twice for a single ventricular contraction (Kopp et al., 2005; Meder et al., 2011). On an ECG trace, this is picked up as two individual P waves for every one QRS complex. This phenotype is only seen in embryos. Adult *kcnh6a*^{tb218} mutants were found to have elongated QT intervals, or defects in the repolarization of the ventricle (Meder et al., 2011). Although these data was recorded with a surface ECG machine, it was custom-made and very low resolution (Hassel et al., 2008). Another allele of *kcnh6a*, the *kcnh6a*^{s290} mutant line has also been used as a model for arrhythmia and QT duration perturbation. Using electrocardiography in adult heterozgyote mutant fish and wild-type fish, a previous group found heterozygote *kcnh6a*^{s290} fish had a prolonged QTc interval, suggesting delayed ventricular repolarization (R Arnaout et al., 2007). This group used an established electrocardiography protocol by Milan et al., where anesthetized fish were perfused and two needle electrodes were inserted into each fish and ECG measurements were captured for hours at a time (Milan et al., 2006). For both of these studies in adult fish, physical parameters including sex and body size were not adjusted for in analysis. Furthermore, no

echocardiography has ever been performed on either line. We decided to test our methods of echocardiography and ECG with these two models, applying the respective models of analysis.

4.2 Results

4.2.1 *kcnh6a^{tb218} mutants do not show electrophysiological dysfunction*

To further demonstrate our newly optimized methods and our analysis, we first studied *kcnh6a^{tb218}* mutant fish. Embryos in our hands show a definitive 2:1 AV block, as described in the literature (two atrial beats to one ventricular beat) (data not shown). We then proceeded to analyze adult mutants with the ECG machine and application of our linear mixed effects model. Analysis via ECG demonstrated no significant differences between homozygous *kcnh6a^{tb218}* fish and wild-type controls (Table 4-1). A longer PR interval is representative of 2:1 AV block, clinically. PR interval was not significantly different between *kcnh6a^{tb218}* fish and wild-type controls. Anticipating that detection of PR interval extension may be obstructed by e.g. a bifurcated P wave, each trace was again examined by eye, but no qualitative differences in traces were seen. Previous studies showed an elongated QT interval, but that too was not seen either by our rigorous methods.

4.2.2 *kcnh6a^{tb218} mutants do not show anatomical dysfunction*

Next, *kcnh6a^{tb218}* fish and wild-type controls were analyzed via echocardiography for structural defects as well as blood flow velocity abnormalities. Echocardiographic analysis has not been published for *kcnh6a^{tb218}* fish. In the analysis of measurements, we adjusted for age, sex, and body size parameters with date of echocardiography as a random effect. We report no significant and meaningful differences between any of the traits examined, including anatomical differences, flow differences through the AV valve, or BV valve (Table 4-2). Although ECG data and echocardiographic data should be

examined separately, the lack of any differences in the structure of the fish heart or blood flow pattern is consistent with the ECG analysis of the *kcnh6a*^{tb218} mutants.

4.2.3 *kcnh6a*^{s290} mutants show elongated QRS and QT intervals by ECG

Next, we examined another mutant line of the gene, *kcnh6a*. We hypothesized a long QT interval in both mutant embryos and adults. However, no overt or gross electrophysiological difference was visualized in mutant embryos (data not shown). Analysis of *kcnh6a*^{s290} by ECG as described in Chapter 3 showed an interesting difference in *kcnh6a*^{s290} traces compared to traces from wild-type controls. Interestingly, there were significant differences between traits QRS complex and QT interval (Table 4-3). For both traits, the *kcnh6a*^{s290} mutants have significantly faster QRS intervals (***$P <$ 0.001) and QT intervals (**$P < 0.01$, Table 4-3). This suggests dysfunction of ventricular repolarization. This is consistent what has been previously described in the literature.

4.2.4 *kcnh6a*^{s290} mutants show an increased velocity time integral through the AV valve by echocardiography

To further characterize the *kcnh6a*^{s290} arrhythmia and long QT model, we performed full analysis via echocardiography. We examined all measurements related to ventricular size in systole and diastole, BA diameter, and blood flow through both the BV and AV valves and applied the linear mixed effects model. This analysis revealed only one significant difference between mutant and wild-type fish – velocity time integral (VTI) through the AV valve. The time integral was significantly decreased (in millimeters) in the mutant fish than the wild-type fish. This suggests there are no

structural phenotypes in *kcnh6a*^{s290} fish, solely an electrophysiological one that may affect blood flow through the AV valve (*$P < 0.05$, Table 4-2). Blood flow through the AV valve is determined in the Visual Sonics echocardiography analysis program, by placing a gate across the AV valve. From this, we calculate late diastolic filling (A peak), early diastolic filling (E peak), IVCT, IVRT, and the velocity time integral. No other traits involving blood flow through the AV valve were different between the two groups of fish. This observation regarding the *kcnh6a*^{s290} mutants has yet to be published.

4.3 Discussion

To apply the methods as well as the model of analysis that I developed in Chapters 2 and 3, we used two mutant lines of the same gene, *kcnh6a*. These two lines each have a specific and unique point mutation generated via ENU mutagenesis. These lines have both been carefully analyzed and phenotyped previously by other groups in the field that report 2:1 AV block in embryos and an elongated QT interval in adults. In our hands with our ECG machine and our model of analysis, we did not determine any cardiac conductance differences between *kcnh6a*^{tb218} mutants and wild-type fish. We also performed echocardiography on these fish and saw no structural defects either. It should be noted that we do see the embryonic cardiac phenotype that was reported by Meder et al. Biologically, little is known regarding heart development in zebrafish between embryonic and adulthood. This line could be used in the future to determine the changes in electrophysiology from early development into adulthood and what could cause a loss of arrhythmia. Potentially, these mutant fish and these adulthood data could be very useful in studying sudden cardiac death, where lethal arrhythmia hits in adulthood. This change in electrophysiology in zebrafish is ripe for discovery.

The second mutant line has also been studied as embryos and adults. This point mutation at homozygosity is lethal and the adult heterozygous fish have been reported to have prolonged QT intervals. In our hands and with our machine and our model of analysis, we see that the *kcnh6a*^{s290} fish do have a significantly prolonged QRS complex and QT interval. This confirms the literature and also illustrates that our methods are working. These fish were also analyzed by echocardiography and were found to have a lower velocity time integral. Since flow velocity varies during the ejection of blood in the

heart, the velocity time integral is used to determine the sum of the flow velocity. Decreased velocity time integral may be suggestive of the effects of the arrhythmia on the ventricle. To conclude, these two well-characterized mutant lines were studied further and these data adds to that characterization. These lines, especially the *kcnh6a*^{s290} line, prove that with the ECG machine and our analysis, we are able to pick up arrhythmias and we can now apply this pipeline to sudden cardiac death candidate genes.

4.4 Methods

4.4.1 ***Zebrafish maintenance*****.** All adult (three months and older) wild type (AB) zebrafish lines were maintained in system water according to standard methods (Westerfield, 2007). Animal upkeep and experimental procedures were in accordance with the ethical permits set by the Johns Hopkins Institutional Animal Care and Use Committee.

4.4.2 ***Electrocardiography.*** Zebrafish cohorts were evaluated by ECG using the iWorx Zebrafish ECG Recording and Analysis System. To facilitate recording, all zebrafish were individually anesthetized using a solution of 2-phenoxyethanol (Fluka Analytical 77699-250ML) diluted 1:1000 in aquarium water. Each fish is placed into the solution for two to three minutes (or until there is minimal gill) movement. Body weight and length measurements for each fish were recorded prior to ECG. The fish is placed dorsal side down (ventral side up) on the provided pedestal and the electrodes are positioned such that the most anterior electrode is sits immediately at the caudal edge of the gills, along the midline of the fish (Figure 2a). Data is recorded for five minutes using the iWorx Zebrafish ECG Recording and Analysis System software before the fish is put into a recovery tank full of clean system water. The Labscribe3 software (iWorx) was used to analyze ECG data and calculate measures of cardiac electrophysiology. To limit the potential for noise introduced into the recordings by electrostatic or electromagnetic interference, the apparatus is maintained within a Faraday cage.

4.4.3 *Echocardiography*. To capture high-resolution images, the Vevo 2100 Imaging System equipped with a 70 MHz ultrasound transducer was used (VisualSonics®, Toronto, ON, Canada). The following settings were used for all reported zebrafish echocardiography sessions: imaging frequency, 50 MHz for B-Mode, 40 MHz for Pulsed-Wave (PW) Doppler and color Doppler, 10-20 Hz pulse repetition frequency, adjusted as necessary, 30-35 Db Doppler gain, 200 frames per second in B-mode, and 7 mm image depth. The zebrafish (n=10 per group) were anesthetized by placing the fish into a plastic cup filled with 100 ml of 168 μg/ml MS-222 (tricaine methane sulfonate). Stage 3 anesthesia (loss of equilibrium, decreased opercular movement rate, no voluntary locomotion, non-responsive to stimuli) was obtained prior to imaging and maintained throughout the period of data recording. Fish were weighed and measured for width and length and then stabilized in the clay mold within the plastic trough filled with MS-222, leaving only the most ventral surface of the ventrum exposed. A thin layer of Parker Aquatic 100 ultrasound gel was then applied to the transducer array (2-3 mm) using a cotton swab. *n.b.* Excessive amounts of ultrasound gel may result in suffocation of the fish.

The transducer probe was positioned in a vertically within the manipulator with the notch facing caudally, meaning the transducer surface lies longitudinally over the ventrum of the fish along the anterior-posterior axis. Thus, the ultrasound beam is thus perpendicular to the long axis of the fish. The transducer was lowered towards the fish until it makes contact with the gel and the heart is visualized in B-Mode. Touching the transducer to the surface of the fish will distort the signal. Two-dimensional B-Mode imaging was used to obtain videos of the heart, including ventricle, atrium, and bulbus

arteriosus, in long axis view. These 100 frame cine loops were then analyzed using the Vevo Lab Software cardiac package.

The left ventricular trace function was used to trace the epicardial surface of the ventricle in systole and diastole, calculating ventricular systolic and diastolic areas and volumes, stroke volume (SV), ejection fraction (EF), and fractional shortening (FS). The diameter of the bulbus arteriosus was measured using the aortic arch function while in ventricular systole. Color Doppler mode was used to determine location, direction, and velocity of blood flow through the heart. While in long axis view and color Doppler mode, PW Doppler mode was used to display the sample volume overlay on the color Doppler mode image. The sample volume wireframe was moved in order to acquire velocity measurements from the ventricular outflow tract (VOT), which should appear blue in color Doppler mode. The Doppler angle was adjusted to align the yellow gate as parallel as possible to blood flow through the VOT. Cine loops were captured as desired and analyzed to calculate the heart rate (HR), mean and peak outflow velocities through the VOT, velocity time integral (VTI), and ventricular ejection time (VET). Next, the wireframe was moved to acquire velocity measurements through the atrioventricular (AV) valve, which should appear red in color Doppler mode. Cine loops were captured and used to calculate early (E) and late (A) diastolic filling velocities, AV VTI, isovolumetric contraction time (IVCT), and isovolumetric relaxation time (IVRT). The Doppler angle was adjusted to align the yellow gate as parallel as possible to the flow of blood through the AV valve and cine loops were captured. The Tei index, also known as the myocardial performance index, was calculated from (IVCT+IVRT)/(VET). The cardiac output was calculated from SV multiplied by HR. The fish were removed from

the imaging trough and placed in a cup of fresh room temperature aquarium water to facilitate recovery from anesthesia. To ensure optimal recovery, imaging sessions lasted no longer than 10 minutes. Evaluated zebrafish were then returned to individual tanks to recover.

4.4.4 ***Statistical Analysis.*** A linear mixed model estimated the effect of group on mutation status. Age, sex, body size parameters, and type were included as covariates with date of echocardiography as a random effect: lmer(trait) ~ group + type + body weight + body length + body width + age + sex + (1 | date of echocardiography/ECG) All statistical analyses were implemented in R version 3.2.3.

4.5 Tables

Measurements	Mean (range) for wild-type	Mean (range) for *kcnh6a*^{tb218}	*P*-value
Heart rate	58.97 (36, 74.12)	59.8 (14, 178)	0.46
PR Interval	62.26 (49.95, 85.12)	57.58 (22.55, 67.13)	0.73
QRS Interval	30.31 (21.03, 44.8)	36.2 (22.55, 67.13)	0.94
QT Interval	227.9 (127.1, 309.5)	206.3 (89.6, 458.7)	0.10

Table 4-1. There are no electrophysiological differences between wild-type and *kcnh6a*^{tb218} mutant adult fish. For each trait, the mean and range values in milliseconds are listed for wild-type fish and *kcnh6a*^{tb218} mutant fish. Each *P*-value was determined using a linear model where each group was analyzed and type, body weight, body length, body width were all adjusted for as covariates and date of ECG was included as a random effect: lmer(trait) ~ group + type + body weight + body length + body width + sex + (1 | date of ECG). $n =$ 49; 44 *kcnh6a*^{tb218} mutants, 5 wild-type fish. A P-value < 0.05 was considered statistically significant.

Parameters and Measurements	Mean (range) wild-type	Mean (range) *kcnh6a*^{tb218}	*P*-value
AV Measurements			
Early (E) Diastolic Filling (mm/s)	20.69 (11.28-30.08)	21.55 (-33.84-40.01)	0.502
Late (A) Diastolic Filling (mm/s)	85.04 (63.92-116.6)	116.8 (41.36-186.8)	0.922
E/A	0.2525 (0.15-0.4118)	0.2201 (-0.2368-0.4545)	0.663
Velocity Time Integral (mm)	6.691 (5.076-9.343)	8.733 (4.775-12.28)	0.681
IVCT (ms)	37.67 (23.33-55)	38.57 (20-50)	0.973
IVRT (ms)	52.67 (23.33-100)	65.24 (30-105)	0.665
BV Measurements			
Heart Rate (bpm)	107.2 (89.22-128.3)	100.8 (81.19-115.9)	0.51
BV Mean Velocity (mm/s)	-43.74 (-65.66--23.84)	-48.44 (-78.48--20.91)	0.828
BV Peak Velocity (mm/s)	-67.39 (-105.3--34.36)	-78.42 (-124.5--32.01)	0.826
Velocity Time Integral (mm)	8.294 (4.773-11.82)	10.44 (4.147-17.71)	0.741
Ventricular Ejection Time (ms)	157.8 (145-175)	180.7 (150-255)	0.368
Ventricular and BA Measurements			
Systolic Area (mm^2)	0.2803 (0.1862-0.4557)	0.3428 (0.1896-0.7017)	0.397
Diastolic Area (mm^2)	0.4286 (0.2765-0.7521)	0.5434 (0.3001-1.094)	0.517
Systolic Volume (mm^3)	0.1091 (0.05622-0.2236)	0.1525 (0.05478-0.4315)	0.421
Diastolic Volume (mm^3)	0.2072 (0.1085-0.4824)	0.2918 (0.1157-0.9241)	0.427
BA Diameter (mm)	0.4966 (0.3902-0.6666)	0.4974 (0.2774-0.7889)	0.639
Stroke Volume (mm^3)	0.09811 (0.03831-0.2588)	0.1393 (0.04042-0.4926)	0.393
Ejection Fraction	47.52 (15.35-60.41)	47.76 (19.15-66.61)	0.884
Fractional Shortening	16.31 (-0.9625-30.97)	21.8 (7.068-42.81)	0.857
Tei Index	0.5729 (0.4-0.871)	0.61 (0.28-1.033)	0.826
Cardiac Output (mm^3/min)	10.86 (4.257-33.22)	13.64 (4.151-39.99)	0.363

Table. 4-2. There are no anatomical differences between wild-type and *kcnh6a*^{tb218} mutant adult fish as determined by echocardiography. For each trait, the mean and range values in the respective units are listed for wild-type fish and *kcnh6a*^{tb218} mutant fish. Each *P*-value was determined using a linear model where each group was analyzed and type, body weight, body length, body width were all adjusted for as covariates and date of echocardiography was included as a random effect: lmer(trait) ~ group + type + body weight + body length + body width + sex + (1 | date of echocardiography), $n = 49; 44$

kcnh6a^{tb218} mutants, 5 wild-type fish. A *P*-value < 0.05 was considered statistically significant.

Measurements	Mean (range) for wild-type	Mean (range) for *kcnh6a*^{s290}	*P*-value
Heart rate	43.82 (21, 78)	61.13 (18, 178)	0.12
PR Interval	57.92 (14.6, 71.68)	71.24 (47.13, 109.76)	0.08
QRS Interval	31.14 (14.54, 53.2)	47.14 (19.04, 78.10)	**0.00018**
QT Interval	192.4 (109.6, 283.3)	263 (164.6, 401.5)	**0.0025**

Table. 4-3. *kcnh6a*^{s290} adult zebrafish have longer QRS and QT intervals compared to wild-type fish. For each trait, the mean and range values in milliseconds are listed for wild-type fish and *kcnh6a*^{s290} mutant fish. Each *P*-value was determined using a linear model where each group was analyzed and type, body weight, body length, body width were all adjusted for as covariates and date of ECG was included as a random effect: lmer(trait) ~ group + type + body weight + body length + body width + sex + (1 | date of ECG), n = 51; 33 *kcnh6a*^{s290} mutants, 18 AB fish. A P-value < 0.05 was considered statistically significant.

Parameters and Measurements	Mean (range) wild-type	Mean (range) *kcnh6a*^{s290}	*P*-value
AV Measurements			
Early (E) Diastolic Filling (mm/s)	13.95 (7.52-26.32)	10.31 (7.52-15.57)	0.533
Late (A) Diastolic Filling (mm/s)	116.8 (60.16-175.5)	132.1 (67.68-240.6)	0.427
E/A	0.1254 (0.04545-0.2105)	0.0898 (0.03125-0.2222)	0.906
Velocity Time Integral (mm)	9.017 (3.471-18.37)	8.312 (3.741-13.25)	**0.0267**
IVCT (ms)	28.8 (20-40)	27.78 (15-36.67)	0.281
IVRT (ms)	71.76 (40-125)	48.33 (20-100)	0.139
BV Measurements			
Heart Rate (bpm)	101.3 (60.2-146.5)	102 (63.38-126.5)	0.937
BV Mean Velocity (mm/s)	-60.86 (-97.39--30.61)	-62.71 (-100.4--24.94)	0.587
BV Peak Velocity (mm/s)	-96.2 (-157.3--44.17)	-99.07 (-170.4--31.9)	0.416
Velocity Time Integral (mm)	13.6 (5.931-21.24)	14.2 (6.208-21.86)	0.732
Ventricular Ejection Time (ms)	185.8 (135-225)	195.4 (130-260)	0.223
Ventricular and BA Measurements			
Systolic Area (mm^2)	0.3319 (0.1705-0.6561)	0.3454 (0.1522-0.5176)	0.593
Diastolic Area (mm^2)	0.4798 (0.1929-0.9675)	0.5033 (0.2048-0.7764)	0.401
Systolic Volume (mm^3)	0.1411 (0.04682-0.3415)	0.1566 (0.04182-0.2891)	0.792
Diastolic Volume (mm^3)	0.2438 (0.06133-0.6316)	0.2641 (0.06652-0.5324)	0.421
BA Diameter (mm)	0.504 (0.2486-0.7224)	0.5256 (0.3414-0.7961)	0.889
Stroke Volume (mm^3)	0.1028 (0.01395-0.3272)	0.1075 (0.008745-0.2685)	0.257
Ejection Fraction	39.77 (10.54-55.66)	39.56 (11.71-65.12)	0.442
Fractional Shortening	17.38 (-1.631-30.85)	19.44 (4.694-32.98)	0.954
Tei Index	0.5695 (0.2667-0.8621)	0.3926 (0.2143-0.6944)	0.0555
Cardiac Output (mm^3/min)	10.62 (0.8396-33.81)	10.91 (0.9464-30.27)	0.26

Table 4-4. *kcnh6a*^{s290} adult zebrafish have longer velocity time integrals through the atrioventricular valve (AV VTI) compared to wild-type fish. For each trait, the mean and range values in the respective units are listed for wild-type fish and *kcnh6a*^{s290} mutant fish. Each *P*-value was determined using a linear model where each group was analyzed and type, body weight, body length, body width were all adjusted for as covariates and date of echocardiography was included as a random effect: lmer(trait) ~ group + type + body weight + body length + body width + sex + (1 | date of echocardiography), $n = 51$;

33 *kcnh6a*^{s290} mutants, 18 AB fish. A *P*-value < 0.05 was considered statistically significant.

Chapter 5: *ROBO4* mutations predispose individuals to bicuspid aortic valve and thoracic aortic aneurysm

5.1 Introduction

Bicuspid aortic valve (BAV) is the most common congenital heart defect, with a population incidence of 1-2%(Fedak et al., 2002; Mack & Silberbach, 2000; Ward, 2000) and a strong association with ascending aortic aneurysm (AscAA) (Tadros, Klein, & Shapira, 2009). BAV/AscAA shows autosomal dominant inheritance with incomplete penetrance and male predominance. Fewer than 1% of cases of nonsyndromic BAV with and without AscAA can be attributed to mutations in known disease genes (e.g. *NOTCH1*, *SMAD6*) (Cripe et al., 2004; Garg et al., 2005; McKellar et al., 2007; Tan et al., 2012), frustrating the development of robust pathogenic models and therapeutic strategies. We report the identification of mutations in *ROBO4*, encoding a factor known to contribute to endothelial performance, that segregate with disease in two families. Additional targeted sequencing of *ROBO4* identified enrichment for rare variants in individual BAV/AscAA probands compared to unrelated controls. Targeted silencing of *ROBO4* or expression of mutant ROBO4 in endothelial cell lines imposes relevant functional deficits, including impaired barrier function, and a synthetic repertoire highly suggestive of endothelial-to-mesenchymal transition (EnMT); concordant findings are observed in patients and animal models with BAV/AscAA-associated phenotypes that are deficient for ROBO4. These data identify a novel etiology for a common human disease phenotype and focus attention on endothelial cell biology.

Kindreds segregating BAV/AscAA often exhibit wide variation in cardiovascular manifestations between related affected individuals, including complete non-penetrance (skewed toward females), isolated BAV, isolated AscAA, and variable location of the site of ascending aortic dilatation including isolated aortic root aneurysm (AoRA), or more distal ascending aortic aneurysm (DAscAA; collectively AscAA) (Clementi, Notari, Borghi, & Tenconi, 1996; Huntington, Hunter, & Chan, 1997; Loscalzo et al., 2007; Mckusick, Logue, & Bahnson, 1957). This observation suggests that BAV and AscAA are both variably penetrant primary manifestations of the same underlying gene defect(s). While enrichment for BAV can be seen in syndromic presentations of thoracic aortic aneurysm (e.g. Loeys-Dietz syndrome caused by mutations in genes encoding primary effectors of the transforming growth factor-β (TGFβ) signaling pathway), isolated DAscAA is exceedingly rare in these conditions suggesting a mechanistic distinction for nonsyndromic BAV/AscAA (Isselbacher, 2005; Van Hemelrijk, Renard, & Loeys, 2010; Williams et al., 2007). The genetic etiology and molecular pathogenesis of nonsyndromic BAV/AscAA remains largely elusive despite intensive effort. Likely obstacles to progress include extreme locus heterogeneity and the confounding influence of incomplete penetrance, sex bias, and environmental and/or genetic modification of disease onset and severity. In this study, we sought to identify genes responsible for nonsyndromic BAV/AscAA using whole exome sequencing (WES) and a familial segregation approach.

5.2 Results

5.2.1 *Enrichment for ROBO4 variants in patients with BAV and AscAA*

A total of nine patient families, 286 individual probands, and 193 unrelated controls without structural heart disease were enrolled in our whole exome sequencing (WES) initiative. In one large family (Family 1), eight individuals showed AoRA with or without DAscAA; two had associated BAV (Figure 5-1a).

Initial sequencing of a panel of genes implicated in familial thoracic aortic aneurysm (*ACTA2*, *FBN1*, *MYH11*, *MYLK*, *SMAD3*, *TGFBR1/2*) (Guo et al., 2007; Loeys et al., 2006; Pereira et al., 1997; van de Laar et al., 2012; L. Wang et al., 2010; Zhu et al., 2006) identified no mutations. WES in five of the affected family members identified a novel heterozygous mutation at the splice acceptor site of *ROBO4* exon 13 (c.2056+1G>T) (Figure 5-1a and Figure 5-2a). We confirmed that all eight affected family members carried the mutation (data not shown). Interestingly, seven of eight affected individuals were male including both with BAV. Two clinically unaffected female family members were heterozygous for the *ROBO4* splice-site mutation. Pathology from one family member with BAV revealed calcium deposition and valve thickening in association with a pronounced fibroproliferative process (Figure 5-2b). Amplification and sequencing of cDNA derived from patient and control fibroblasts showed that the splice-site mutation results in the skipping of the 108 base pairs encoding exon 13 of *ROBO4*, resulting in an in-frame transcript encoding a protein isoform missing 36 amino acids from the intracellular domain (Figure 5-1b). In a separate family (Family 2), WES revealed a heterozygous *ROBO4* missense variant (c.190C>T; p.Arg64Cys) in a woman with atrial septal defect (ASD) and aortic valve stenosis (AVS)

that required surgery and her son with ASD, BAV and significant AVS (Figure 5-1c and Figure 5-2c). This variant is exceedingly rare in population databases (ExAC frequency: 19/98,998), predicted deleterious by Polyphen and SIFT, and predicted to be among the 1% most deleterious substitutions possible in the human genome by the Combined Annotation Dependent Depletion (CADD) algorithm with a score of 21.6. The mutation changes an evolutionarily conserved residue in the Ig-like C2-type 1 extracellular domain of ROBO4. Of the 286 individual probands, four variants were determined to meet our *a priori* filtering to focus on all variants that are exceedingly rare (MAF<0.01%), or rare and predicted highly deleterious (MAF<0.1% and CADD>20) (Figure 5-1d and Table 5-1). All variants were confirmed by Sanger sequencing (data not shown).

We then sequenced an additional 441 probands with BAV/AscAA and 183 unrelated controls with echocardiogram-confirmed absence of structural cardiovascular disease for *ROBO4* mutations using the Haloplex target enrichment system. 99.47% of base positions exceeded 10x coverage for *ROBO4* in 90% of samples. We identified an additional seven BAV/AscAA probands harboring heterozygous *ROBO4* variants that fulfilled filtering criteria, including five missense mutations and one frameshift mutation (Figure 5-1d and Table 5-1). The missense mutations observed in the targeted sequencing cohort include an additional example of the p.Arg64Cys variant previously observed in Family 2 and two independent occurrences of an exceedingly rare (ExAC frequency: 4/110,004) and predicted highly deleterious (CADD score 21.3) variant (p.Asp622His) in two unrelated probands that were recruited at distant sites. In sum, among familial and individual probands (WES and targeted sequencing), 13/736 (1.77%) had a *ROBO4*

variant that passed *a priori* filtering constraints while one rare (absent in ExAC) missense mutation was observed among 376 rigorously phenotyped controls ($P < 0.05$).

5.2.2 *Cellular consequences of ROBO4 variants*

We next sought to elucidate the functional consequence of mutant *ROBO4* alleles. Histologic and immunofluorescent analyses were performed on resected ascending aortic aneurysm tissue from patient 1.II:1 and compared to normal ascending aorta derived from an age- and sex-matched control individual. ROBO4 was strongly expressed in endothelial cells in control aorta as evidenced by co-localization with platelet endothelial cell adhesion molecule 1 (CD31), but was diminished in the endothelium in the BAV/AscAA sample (Figure 5-3a, c). Both control and diseased aorta showed expression of ROBO4 in the intima in the absence of co-expression of α-smooth muscle actin (α-SMA), a vascular smooth muscle cell mesenchymal marker (Figure 5-3b). However, the aneurysm tissue uniquely showed infiltration of ROBO4+ cells into the aortic media with co-staining for α-SMA. Given expression of ROBO4 in the endothelial lining of the vasculature (Park et al., 2003) and its described role in establishing endothelial barrier function (Cai et al., 2015; Jones et al., 2008), we hypothesized enhanced vascular permeability in the ascending aorta of patients with BAV/AscAA. In keeping with this hypothesis, immunostaining for albumin was restricted to the endothelial surface in control aorta, but substantial penetration into the aortic intima was observed in patient tissue (Figure 5-3d). Histologic analyses showed a strong fibroproliferative response in the intima and superficial medial layer of patient aorta, as evidenced by increased cellularity and the accumulation of collagen upon Masson's trichrome staining. There

was also decreased elastin content and fragmentation and disarray of elastic fibers in the superficial media revealed upon Verhoeff-Van Gieson (VVG) staining (Figure 5-3e). Taken together, these data suggest that *ROBO4* mutations disrupt endothelial cellular performance and barrier function and contribute to pathological remodeling of the aortic media.

5.2.3 *In vitro functional analysis of ROBO4 variants*

To further address the hypothesis that *ROBO4* mutations directly influence endothelial cell performance, cultured human aortic endothelial cells (HAECs) were treated with short interfering RNA (siRNA) to silence ROBO4 expression or were transiently transfected with expression constructs that overexpress wild-type ROBO4, a form lacking exon 13, or a form with the p.Arg64Cys missense variant. In addition, HAECs with silenced endogenous ROBO4 expression by siRNA targeting sequence in exon 13 were transfected with the expression construct lacking exon 13 (termed SS-Alone) to assess the individual performance of the mutant form of ROBO4 seen in Family 1. The expression of wild-type and mutant *ROBO4* mRNA was assessed by quantitative reverse transcription-PCR (qRT-PCR) (Figure 5-4a). Either *ROBO4* silencing or expression of mutant forms resulted in loss of endothelial barrier function in a dextran permeability assay, with significantly worse performance of SS-Alone cells compared to cells lacking any ROBO4 expression (Figure 5-4b). These data document that ROBO4 is critical for endothelial barrier function, that *ROBO4* mutations have dominant-negative potential, and that isolated expression of selected mutant forms of ROBO4 can perturb cellular function. Potentially, mutant ROBO4 competes with other

members of the Roundabout family in the binding of SLIT ligands despite inability to propagate signal or (less likely) through neomorphic activity. Loss of barrier function associated with down regulation of expression of TJP1 and VE-cadherin mRNA and protein is indicative of loss of tight- and adherens-junction integrity, respectively (Figure 5-4c). Other phenotypes seen upon either *ROBO4* silencing or expression of mutant forms in HAECs included induction of expression of α-SMA and cellular elongation and invasion (Figure 5-5). Together, these results suggest that ROBO4 contributes to maintenance of endothelial identity and performance, and to the suppression of the transition to a more mesenchymal invasive character and synthetic repertoire. Both functions appear compromised upon expression of *ROBO4* alleles seen in patients with BAV/AscAA.

5.2.4 *Animal models have been used previously to study ROBO4*

Mommersteeg and colleagues described expression of ROBO1, ROBO2, SLIT2 and SLIT3 in or adjacent to the endocardial cushions and heart valves during mouse development(Mommersteeg, Yeh, Parnavelas, & Andrews, 2015). Targeted homozygous disruption of both *Robo1* and *Robo2* or *Slit3* resulted in highly penetrant septal defects with variably penetrant valve anomalies, including BAV. By report, ROBO4 expression was only observed in the coronary circulation and was therefore excluded from the study. In developing mice, we observed that ROBO4 was expressed in the endocardial layer of the cushions and delamination zones at embryonic day 11.5 (E11.5; Figure 5-6a). By E17, ROBO4 was detected in both the endothelial and interstitial cells of the developing aortic valve and endothelial cells of the proximal aorta (Figure 5-6a, b). At 5 weeks after

birth, ROBO4 was localized to the endothelial layer of the ascending aorta and expression was sustained throughout postnatal development (Figure 5-6b). Previous studies in zebrafish demonstrated robo4 expression in the developing vasculature beginning at the 19-somite stage and continuing in the intersomitic vessels through 29 hours post-fertilization(Bedell et al., 2005). In normal adult human ascending aorta, ROBO4 is expressed in endothelial and intimal cells (Figure 5-3 and Figure 5-6c). Together, these results confirm expression of ROBO4 in cells relevant to the pathogenesis of BAV/AscAA.

5.2.5 *Loss-of-function robo4 zebrafish demonstrate defects in cardiac function*

Next, functional evaluation of the *ROBO4* ortholog was conducted in zebrafish (*Danio rerio*). Using CRISPR/Cas9 engineering technology, we established a mutant zebrafish line harboring a seven bp deletion in exon 6 of the endogenous robo4 gene (*robo4*$^{\Delta 7}$; Figure 5-7a). This mutation establishes a frameshift resulting in the genesis of a premature termination codon. We confirmed nonsense mediated mRNA decay of the mutant transcript by qRT-PCR, demonstrating a significant reduction in robo4 RNA in both *robo4*$^{\Delta 7}$ heterozygote and homozygote zebrafish (Figure 5-7b). Gross examination of the mutant genotypes did not reveal an overt larval phenotype (Figure 5-8). Further, all genotypes were represented in appropriate Mendelian proportion into adulthood in crosses between mutant heterozygotes (Table 5-2). The absence of an overt embryonic phenotype or lethality prompted analysis in adult robo4 deficient zebrafish by echocardiography. Importantly, ≥26% of assayed mutant zebrafish (7/26 *robo4*$^{\Delta 7/+}$ and 4/15 *robo4*$^{\Delta 7/\Delta 7}$) displayed an aberrant echocardiogram characterized by regurgitation,

blood flow turbulence, or extreme outflow tract velocity (Figure 5-7c and Table 5-3). In wild-type zebrafish, color Doppler echocardiography shows a predictable flow pattern of inflow from the atrium into the ventricle (red) and outflow from the ventricle into the bulbus arteriosus (blue; Figure 5-7c). Heterozygote and homozygote *robo4*$^{\Delta 7}$ mutant fish displayed regurgitation of blood through the bulboventricular valve, as seen by aberrant flow via color Doppler (blue outflow immediately preceded by red backflow) and PW Doppler (negative outflow immediately preceded by positive backflow) (Figure 5-7c). Histological analysis demonstrated mutant fish have increased trabeculation of the apex of the ventricle as seen by H&E staining (Figure 5-7e). Masson's trichome stain revealed increased collagen (blue) in the bulbus arteriosus of mutant fish compared to wild-type fish, suggestive of elastin degradation and reduced integrity of the bulbus arteriosus (5-7e). In contrast, only four of 45 wild-type (AB and clutch mates) (8.9%) displayed any abnormal flow patterns of regurgitation/turbulence (Figure 5-7d). These data are statistically significant ($P < 0.05$). Thus, in zebrafish, loss-of-function mutations in *robo4* result in haploinsufficiency with incomplete penetrance for aberrant cardiac structure and function.

5.2.3 *Robo4 knockout mice show aberrant heart function*

We next examined the effect of loss of ROBO4 function in mice using the *Robo4*^{tm1Lex} model, which lacks exons 1 through 3. *Robo4* transcripts were not detected in homozygous *Robo4*$^{tm1Lex/tm1Lex}$ mice via qRT-PCR (Figure 5-9a). None of the evaluated heterozygotes (*Robo4*$^{tm1Lex/+}$) presented with any structural or functional abnormality. Homozygous *Robo4*$^{tm1Lex/tm1Lex}$ knockout mice exhibited a complex cardiovascular

phenotype that includes a combination of aortic valve thickening with or without BAV, aortic valve stenosis and/or regurgitation and/or AscAA. In general, these phenotypes were observed with low penetrance and male predominance. Overall, at 20 weeks of age, 5/28 (17.9%) male and 2/18 (11.1%) female *Robo4*$^{tm1Lex/tm1Lex}$ mice were affected compared to 0/22 (0%) and 0/19 (0%) *Robo4*$^{+/+}$ males and females, respectively ($P <$ 0.01; Figure 5-10). Additionally, one mouse with aortic regurgitation presented with a quadricuspid aortic valve (Figure 5-9b).

5.2.4 *Generation of a mutant mouse with splice site mutation from Family 1*

We next sought to evaluate the *in vivo* consequence of the splice mutation (c.2056+1G>T) that we had observed in Family 1 by establishing a knock-in mouse line harboring a mutation (*Robo4*^{Skip13}) at the splice donor site in intron 13 of *Robo4* (c.2089+1G>T) (Figure 5-11a). Sanger sequencing of cDNA amplicons spanning exons 11-14 using mRNA derived from the ascending aorta of targeted animals revealed either in-frame skipping of exon 13 (Exons 12/14) or inclusion of exon 13 with activation of a cryptic splice donor in intron 13 (Figure 11b, c). Using TaqMan™ probes specific to individual exons or splice junctions we determined that wild-type mice show 100% normal splicing (Exons 12/13/14). Representation of Exons 12/13/14, Exons 12/13+Intron 13 and Exons 12/14 transcripts was ~50%, 28% and 22% or ~0%, 55% and 45% in *Robo4*$^{+/Skip13}$ or *Robo4*$^{Skip13/Skip13}$ animals, respectively (Figure 11d). We conclude that the *Robo4*^{Skip13} mutation alters pre-mRNA splicing with significant representation of mature mRNA lacking exon 13.

5.2.5 *Mice with the Robo4 splice site mutation show abnormal heart function*

Like the knockout mice, *Robo4*^{Skip13} mice presented with an incompletely penetrant complex cardiovascular phenotype that included aortic valve defects and aortic valve dysfunction and AscAA. At 20 weeks, 1/31 (3.2%) *Robo4*$^{Skip13/+}$ and 4/35 (11.4%) *Robo4*$^{Skip13/Skip13}$ male mice were affected compared to 0/18 *Robo4*$^{+/+}$ mice ($P < 0.05$; Figure 5-12).

5.3 Discussion

This study demonstrates that heterozygous mutations in *ROBO4* are sufficient to cause a nonsyndromic presentation of BAV/AscAA. The distribution of expression of ROBO4 in both the developing valve and the ascending aorta is consistent with the view that BAV and aortic aneurysm present as independent primary manifestations of the same underlying gene defect, a concept further supported by the presence of either BAV/AscAA, isolated BAV, or isolated AscAA in family members segregating the same *ROBO4* mutation. This study highlights many obstacles in the elucidation of etiologies for BAV/AscA. These include a relatively low frequency for involvement of any specific disease gene (also evident for *NOTCH1* and *SMAD6*), extreme locus heterogeneity, functional redundancy within relevant pathways, low penetrance with sex bias, and finally, the lack of signature for loss-of-function intolerance which is likely related to both the penetrance issue and to later onset of the phenotype and hence minimal, if any, impact on reproductive fitness. This study focuses attention on endothelial cell biology in BAV/AscAA, with impairment of barrier function and/or dysregulation of mesenchymal transition potentially contributing to disease expression. Interestingly, prior work has

suggested descriptive association between BAV/AscAA and an EnMT-like phenotype in the aortic wall (Maleki et al., 2016) and decreased mesenchymal potential of endothelial cells derived from such patients (Kostina et al., 2016), but neither study had defined the etiology or mechanism for these findings. Given prior data that link NOTCH signaling, enhancement of TGF-β, bone morphogenetic protein signaling, or suppression of signaling by SMAD6 to the induction of EnMT (Gonzalez & Medici, 2014), our findings provide further incentive to interrogate altered mesenchymal transition as a pathogenic driver and a therapeutic target in BAV/AscAA.

5.4 Methods

5.4.1 ***Study participants***. Affected individuals were recruited from the Connective Tissue Clinic at Johns Hopkins Hospital (H.C.D.), Duke University (G.C.H.), Radboud University Hospital/Antwerp University Hospital (B.L.L.), Centre Hospitalier Universitaire Sainte-Justine (G.A.), Karolinska University Hospital (P.E.), University of Luebeck (S.A.M.), Sickkids Hospital (S.M.), and Erasmus University Medical Center (M.W.). All skin biopsies and research protocols were collected in compliance with the Institutional Review Board at each respective institution after informed consent was obtained. Echocardiograms were performed and interpreted as previously described (Brooke et al., 2008).

5.4.2 ***Whole exome sequencing.*** Genomic DNA was extracted from peripheral blood lymphocytes using standard protocols. DNA fragmentation was performed using a Covaris S2 system, and exon capture was performed using the Agilent SureSelect 38 Mb Human All Exon Target Enrichment system. DNA sequencing was performed on an Illumina Genome Analyzer IIx instrument with using standard protocols for 75 base pair paired-end runs.

5.4.3 ***Bioinformatics analysis.*** Reads were mapped to the human reference genome (UCSC hg19) using the Burrows-Wheeler Aligner (BWA) and a variant list created using SAMtools, which were annotated using ANNOVAR (Li et al., 2009; Li & Durbin, 2009; K. Wang, Li, & Hakonarson, 2010). Local realignment and recalibration of base call quality scores was performed using the Genome Analysis Toolkit (GATK) (DePristo et

al., 2011; McKenna et al., 2010). Duplicates were identified using Picard. We selected for rare variants (dbSNP, exome variant server, ExAC) and focused only on exonic non-synonymous, splice-site and insertion and/or deletion (indel) variants. Variants were viewed directly using the Integrated Genome Viewer (IGV) and excluded if reads were only present in one direction, if ambiguously mapped reads were present, or if an indel occurred within 3 base pairs of the end of the read (Robinson et al., 2011).

5.4.4 ***Mutation validation and Sanger sequencing of candidate genes.*** Bidirectional Sanger DNA sequencing assays were performed using primers designed 60–120 base pairs from the variants or intron-exon boundaries to confirm candidate variants or sequence candidate genes. PCR was performed using a DNA Engine Dyad thermal cycler (Bio-Rad). Phusion Flash High Fidelity PCR Master Mix was used in accordance with the manufacturer's instructions for each primer set (Thermo Scientific). Cycle sequencing was performed using the BigDye Terminator v3.1 kit and an ABI 3730xl DNA Analyzer in accordance with the manufacturer's instructions (Life Technologies). Samples were purified using the QIAquick PCR Purification kit (Qiagen).

5.4.5 ***Targeted sequencing.*** Enrichment for all exons of *ROBO4*, including ±10 nucleotides of adjacent intronic sequences, was performed with a custom Haloplex target enrichment kit per instructions of the manufacturer (Agilent Technologies, USA). Probe design covered a theoretical 99.7% of the complete target region. Pooled samples were sequenced either on a HiSeq 2500 (Illumina, USA) with 2x150 base pair reads or on a HiSeq 1500 (Illumina, USA) with 2x100 base pair reads.

5.4.6 ***Cell culture and transfection.*** Primary human dermal fibroblasts were derived from forearm skin biopsies from one control individual, a control cell line (ATCC), or a single proband. Cells were cultured in DMEM supplemented with 10% FBS in the presence of antibiotics and were passaged at confluence. Human aortic endothelial cells (HAEC) (Promocell, Heidelberg) were cultured in EGM2 BulletKi (Lonza, CC-3156/CC-4176) and used for experiments at P2-P4. For transfection experiments, cells were seeded at 60-70% confluence. *ROBO4* constructs were mixed with Lipofectamine 3000 (Invitrogen), diluted in EGM2 (without antibiotics) (for constructs, see Table 5-4), and treated for 24 hours. HAEC media was then replaced and allowed to culture for an additional 48 hours. Transfection efficiency was measured via qRT-PCR and immunofluorescence.

5.4.7 ***RNA isolation and qRT-PCR.*** For human and mice samples, RNA extractions were performed using a Qiagen total RNA purification kit (Qiagen) and RNA was reverse transcribed to cDNA using the SuperScript III RT-PCR kit with oligo(dT) primer (Invitrogen). Real-time PCR experiments were conducted using the FAM-MGB PCR system (Applied Biosystems) on QuantStudio 7 Real-Time ABI 384 cycler, with 40 cycles per sample. Primers were normalized to 18S or GAPDH. The following pre-validated probes were used for mRNA analysis: H200219408_m1 (*Robo4*), Hs01551861_m1 (*TJP1*), Hs00901463_m1 (*CDH5*), Hs00426835_g1 (*ACTA2*), Hs03003631_g1 (18S), and Hs02758991_g1 (*GAPDH*) (Life technologies). For zebrafish, RNA extracts were prepared from isolated wild-type or *robo4* knockout adult hearts using RNA TRIzol (Ambion) and cDNA was synthesized using SuperScript III

Reverse Transcriptase kit (ThermoFisher Scientific). Two sets of specific primers spanning the junctions of exons 9 and 10 and of exons 16 and 17 were designed (see Table 5-5). All qRT-PCR data was obtained using the ViiA 7 Real-Time PCR System (Applied Biosystems) and SYBR Green PCR Mix (ThermoFisher).

5.4.8 ***Antibody staining.*** Samples were fixed in 4% paraformaldehyde overnight at 4°C. Samples were then washed for 15 minutes on a rocker 3 times with PBS, permeabilized with 0.2% Triton-X 100 (VWR International, Radnor, PA) for 10 minutes, and washed another 3 times with PBS. Samples were incubated overnight at 4°C in a 1% BSA (Rockland Immunochemicals) blocking solution followed by another 4°C overnight incubation with ROBO4 (Abcam, ab103674), ROBO4 (Santa Cruz, sc-46497), CD31 (Biocare Medical, CM303A), PECAM1 (Santa Cruz, sc-1506), CDH5 (Santa Cruz, sc-28644), TJP1 (Santa Cruz, sc-8146), ACTA2 (Abcam, ab7817), or ALB (Santa Cruz, sc-46293). After 3 washes for 15 minutes with PBS, samples were exposed to Alexa Fluor 488 or 568 conjugated (Invitrogen), species-specific secondary antibodies at 1:100 in 1% BSA for 2 hours at room temperature. Three more washes with PBS for 15 minutes were followed by incubation with either DRAQ5 (far-red) nuclear stain or DAPI (UV) nuclear stain (Enzo Life Sciences) at 1:1000.

5.4.9 ***Permeability assay.*** Permeability assays were performed as described previously (Anderl, Ma, & Armstrong, n.d.). HAECs were utilized at or before passage six. Cells were detached using 0.05% trypsin-EDTA, pelleted, then re-suspended in a growth medium to a concentration of 0.5-1X at 10^6 cells/mL. Dry collagen pre-coated porous

inserts were rehydrated for 15 minutes in a growth medium prior to cell seeding (1.0um pores, EMD Millipore). HAECs were seeded in 200 µL of growth medium per 24 well insert. 500 µL were added to each receiver plate well. HAECs were cultured in a 37°C/5% CO_2 tissue culture incubator for 72 hours to allow for a monolayer formation. Following endothelial monolayer formation, growth medium was carefully removed. This was replaced with medium containing different *ROBO4* constructs (see Table 5-4). Samples were returned to 37°C incubation for 24 hours. Afterwards, the treatment medium was carefully removed. A high molecular weight FITC-dextran solution (40kDA) was created by 1:40 dilution in a growth medium and added at 150 µL. Growth medium was added to each receiver plate well at 500 µL (24-well). The FITC-dextran permeated the monolayers for 2 hours. The inserts were removed from the receiver wells to stop permeation. The medium in the receiver wells was then thoroughly mixed and 100 µL was removed from each well to a black 96-well opaque plate for fluorescence measurement. Permeability was quantified on a Synergy-II fluorescent plate reader (Biotek) via fluorescence at 485nm excitation/535nm emission wavelengths (1 second fluorescent count time). The endothelial monolayer was stained after completion of FITC-dextran permeability testing for subsequent confocal imaging.

5.4.10 ***Cell morphology assay.*** Cell shape was calculated as previously described using ImageJ (https://imagej.nih.gov/ij/plugins/circularity.html) (Gould, Sinha, et al., 2012). Cell shape changes were automatically tracked over subsequent images, and quantified as a cell circularity index (CI=4*Pi*(Area/Perimeter2)). A circularity value of 1.0 indicates

a perfect circle. As the value approaches 0.0, it indicates an increasingly elongated polygon.

5.4.11 ***Endothelial aggregate invasion assay.*** For invasion assays, cells were re-suspended in culture media and allowed to aggregate overnight in hanging drop culture (20 μL; 20,000 cells). The aggregates were then placed on the surface of neutralized type I collagen hydrogels (1.5 mg/mL) as previously described (Chiu, Norris, Mahler, Recknagel, & Butcher, 2010) and allowed to adhere for 2 hours before adding treatments. Cultures were then transfected for 24 hours with the *ROBO4* constructs (see Table 5-4) and maintained for another 72 hours. Cell invasion was quantified manually at a 50-μm depth into the gel and normalized to control.

5.4.12 ***Scratch assay.*** Migratory ability was tested as described previously (Liang, Park, & Guan, 2007). Briefly, cells were cultured to confluency and then transfected for 24 hours with the *ROBO4* constructs. A scratch was then introduced using a 200-μl pipette tip. The cells were then incubated at 37°C and observed at 24 hours. Differences in filling in the scratch were observed to establish the capability of cellular migration.

5.4.13 ***Proliferation assay.*** 5-bromo-2′-deoxyuridine (BrdU) incorporation was used to detect proliferating cells as described previously (Gould, Chin, et al., 2012). Cultures were transfected for 24 hours with the *ROBO4* constructs (see Table 5-4). BrdU labeling reagent (Invitrogen) was added to the culture media for 12 hours after treatment. After 24 hours, cells were fixed and targeted with a monoclonal Anti-BrdU Alexa Fluor 488

conjugate (PRB-1, Invitrogen) while total DNA was counterstained using a DAPI dye. Positive fluorescent areas for each cell were measured using ImageJ and normalized by cell nuclei.

5.4.14 ***Zebrafish and mouse maintenance.*** Adult AB and *robo4*$^{\Delta 7}$ mutant zebrafish lines were maintained in system water according to standard methods (Westerfield, 2007). Mice were housed in the Johns Hopkins University School of Medicine East Baltimore campus. All strains were maintained on a mixed C57BL/6J and F129/SVE background. All zebrafish and mice upkeep and experimental procedures were in accordance with the ethical permits set by the Johns Hopkins Institutional Animal Care and Use Committee.

5.4.15 ***Generation of robo4 knockout line by CRISPR/Cas9.*** We designed a single guide RNA (gRNA, see sequences in Table 5-5) to target the *robo4* gene (gRNA^{robo4}), using ZiFit (Sander et al., 2010; Sander, Zaback, Joung, Voytas, & Dobbs, 2007). Cas9 RNA was synthesized from linearized pCS2-nls-zCas9-nls (AddGene, no. 47929) (Jao, Wente, & Chen, 2013). We injected 100 ng/nL of gRNA and 300 ng of Cas9 in a 5-μL solution into 1-cell wild-type (AB) zebrafish embryos and raised them to maturity (F_0). To identify fish capable of germline transmission, we crossed F_0 males with AB females. Germline transmission was confirmed by Surveyor Assay (IDT) in pooled F_1 embryos (n = 50) followed by Sanger sequencing. Heterozygous F_1 adults with the same seven base pair deletion were inbred to establish the line (*robo4*^{jh176}). All subsequent generations were genotyped using primer set F2 and R2 (see Table 5-5).

5.4.16 ***Robo4 knockout mice and generation of Robo4 knock-in mice.*** *Robo4*^{tm1Lex} knockout mice were purchased through the mutant mouse resource and research centers supported by the NIH (MGI:5007309, Lexicon Pharmaceuticals). The mice were bred in a heterozygous state on a mixed background of 129S5/SvEvBrd and C57BL6/J. To generate *Robo4* knock-in mice, we targeted the *Robo4* locus using CRISPR/Cas9. Two single-guide RNA (sgRNA) sequences (see Table 5-6) were designed to target exon 13 of *Robo4* (NC_000074.5) using a gRNA CRISPR design tool (http://crispr.technology/) (Jaskula-Ranga & Zack, 2016). Neither gRNA was predicted to have any off-target effects. These oligonucleotides were cloned into a pX459 plasmid (Ran et al., 2013) (Addgene, no. 48139) and appended with a T7 promoter. The sgRNA was transcribed in vitro. The homology directed repair (HDR) template was purchased as a 4nm Ultramer (IDT, see Table 5-6). The sgRNA, Cas9 (TriLink BioTechnologies), and HDR were co-injected into C57BL/6J zygotes (Johns Hopkins University Transgenic Core). Pups (n = 41) were screened for locus editing by Sanger sequencing (IDT, see Table 5-6). Mice (*Robo4*^{Skip13}) were subsequently genotyped by Sanger sequencing (271 base pair amplicon). Mice were then crossed to a mixed background (129S5/SvEvBrd and C57BL6).

5.4.17 ***Zebrafish and Mice Echocardiography.*** For zebrafish, we used the Vevo 2100 Imaging System equipped with a 70 MHz ultrasound transducer (VisualSonics®, Toronto, ON, Canada). The zebrafish were anesthetized by placing the fish into a plastic cup filled with 100 ml of 168 μg/ml MS-222 (Tricaine methanesulfonate, Fluka Analytical). For mice, echocardiograms were undertaken on awake, unsedated mice using

the Vevo 2100 Imaging System (VisualSonics®, Toronto, ON, Canada) and a 40 MHz transducer. Echocardiographic recordings for the mice were taken using a parasternal long-axis or sagittal short axis view; 3 independent measurements of the maximal internal dimension at the sinus of Valsalva and ascending aorta were made and averaged. All data acquisition and measurements for mice and zebrafish were performed blinded to the genotype.

5.4.18 ***Statistical analysis.*** For experiments including multiple comparisons, *P* values refer to one-way ANOVA followed by Tukey's post-hoc test. For experiments including only one comparison, *P* values refer to unpaired two-tailed Student's *t*-test, two-tailed Welch's *t*-test, or two- or one-tailed Fisher's exact test. *P* values less than 0.05 were considered significant. Data are shown as mean ± standard error (SE) or standard deviation (SD).

5.5 Tables

Sample	Variant	Depth 1	Depth 2	Domain	Fusion pattern	Family history	ExAC	CADD
BAV/AscAA	c.C190T p.Arg64Cys	63	69	IG-L 1	L-R	Yes	19/98998	21.6
BAV/AscAA	c.C190T p.Arg64Cys	312	260	IG-L 1	L-R	N/A	19/98998	21.6
BAV/AscAA	c.G238A p.Ala95Thr	7	6	IG-L 1	R-N	No	5/117304	6.42
BAV/AscAA	c.C695T p.Thr232Met	42	36	/	R-L	Yes	10/121068	19.56
BAV/AscAA	c.T740C p.Val247Ala	1204	1187	/	L-R	N/A	1/121370	10.5
BAV/AscAA	c.A839C p.Tyr280Ser	590	469	FN1	R-N	N/A	5/117546	22
BAV/AscAA	c.T1233A p.His411Gln	31	30	FN2	R-N	Yes	Absent	0.002
Control	c.A1529T p.Asp510Val	69	51	/	N/A	N/A	Absent	11.6
BAV/AscAA	c.1601_1614del p.Gly534Glufs*49	124	114	/	N/A	Yes	Absent	N/A
BAV/AscAA	c.C1702T p.Arg568Ter	43	49	/	R-L	No	12/120920	N/A
BAV/AscAA	c.G1864C p.Asp622His	767	721	/	L-R	N/A	4/110004	21.3
BAV/AscAA	c.G1864C p.Asp622His	1300	1118	/	L-R	No	4/110004	21.3
BAV/AscAA	c.2056+1G>T	12	10	/	R-N	Yes	Absent	17.6
BAV/AscAA	c.G2245C; c.C2246T p.Ala749Leu	195	173	/	R-N	N/A	Absent	16.7

Table 5-1. *ROBO4* mutations are more frequent in cases than in controls. In the study, 13/736 (1.77%) of BAV/AscAA individuals were heterozygous for a rare and deleterious (MAF<0.1% and CADD>20 or MAF<0.01%) compared to 1/376 controls (0.27%). These data suggest enrichment for deleterious *ROBO4* variants in the patient cohort using a strict *a priori* filtering constraints (Fisher's exact test, two-tailed *P*-value, $n = 736$ cases, $n = 376$ controls, $*P = 0.0432$).

Genotype	Percentage at 24 h.p.f.
robo4$^{+/+}$	26.42% (n=28)
robo4$^{\Delta 7/+}$	50.94% (n=54)
robo4$^{\Delta 7/\Delta 7}$	22.64% (n=24)

Table 5-2. *robo4* mutant embryos survive in Mendelian ratios through gastrulation. Embryos were genotyped at 24 hours post-fertilization (h.p.f.) to confirm all genotypes survived through gastrulation at Mendelian ratios (n = 106, P = 0.8433, chi-squared test).

Parameters and Measurements	Mean for wild-type	Mean for *robo4*$^{\Delta 7}$	*P*-value
AV Measurements			
Early (E) Diastolic Filling (mm/s)	26.9	27.8	0.23
Late (A) Diastolic Filling (mm/s)	59.4	65.8	0.28
E/A	0.34	0.31	0.46
AV Mean Velocity (mm/s)	34.3	41.2	0.80
AV Peak Velocity (mm/s)	75.8	93.6	0.32
Velocity Time Integral (mm)	7.6	8.7	0.39
BV Measurements			
Heart Rate (bpm)	95	92.1	0.25
BV Mean Velocity (mm/s)	49.4	57.84	**0.031**
BV Peak Velocity (mm/s)	77.7	91.9	**0.046**
Velocity Time Integral (mm)	10.0	11.8	**0.03**
Ventricular Ejection Time (ms)	171.1	171.9	0.97
Ventricular and BA Measurements			
Systolic Area (mm^2)	0.30	0.42	0.34
Diastolic Area (mm^2)	0.41	0.58	0.14
Systolic Volume (mm^3)	0.12	0.20	0.29
Diastolic Volume (mm^3)	0.19	0.35	0.13
BA Diameter (mm)	0.52	0.58	0.59
Stroke Volume (mm^3)	0.071	0.14	0.15
Cardiac Output (mm^3/min)	6.4	12.4	0.14

Table 5-3. Parameters and measurements for wild-type and *robo4*$^{\Delta 7}$ mutants (heterozygotes and homozygotes). Comparison of physical parameters or measurements via echocardiography of *robo4*$^{\Delta 7}$ mutants without severe blood flow turbulence and wild-type fish (clutch mates or AB) determined significant differences between the two groups of fish (bolded). A linear mixed model estimated the effect of group on mutation status. Age, sex, body size parameters, and type were included as covariates with date of echocardiography as a random effect: lmer(trait) ~ group + type + body weight + body length + body width + age + sex + (1 | date of echo) (n = 82 total; 37 *robo4*$^{\Delta 7}$ mutants, 45 wild-type or AB fish). All statistical analyses were implemented in R version 3.2.3. AV:

atrioventricular valve, BV: bulboventricular valve, BA: bulbus arteriosus

Name (Abbreviation)	Construct
Control GFP plasmid (co-plasmid)	pCMV6-AC-GFP (Origene, PS100010)
Control siRNAs (co-siRNA)	siGENOME Non-Targeting siRNA Pool (Dharmacon, D-001206-13-50)
Global ROBO4 knockdown (siRNA)	siGENOME-*ROBO4* (Dharmacon, M-015216-00-0005)
Overexpression of ROBO4 wild-type plasmid (OE-WT)	*ROBO4*-GFP-pCMV6-AC-GFP (Origene, RG213730**)**
Targeted ROBO4 knockdown of exon 13 (siRNA-Ex13)	DsiRNA-*Robo4*-Ex13 (IDT, CUSTOM**)** Sense: AUAGAGGUUCCAAGAACCUUUCC AntiSense: UUUAUCUCCAAGGUUCUUGGAAAGGGU
Overexpression of ROBO4 cDNA plasmid without exon 13 (OE-SS)	*ROBO4*-GFP-pCMV6-AC-GFP (BLUE HERON, CUSTOM**)**
Overexpression of ROBO4 cDNA plasmid with p.Arg64Cys (OE-R64C)	*ROBO4*-GFP-pCMV6-AC-GFP (BLUE HERON, CUSTOM**)**

Table 5-4. ROBO4 constructs used in functional studies in cell culture and TaqMan™ probes for mRNA analysis.

robo4 primer	Forward	Reverse
1	CCAAACAACAAGGCCAAAAC	GCACTCCCAAAGAGTGGTCT
2	AACCCAGATCACAGTCTGCA	TACAAGAAGCTGTGCACTGG
3	TATCAGGTGTGGTGTGTGGA	TATGGATCGCTCTGGACACC
4	GGACAGAGCACATCCCATCA	TCCCATTCGCTGCAGTAAGA
robo4 CRISPR/Cas9 Target site	Oligonucleotide 1	Oligonucleotide 2
GGGCAGATACAGCTGCACAG	TAGGGCAGATACAGCTGCACAG	AAACCTGTGCAGCTGTATCTGC

Table 5-5. List of primers and oligonucleotide sequences used in the zebrafish study.

Robo4 Primer	Forward	Reverse
1	CCCTTCTAGAATTGCACCAAGC	ACGGATTCCAACCTGCTCAG
gRNA Target Site	gRNA 1	gRNA 2
Exon13	AAGAACCTTTCTCAAAGCCCAGG	CTCACTTCCCCACTCTCACCTGG
Homology Directed Repair Template	CCGGGGCAGCCACCCCATGGAAATCTGGGCCTGGGAGTTGGGAAGCAGAGCCTCCAAGAACCTTTCTCAAAGCCCAG**(T)**TGAGAGTGGGGAAGTGAGGGTAAGGCAGGTTTTCAGGTCCACCAGTCCAGGCCCTTCTTGGTTCTGCTATGGTGTG	

Table 5-6. List of primers and oligonucleotide sequences used in the mice study.

5.6 Figures

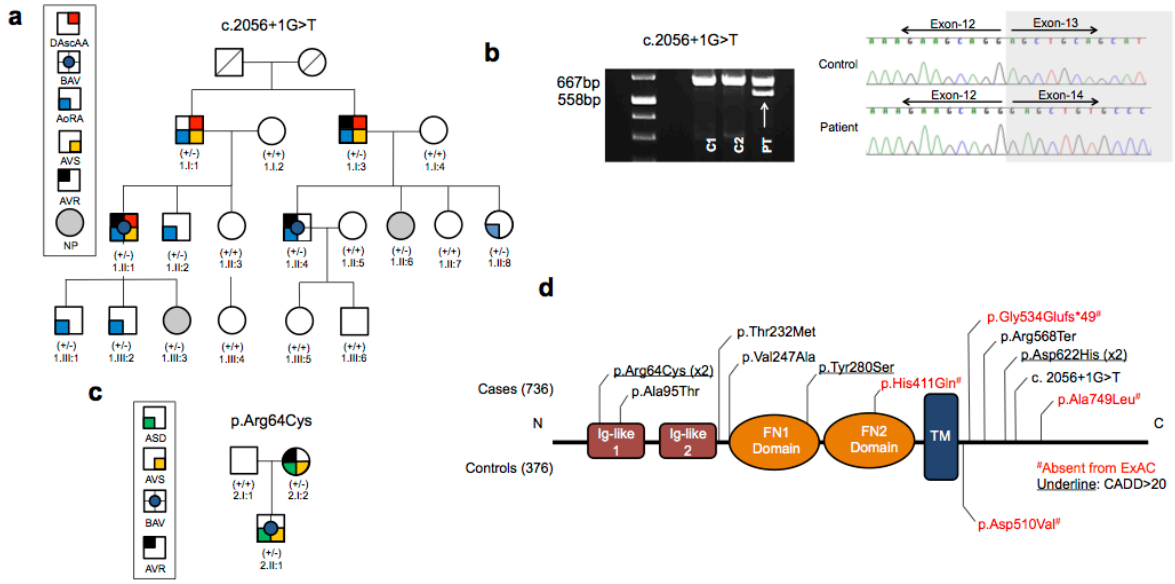

Figure 5-1. Identification of *ROBO4* variants segregating in families with bicuspid aortic valve and aortic aneurysms. (**a**) In this large family, eight individuals showed AoRA with or without DAscAA and two had associated BAV. Whole exome sequencing (WES) revealed segregation of a heterozygous obligate splice site mutation (c.2056+1G>T) in a multigenerational family. (**b**) cDNA amplicons spanning exons 11-14 were analyzed from patient (proband 1.II:4) and control fibroblasts. Sanger sequencing confirmed skipping of exon 13 (108 base pair). (**c**) A missense mutation (p.Arg64Cys) was observed in a small family. The missense mutation resides at the Ig-like C2-type-1 (extracellular domain). (**d**) Sequencing of 736 individuals with BAV/TAA and 376 controls. Thirteen rare mutations (MAF<0.1% with CADD>20 or MAF<0.01%) were identified in 736 patients and one in 376 controls. AscAA: ascending aortic aneurysm, BAV: bicuspid

aortic valve, AoRA: aortic root aneurysm, AVS: aortic valve stenosis, ASD: atrial septal defect, AVR: aortic valve replacement, NP: non-penetrant

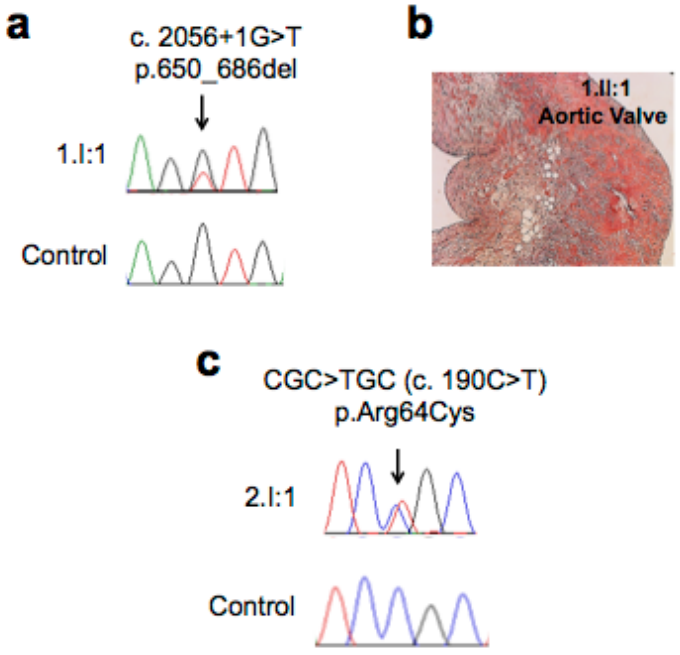

Figure 5-2. (**a**) Sanger sequencing verification of the heterozygous obligate splice site mutation (c.2056+1G>T) in Family 1. (**b**) H&E stain of the affected patient (1:II:1) aortic valve, *n* = 1. (**c**) Sanger sequencing verification of the missense mutation p.Arg64Cys in Family 2.

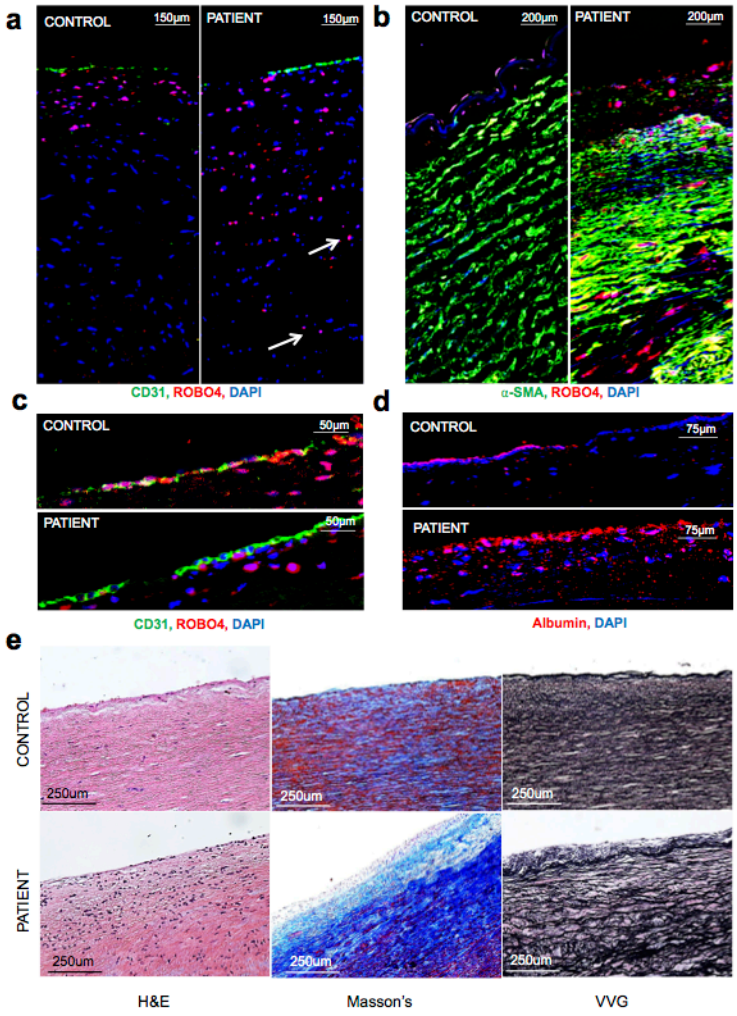

Figure 5-3. Evaluation of ascending aortic aneurysm tissue resected from patient 1.II:1, compared to an age- and sex-matched control. (a) Immunofluorescent staining of CD31 (green), ROBO4 (red), and DAPI (blue) at the intima-media interface. Arrows indicate ROBO4+ cells deep within the aortic media. (b) Immunofluorescent staining of α-SMA (green), ROBO4 (red), and DAPI (blue) at the intima-media interface. (c) Immunofluorescent staining of CD31 (green), ROBO4 (red), and DAPI (blue) at the endothelial layer. (d) Immunofluorescent staining of albumin (red) and DAPI (blue) at

the luminal surface. (e) Histological staining (H&E, Masson's, and VVG) of patient and control ascending aortic tissue. VVG: Verhoeff-Van Gieson

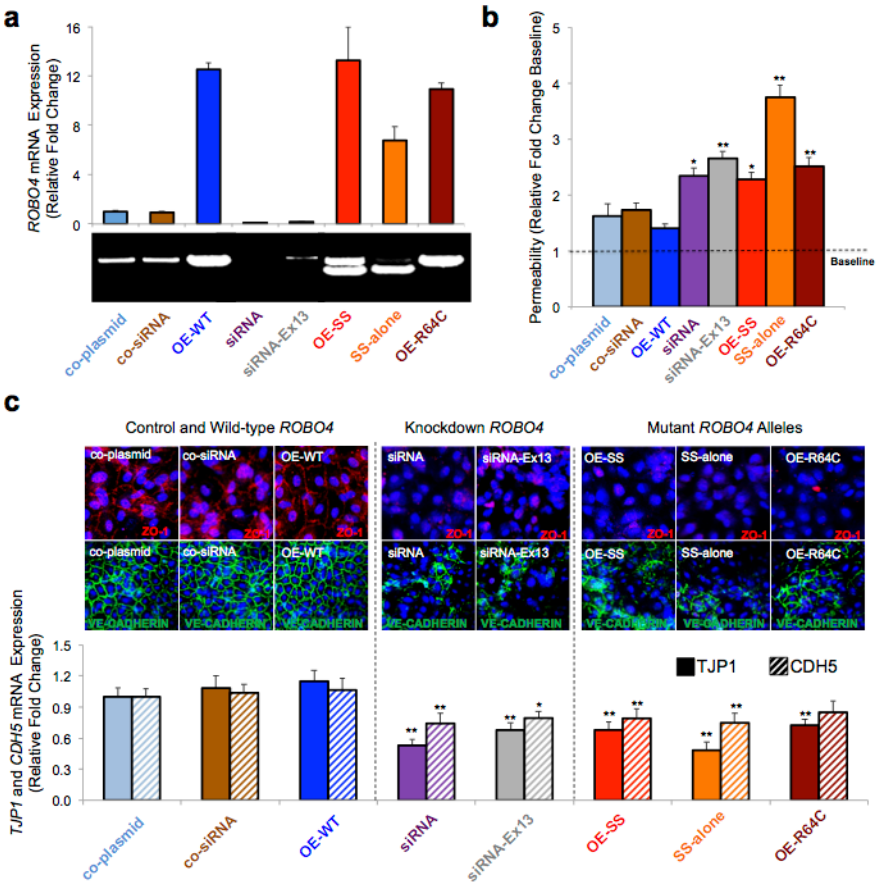

Figure 5-4. *ROBO4* mutant alleles impair endothelial barrier function. (**a**) HAECs were transfected with either co-plasmid (control GFP plasmid), co-siRNA (control siRNA), OE-WT (overexpression of ROBO4 wild-type plasmid), siRNA (global ROBO4 knockdown), siRNA-Ex13 (ROBO4 knockdown through targeting of exon 13), OE-SS (overexpression of ROBO4 cDNA plasmid without exon 13), SS-alone (overexpression of ROBO4 cDNA plasmid without exon 13 plus silencing of endogenous ROBO4 using siRNA targeting exon 13), OE-R64C (overexpression of ROBO4 cDNA plasmid with p.Arg64Cys) and *ROBO4* mRNA expression was quantified. (**b**) HAECs were cultured to confluency and a dextran permeability assay was used to assess the integrity of the endothelial barrier. Error bars show ± SE, $n = 6$. Asterisks signify significant differences

per one-way ANOVA with Tukey's Post-hoc, *$P < 0.05$, **$P < 0.01$. (**c**) Immunofluorescent staining of VE-cadherin (green), tight junction protein ZO-1 (red), and DAPI (blue). *TJP1* (encoding tight junction protein ZO-1) expression and *CDH5* (encoding VE-cadherin) expression were analyzed via qRT-PCR. For both **a** and **c**, error bars show ±SD, $n = 6$. Asterisks signify significant differences per a one-way ANOVA with Tukey's Post-hoc, *$P < 0.05$, **$P < 0.01$.

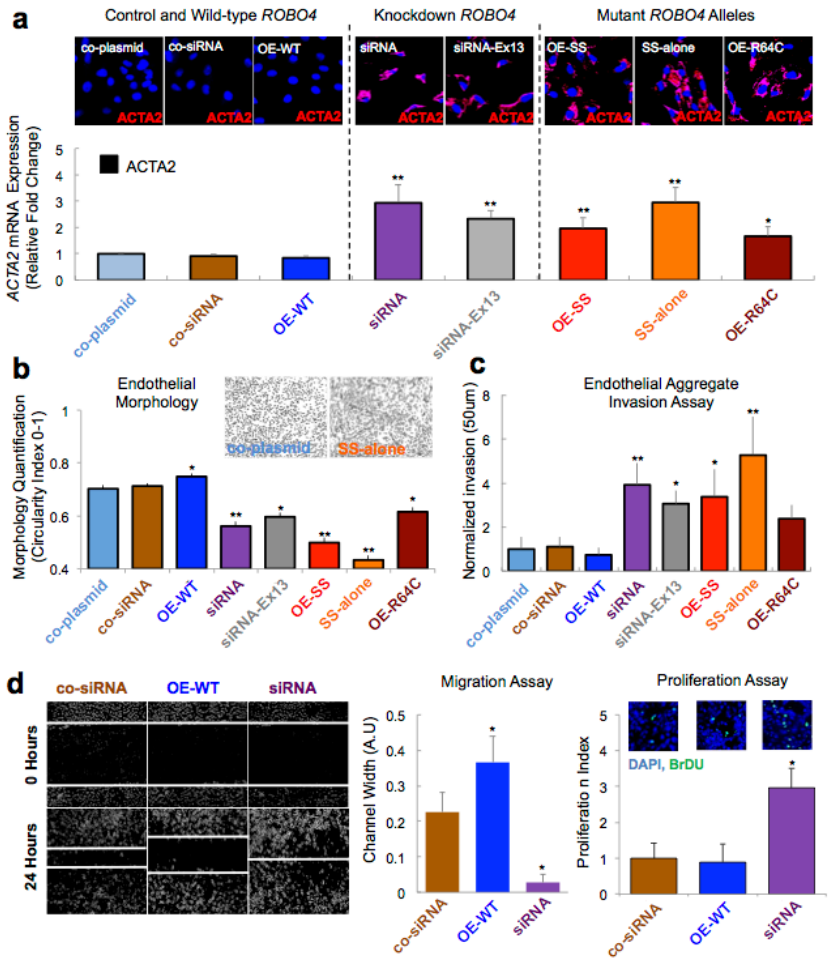

Figure 5-5. Cellular phenotypes observed in HAECs transfected with *ROBO4* mutant alleles or siRNA to silence ROBO4 expression. (**a**) HAECs were transfected with either co-plasmid (control GFP plasmid), co-siRNA (control siRNAs), OE-WT (overexpression of ROBO4 wild-type plasmid), siRNA (global ROBO4 knockdown), siRNA-Ex13 (ROBO4 knockdown through targeting of exon 13), OE-SS (overexpression of ROBO4 cDNA plasmid without exon 13), SS-alone (overexpression of ROBO4 cDNA plasmid without exon 13 plus silencing of endogenous ROBO4 using siRNA targeting exon 13), OE-R64C (overexpression of ROBO4 cDNA plasmid with p.Arg64Cys) and mRNA

expression levels for *ACTA2* (encoding α-smooth muscle actin; α-SMA) were quantified via qRT-PCR and immunofluorescence, respectively. Error bars show ± SD, $n = 6$. Asterisks signify significant differences per a one-way ANOVA with Tukey's post-hoc, * $P < 0.05$, ** $P < 0.01$. (**b**) Cellular morphology was captured via bright-field microscopy and quantified as a circularity index using ImageJ, $n = >200$ cells were assessed per condition. (**c**) Endothelial invasion was assessed using an endothelial aggregate invasion assay on collagen gels. (**d**) Migration and proliferation were measured using a scratch assay and 5-bromo-2′-deoxyuridine (BrDU) proliferation assay, respectively. For **b**, **c**, **d**, error bars show ± SE, $n = 3$. Asterisks signify significant differences per a one-way ANOVA with Tukey's post-hoc, * $P < 0.05$.

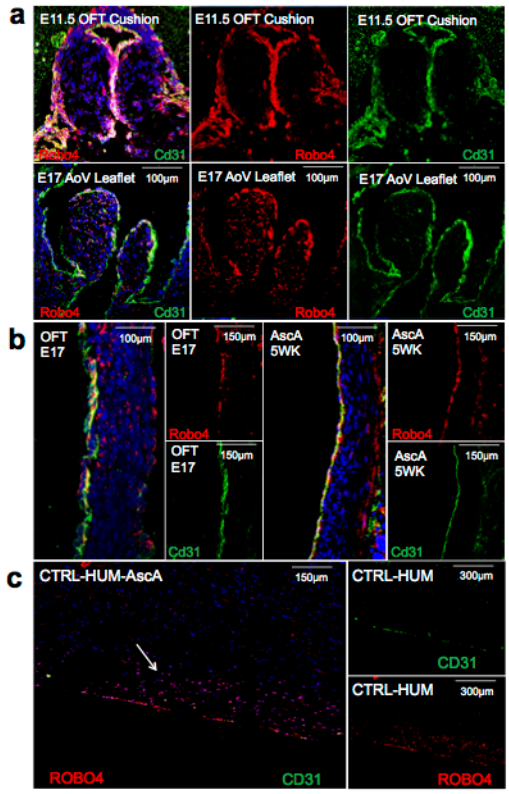

Figure 5-6. Immunofluorescent staining for ROBO4 in the developing murine outflow tract (OFT) and human adult ascending aorta. (a) Murine ROBO4 expression in the endothelial layer of the embryonic endocardial OFT cushions and the primordial aortic valve leaflets at E11.5 and E17, respectively. (b) Murine ROBO4 expression in the endothelium of the OFT (E17) and ascending aorta (5wk). (c) Human control ROBO4 expression in an ascending aorta. The arrow indicates ROBO4 expressing cells in the intima.

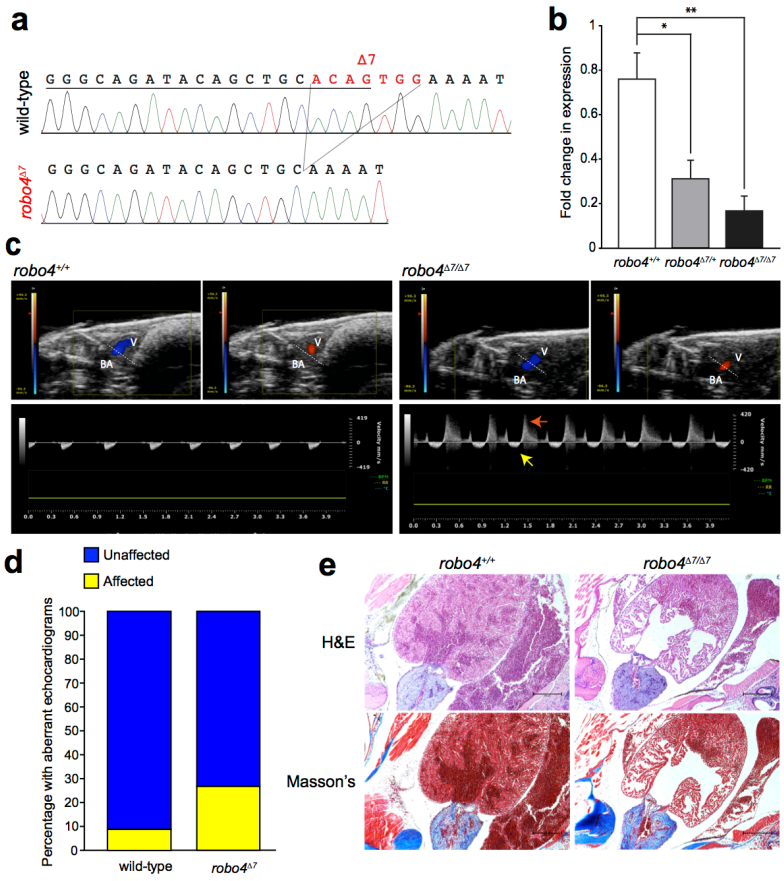

Figure 5-7. *robo4* deficiency results in aberrant blood flow in the adult zebrafish. (**a**) A mutant line for *robo4* was generated using CRISPR/Cas9. A seven-base pair deletion was induced in exon 6 ($robo4^{\Delta 7}$). (**b**) *robo4* expression was analyzed by qRT-PCR on 4 hearts per genotype and then averaged. Results are shown normalized to β-actin mRNA expression. Graph shows mean ±SE, $n = 4$ biological replicates per genotype run on the same plate. Asterisks signify significant differences per a two-tailed Welch's *t*-test, * $P < 0.05$; ** $P < 0.01$. (**c**) Representative color Doppler echocardiograms for wild-type zebrafish show blood flow during systole (blue) and during diastole (red). A representative pulsed wave Doppler image of a wild-type zebrafish shows normal flow pattern. Representative color Doppler echocardiograms for $robo4^{\Delta 7/\Delta 7}$ mutant zebrafish

show blood flow during systole (blue) and regurgitation (red) during diastole from the bulbus arteriosus (BA) into the ventricle (V). A representative pulsed wave Doppler image of *robo4*$^{\Delta 7/\Delta 7}$ zebrafish shows regurgitant flow through the ventriculo-bulbar valve (orange arrow). The white arrow marks normal flow through the ventriculo-bulbar valve. (**d**) Approximately 11/41 (26.8%) of *robo4*$^{\Delta 7}$ mutants (heterozygous and homozygous) exhibit aberrant echocardiograms with regurgitation or turbulence while only 4/45 (8.88%) of wild-type fish showed this phenotype. Statistical differences calculated per a Fisher's exact test, one-tailed *P*-value, $*P = 0.028$, $P < 0.05$ is considered statistically significant. (**e**) Histological staining (H&E and Masson's trichrome) of the ventricle and bulbus arteriosus for wild-type and *robo4*$^{\Delta 7/\Delta 7}$ zebrafish. V: ventricle, BA: bulbus arteriosus

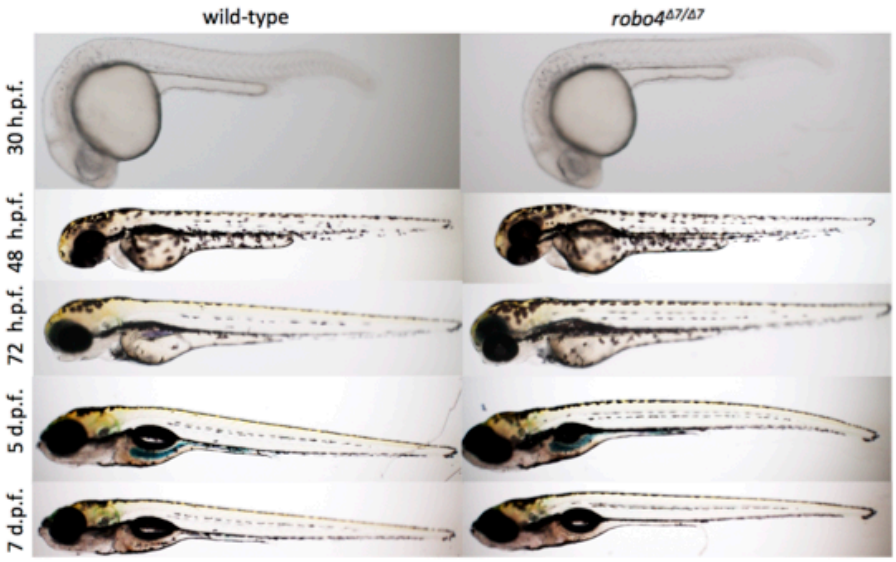

Figure 5-8. *robo4* loss-of-function mutants do not show an overt embryonic phenotype. At all stages, mutants did not show gross cardiac, craniofacial, or trunk defects. h.p.f.: hours post-fertilization and d.p.f.: days post-fertilization.

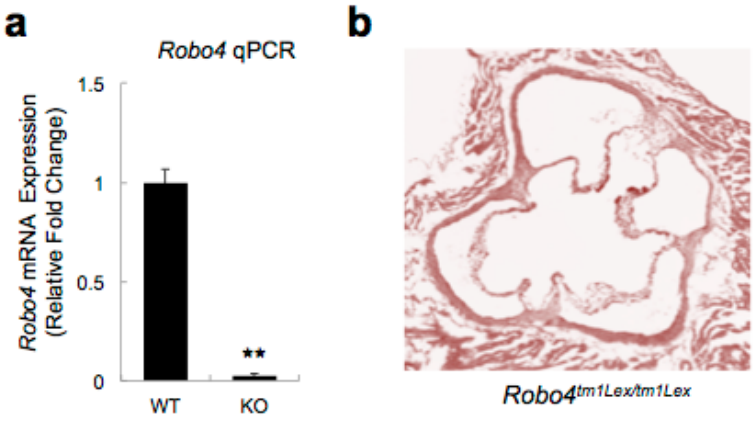

Figure 5-9. Phenotype data for *Robo4*^{tm1Lex} knockout mice with AscAA. (**a**) *Robo4* mRNA expression, normalized to *Gapdh*, was analyzed by pooling 4 samples per genotype and performing qPCR. Error bars show ± SD, $n = 4$ per genotype pooled, one experiment. Asterisks signify statistical differences per a two-tailed Student's *t*-test relative to control, * $P < 0.05$, ** $P < 0.01$. (**b**) H&E histology of a quadricuspid valve in a regurgitant *Robo4*$^{tm1Lex/tm1Lex}$ mouse. WT: wild-type and KO: knockout mice

a

	Robo4$^{+/+}$		*Robo4*$^{+/tm1Lex}$		*Robo4*$^{tm1Lex/tm1Lex}$		
	Male	Female	Male	Female	Male	Female	WT vs. KO
Regurgitation	0/22	0/19	0/14	0/11	4/28	1/18	$P = 0.037$
Flow >600mm/s	0/22	0/19	0/14	0/11	5/28	1/18	$P = 0.019$
DAscAA (Z>2)	0/22	0/19	0/14	0/11	3/28	0/18	$P = 0.143$
AoRA (Z>2)	0/22	0/19	0/14	0/11	2/28	0/18	$P = 0.277$
Total Affected	0/22	0/19	0/14	0/11	5/28	2/18	$P = 0.009$
AoV Defect*	0/3	N/A	N/A	N/A	5/5	2/2	$P = 0.008$
Pure BAV**	0/25	N/A	N/A	N/A	1/41	N/A	$P = 0.627$

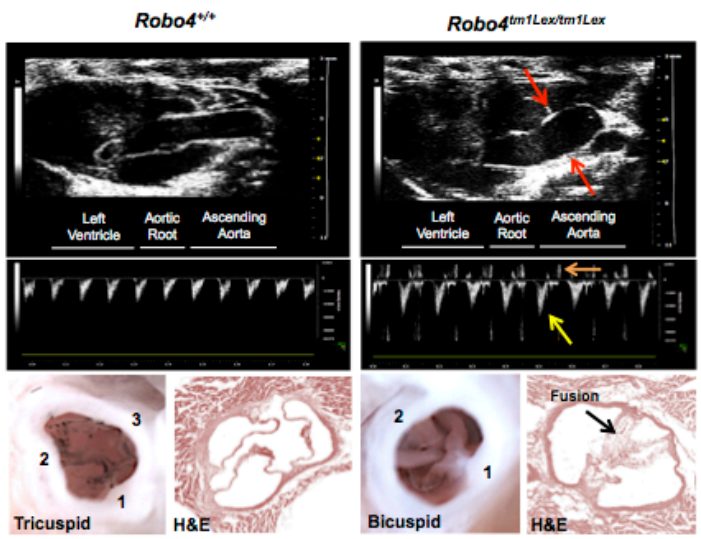

Figure 5-10. *Robo4* knockout causes aortic valve defects and aortic aneurysm in mice. (**a**) Wild-type (*Robo4*$^{+/+}$), heterozygous (*Robo4*$^{+/tm1Lex}$), and knockout (*Robo4*$^{tm1Lex/tm1Lex}$) mice were aged to 20 weeks and the cardiovascular phenotype was determined. Aortic dilatation was defined as a Z-score greater than two when compared to wild-type male mice by echocardiography. Statistical differences per a one-tailed Fisher's exact test, n = 112 total male and female mice, $P < 0.05$ was considered statistically significant. (**b**) Representative parasternal long axis and pulsed-wave Doppler images. Red arrows indicate a dilated segment of the ascending aorta. The yellow arrow shows increased velocity of outflow across the aortic valve during systole while the orange arrow shows regurgitant flow during diastole in a *Robo4*$^{tm1Lex/tm1Lex}$ mouse. (**c**) Gross and histological

examination of the aortic valve. Numbers refer to individual commissures. AscAA: ascending aortic aneurysm, AoRA: aortic root aneurysm, *abnormal aortic valve morphology including BAV, distal commissure fusion, leaflet thickening, or quadricuspid aortic valve among mutant mice with flow abnormalities by echocardiogram. Comparison is made to a representative sample of wild-type mice. **pure bicommissural aortic valve that was definitively evident by gross inspection

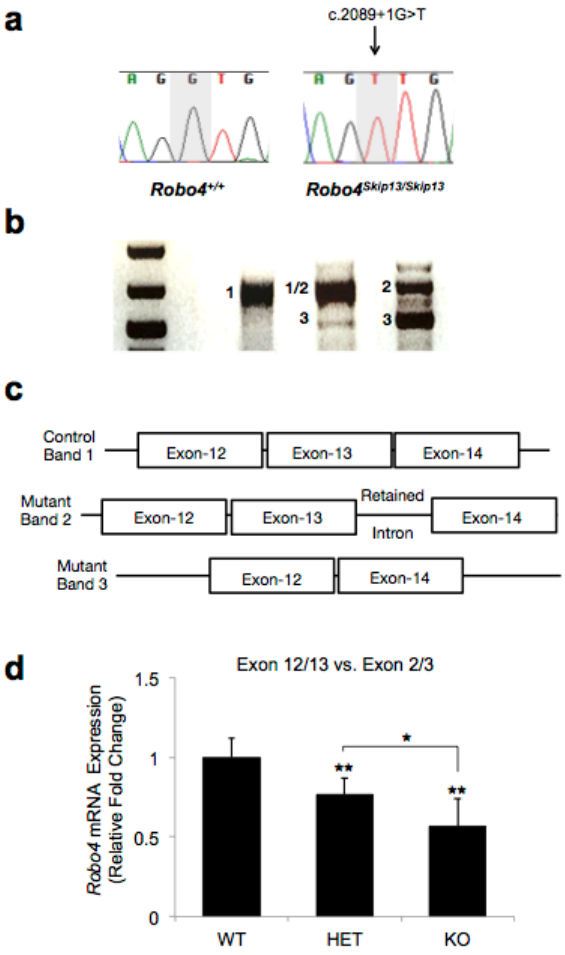

Figure 5-11. A knock-in line harboring a mutation (*Robo*^{Skip13}) at the splice acceptor site in exon 13 (c.2089+1G>T). (**a**) Sanger sequencing of the splice site mutation. (**b, c**) In-frame skipping of exon 13 (Ex12/14) or inclusion of exon 13 with activation of a cryptic splice donor in intron 13 that adds 15 base pairs to the mature mRNA (Ex12/13+15bp/14) that are predicted to add five extra amino acids between those encoded by exons 13 and 14. (**d**) TaqMan™ probes were used to directly compared exon 12/13 and exon 2/3 expression as this would provide a relative ratio of exon 13 skipping versus wild-type.

Error bars show ±SD, $n = 4$. Asterisks signify statistical differences per a one-way ANOVA with Tukey's post-hoc, * $P < 0.05$, ** $P < 0.01$.

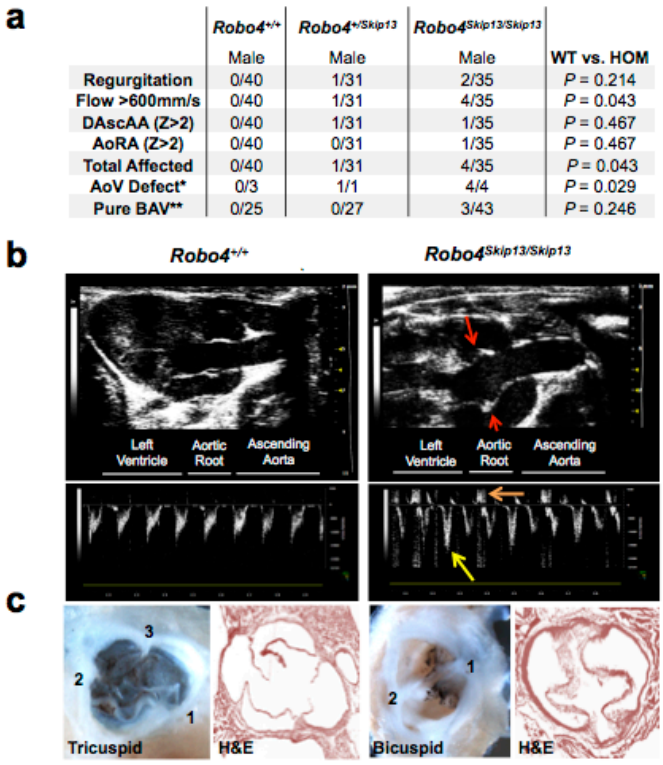

Figure 5-12. Knock-in splice site mutation (c.2089+1G>T; *Robo4*^{Skip13}) causes aortic valve defects and aortic aneurysm in mice. (**a**) Wild-type (*Robo4*$^{+/+}$), heterozygous (*Robo4*$^{+/Skip13}$), and homozygous (*Robo4*$^{Skip13/Skip13}$) mice were aged to 20 weeks and the cardiovascular phenotype was determined. Aortic dilatation was defined as a Z-score greater than two when compared to wild-type male mice by echocardiography. Significant differences per a one-tailed Fisher's exact test, n = 106 total male mice, P < 0.05 was considered statistically significant. (**b**) Representative parasternal long axis and pulsed-wave Doppler images. Red arrows indicate a dilated segment of the aortic root. The yellow arrow shows increased velocity of outflow across the aortic valve during systole while the orange arrow shows regurgitant flow during diastole in a *Robo4*^{Skip13} mouse. (**c**) Gross and histological examination of the aortic valve. Numbers refer to

individual commissures. AscAA: ascending aortic aneurysm, AoRA: aortic root aneurysm. *abnormal aortic valve morphology including BAV, distal commissure fusion, leaflet thickening, or quadricuspid aortic valve among mutant mice with flow abnormalities by echocardiogram. Comparison is made to a representative sample of wild-type mice. **pure bicommissural aortic valve that was definitively evident by gross inspection

Chapter 6: Conclusions

The heart is a pump. It has two main components: first is the structural component. Blood flows through the right atrium, to the right ventricle and into the pulmonary artery then to the lungs, where the blood becomes oxygenated. Blood then flows into the left atrium, to the left ventricle and into the aorta. The aorta is the structure that works as a capacitor to maintain blood flow through the body. Heart valves, between each of the four chambers, work to maintain this very specific blood flow pattern. Diseases that affect the structure are called congenital heart disease and affect approximately 1% of individuals. A specific congenital heart disease of interest in our laboratory is bicuspid aortic valve (BAV) and associated ascending aortic aneurysm (AscAA). The second component of the heart is electrical. In order to move blood through the heart, the heart contracts. An electrical pulse first contracts the atria and then the ventricles. This electrical pulse is commonly illustrated as a P wave, a QRS complex, and a T wave as seen in an electrocardiogram. Diseases that affect the conductance are arrhythmias, including sudden cardiac death and long QT syndrome.

In order to study these diseases, our laboratory is part of two larger groups studying bicuspid aortic valve and sudden cardiac death and arrhythmias. As part of these larger groups, genetic studies are performed using patient data and our laboratory specifically performs functional studies *in vivo*, using zebrafish. My thesis objectives were to first expand the functional analysis toolbox in zebrafish and thereby, facilitate the evaluation of cardiovascular phenotypes, including both structural and conductance issues. Next, I wanted to establish baseline measurements for wild-type zebrafish using

these tools (echocardiography and electrocardiography) as well as apply new models of analysis. Finally, I applied these techniques to determine the biological significance of candidate genes implicated in cardiac diseases including sudden cardiac death and bicuspid aortic valve.

Zebrafish are a great model organism with which to study cardiovascular malformations. First, they are cost-effective vertebrates. Zebrafish fertilize externally and they are transparent as embryos. Interestingly, they are not dependent on a fully functioning cardiovascular system until seven days post-fertilization, which allows us to cause cardiac malformations or disrupt the heart function, without lethality. Zebrafish have a two-chambered heart, which simplifies the heart system as well. Most importantly, however, the cardiac electrophysiology of zebrafish is remarkably similar to human cardiac electrophysiology (I. U S Leong et al., 2010).

In order to study the heart anatomy, we developed a new procedure to perform echocardiography in zebrafish. No other group has published with the resolution we can capture using a high-resolution transducer and using ultrasound gel directly on the fish. Incredibly, we are still able to keep the fish alive during these studies. In a longitudinal study on wild-type fish, we determined the normal echocardiographic measurements for wild-type fish of commonly used ages. These baseline measurements can be used as standards for all future studies on fish in the facility.

From these measurements, we determined the best and most accurate way to analyze the data. Echocardiographic studies in zebrafish fail to account for the size of the heart and for the fish generally (L. W. Wang et al., 2017). Wang et al. did look into adjusting for body mass index (BMI) or body surface area (BSA), but simply divided

each anatomical measurement by BMI or BSA. This does not accurately account or adjust for appropriate size measurements of the fish nor were any tests performed to determined whether BSA or BMI were better to use. It is common in humans studies to control for sex, age, and body size (Pettersen, Du, Skeens, & Humes, 2008; Roman, Devereux, Kramer-Fox, & O'Loughlin, 1989; Sluysmans, 2005). With our data, we performed a correlation analysis and saw that body size parameters are highly correlated (directly or anti-) with echocardiographic measurements. Thus measurements of zebrafish cardiac function and structure, captured by echocardiography, must be adjusted for body size parameters. The most accurate way to model this is with a linear mixed effects model, where sex, age, and body size parameters are fixed effects and date of echocardiography is a random effect.

In order to study the sudden cardiac death and arrhythmia candidate genes, we established an ECG protocol using the iWorx Zebrafish ECG Recording and Analysis System. Very few studies have been published on adult zebrafish ECG and most use a procedure that requires perfusion of the animal. The iWorx System allows us to perform surface ECG, keeping the fish alive and stable, with minimal interference in the normal conductance of the fish. We performed ECG analysis in parallel with the echocardiography study and captured normal measurements for wild-type fish in a longitudinal study. Similar to the echocardiography data, by correlation analysis, we determined that sex, age, and body size must be adjusted for in ECG studies. This has not been done previously. This linear mixed effects model includes sex, age, and body size parameters as fixed effects and date of ECG as a random effect. Together with the echocardiography data, this study provides a comprehensive analysis of wild-type

zebrafish at ages crucial to the zebrafish community and sets guidelines on all future studies, in our laboratory and others'.

We next applied this working pipeline for zebrafish cardiovascular phenotypes to two well-characterized models of arrhythmia and long QT syndrome for the gene, *kcnh6a*. The first long QT model is called *kcnh6a*^{tb218}. With our machine and our analysis, we did not detect any cardiac conductance defect in these mutant fish. Interestingly, we do see a 2:1 AV block in the embryos. This change in heart function between larval and adult stages is fascinating and is open for future investigation. By echocardiography, we saw no structural defects either. The second model is called *kcnh6a*^{s290}. This model had both prolonged QRS and QT intervals in adults, as shown in previous studies (Rima Arnaout et al., 2007). No embryonic phenotype was detected. By echocardiography, the mutant fish had a decreased velocity time integral through the AV valve, which could be caused by disruption in the contraction of the ventricle. The detection of arrhythmia in this model confirmed our abilities to perform ECG, echocardiography, and analyze mutant fish.

We then applied these methods to a novel candidate gene of interest for bicuspid aortic valve and aneurysm. *ROBO4* encodes a factor known to contribute to endothelial performance. It is expressed in vascular endothelial cells and has been implicated in the regulation of angiogenesis and involved in endothelial cell barrier integrity. We found a total of 13 variants in cases of BAV with and without AscAA and one variant in controls (735 cases, and 376 controls). Cellular and molecular assays performed on patient and control cells demonstrated a fibroproliferative response in patient cells as well as a decreased endothelial layer barrier. These data fit with the hypothesis and we moved to *in*

vitro studies using zebrafish. We generated a line with a seven base pair deletion in exon six, which resulted in a loss-of-function allele. Mutant embryos showed no gross defects in cardiovascular development. However, about 27% percent of heterozyous and homozgyous adult fish combined showed blood flow regurgitation and turbulence in the outflow tract. Only four out of 45 wild-type fish showed a similar gross phenotype as detected by color Doppler. For all 86 fish, we also determined all capable echocardiographic measurements and parameters. We found that the blood flow velocity through the bulboventricular valve, which is analogous to the aortic valve, is significantly faster in *robo4* mutant fish than wild-type fish. Faster flow through the aortic valve is a common sign of aortic stenosis and found commonly in patients with bicuspid aortic valve. This observation of a diseased state in the zebrafish was confirmed by histology. Data from the knockout mice are consistent with the zebrafish. These data together establish *ROBO4* as a gene critical for the normal development and homeostasis of outflow tract and establish a robust system and protocols for functional validation of other candidate genes of BAV/AscAA including *SEMA3C* and *SMAD6*.

To conclude, I have established a working pipeline for phenotyping adult zebrafish heart using echocardiography and ECG. I gathered wild-type baseline measurements for the zebrafish in our facility at different ages typically used for study. I determined a linear mixed effects model of analysis to adjust for variation between zebrafish that can affect the analysis of data. These variants include sex, age, and body size parameters. These covariates must be adjusted for in echocardiography and ECG analysis in zebrafish. I have successfully generated a loss-of-function mutant zebrafish line for *robo4.* This model shows a turbulent and blood flow phenotype consistent with

the mouse model. Finally, this work sets the groundwork for future translational research for zebrafish, other model organisms, and human data.

References

Alexander, J., Stainier, D. Y. R., & Yelon, D. (1998). Screening mosaic F1 females for mutations affecting zebrafish heart induction and patterning. *Developmental Genetics*, *22*(3), 288–299. http://doi.org/10.1002/(SICI)1520-6408(1998)22:3<288::AID-DVG10>3.0.CO;2-2

Anderl, J., Ma, J., & Armstrong, L. (n.d.). Improved Assays for Quantification of In Vitro Vascular Permeability, 10–14. http://doi.org/10.1038/an8623

Arnaout, R., Ferrer, T., Huisken, J., Spitzer, K., Stainier, D. Y. R., Tristani-Firouzi, M., & Chi, N. C. (2007). Zebrafish model for human long QT syndrome. *Proceedings of the National Academy of Sciences of the United States of America*, *104*(27), 11316–21. http://doi.org/10.1073/pnas.0702724104

Arnaout, R., Ferrer, T., Huisken, J., Spitzer, K., Stainier, D. Y., Tristani-Firouzi, M., & Chi, N. C. (2007). Zebrafish model for human long QT syndrome. *Proc Natl Acad Sci U S A*, *104*(27), 11316–11321. http://doi.org/10.1073/pnas.0702724104

Babij, P., Askew, G., Nieuwenhuijsen, B., & Su, C. (1998). Inhibition of cardiac delayed rectifier K+ current by overexpression of the long-QT …. *Circulation Research*, *83*(6), 668–678.

Bedell, V. M., Yeo, S.-Y., Park, K. W., Chung, J., Seth, P., Shivalingappa, V., … Ramchandran, R. (2005). Roundabout4 Is Essential for Angiogenesis in Vivo. *Proceedings of the National Academy of Sciences of the United States of America*, *102*(18), 6373–8. http://doi.org/10.1073/pnas.0408318102

Beis, D., Bartman, T., Jin, S.-W., Scott, I. C., D'Amico, L. a, Ober, E. a, … Jungblut, B. (2005). Genetic and cellular analyses of zebrafish atrioventricular cushion and valve development. *Development (Cambridge, England)*, *132*(18), 4193–4204. http://doi.org/10.1242/dev.01970

Braverman, A. C., Güven, H., Beardslee, M. A., Makan, M., Kates, A. M., & Moon, M. R. (2005). The Bicuspid Aortic Valve. *Current Problems in Cardiology*, *30*(9), 470–522. http://doi.org/10.1016/j.cpcardiol.2005.06.002

Brooke, B. S., Habashi, J. P., Judge, D. P., Patel, N., Loeys, B., & Dietz, H. C. (2008). Angiotensin II blockade and aortic-root dilation in Marfan's syndrome. *The New England Journal of Medicine*, *358*(26), 2787–95. http://doi.org/10.1056/NEJMoa0706585

Cai, H., Liu, W., Xue, Y., Shang, X., Liu, J., Li, Z., … Liu, Y. (2015). Roundabout 4 Regulates Blood-Tumor Barrier Permeability Through the Modulation of ZO-1, Occludin, and Claudin-5 Expression. *Journal of Neuropathology and Experimental Neurology*, *74*(1), 25–37. http://doi.org/10.1097/NEN.0000000000000146

Chen, J. N., Haffter, P., Odenthal, J., Vogelsang, E., Brand, M., van Eeden, F. J., … Nüsslein-Volhard, C. (1996). Mutations affecting the cardiovascular system and other internal organs in zebrafish. *Development (Cambridge, England)*, *123*, 293–302.

Chi, N. C., Shaw, R. M., Jungblut, B., Huisken, J., Ferrer, T., Arnaout, R., … Stainier, D. Y. R. (2008). Genetic and physiologic dissection of the vertebrate cardiac conduction system. *PLoS Biology*, *6*(5), 1006–1019. http://doi.org/10.1371/journal.pbio.0060109

Chiu, Y.-N., Norris, R. a, Mahler, G., Recknagel, A., & Butcher, J. T. (2010). Transforming growth factor β, bone morphogenetic protein, and vascular endothelial growth factor mediate phenotype maturation and tissue remodeling by embryonic valve progenitor cells: relevance for heart valve tissue engineering. *Tissue Engineering. Part A*, *16*(11), 3375–3383. http://doi.org/10.1089/ten.tea.2010.0027

Clementi, M., Notari, L., Borghi, A., & Tenconi, R. (1996). Familial congenital bicuspid aortic valve: A disorder of uncertain inheritance. *American Journal of Medical Genetics*, *62*(4), 336–338. http://doi.org/10.1002/(SICI)1096-8628(19960424)62:4<336::AID-AJMG2>3.0.CO;2-P

Cripe, L., Andelfinger, G., Martin, L. J., Shooner, K., & Benson, D. W. (2004). Bicuspid aortic valve is heritable. *Journal of the American College of Cardiology*, *44*(1), 138–143. http://doi.org/10.1016/j.jacc.2004.03.050

DePristo, M. a., Banks, E., Poplin, R. E., Garimella, K. V., Maguire, J. R., Hartl, C., … Daly, M. J. (2011). A framework for variation discovery and genotyping using next-generation DNA sequencing data. *Nat Genet*, *43*(5), 491–498. http://doi.org/10.1038/ng.806.A

Dore, A., Brochu, M.-C., Baril, J.-F., Guertin, M.-C., & Mercier, L.-A. (2003). Progressive dilation of the diameter of the aortic root in adults with a bicuspid aortic valve. *Cardiology in the Young*, *13*(6), 526–31. http://doi.org/10.1017/S1047951103001112

Enomoto, S., Mitsui, K., Kawamura, T., Iwanari, H., Daigo, K., Horiuchi, K., … Hamakubo, T. (2016). Suppression of Slit2/Robo1 mediated HUVEC migration by Robo4. *Biochemical and Biophysical Research Communications*, *469*(4), 797–802. http://doi.org/10.1016/j.bbrc.2015.12.075

Fedak, P. W. M., Verma, S., David, T. E., Leask, R. L., Weisel, R. D., & Butany, J. (2002). Clinical and pathophysiological implications of a bicuspid aortic valve. *Circulation*. http://doi.org/10.1161/01.CIR.0000027905.26586.E8

Fritz, R. D., Menshykau, D., Martin, K., Reimann, A., Pontelli, V., & Pertz, O. (2015). SrGAP2-Dependent Integration of Membrane Geometry and Slit-Robo-Repulsive Cues Regulates Fibroblast Contact Inhibition of Locomotion. *Developmental Cell*, *35*(1), 78–92. http://doi.org/10.1016/j.devcel.2015.09.002

Garg, V., Muth, A. N., Ransom, J. F., Schluterman, M. K., Barnes, R., King, I. N., … Srivastava, D. (2005). Mutations in NOTCH1 cause aortic valve disease. *Nature*, *437*(7056), 270–274. http://doi.org/10.1038/nature03940

Gonzalez, D. M., & Medici, D. (2014). Signaling mechanisms of the epithelial-mesenchymal transition. *Science Signaling*, *7*(344), re8-re8. http://doi.org/10.1126/scisignal.2005189

Gould, R. A., Chin, K., Santisakultarm, T. P., Dropkin, A., Richards, J. M., Schaffer, C.

B., & Butcher, J. T. (2012). Cyclic strain anisotropy regulates valvular interstitial cell phenotype and tissue remodeling in three-dimensional culture. *Acta Biomaterialia*, *8*(5), 1710–1719. http://doi.org/10.1016/j.actbio.2012.01.006

Gould, R. A., Sinha, R., Aziz, H., Rouf, R., Dietz, H. C., Judge, D. P., & Butcher, J. (2012). Multi-Scale Biomechanical Remodeling in Aging and Genetic Mutant Murine Mitral Valve Leaflets: Insights into Marfan Syndrome. *PLoS ONE*, *7*(9). http://doi.org/10.1371/journal.pone.0044639

Guo, D.-C., Pannu, H., Tran-Fadulu, V., Papke, C. L., Yu, R. K., Avidan, N., … Milewicz, D. M. (2007). Mutations in smooth muscle alpha-actin (ACTA2) lead to thoracic aortic aneurysms and dissections. *Nature Genetics*, *39*(12), 1488–1493. http://doi.org/10.1038/ng.2007.6

Hassel, D., Scholz, E. P., Trano, N., Friedrich, O., Just, S., Meder, B., … Rottbauer, W. (2008). Deficient zebrafish ether-à-go-go-related gene channel gating causes short-QT syndrome in zebrafish reggae mutants. *Circulation*, *117*(7), 866–875. http://doi.org/10.1161/CIRCULATIONAHA.107.752220

Hein, S. J., Lehmann, L. H., Kossack, M., Juergensen, L., Fuchs, D., Katus, H. A., & Hassel, D. (2015a). Advanced echocardiography in adult zebrafish reveals delayed recovery of heart function after myocardial cryoinjury. *PLoS ONE*, *10*(4). http://doi.org/10.1371/journal.pone.0122665

Hein, S. J., Lehmann, L. H., Kossack, M., Juergensen, L., Fuchs, D., Katus, H. A., & Hassel, D. (2015b). Advanced echocardiography in adult zebrafish reveals delayed recovery of heart function after myocardial cryoinjury. *PLoS ONE*, *10*(4), 1–21. http://doi.org/10.1371/journal.pone.0122665

Hu, N., Joseph Yost, H., & Clark, E. B. (2001). Cardiac morphology and blood pressure in the adult zebrafish. *Anatomical Record*, *264*(1), 1–12. http://doi.org/10.1002/ar.1111

Huminiecki, L., Gorn, M., Suchting, S., Poulsom, R., & Bicknell, R. (2002). Magic Roundabout Is a New Member of the Roundabout Receptor Family That Is Endothelial Specific and Expressed at Sites of Active Angiogenesis. *Genomics*, *79*(4), 547–552. http://doi.org/10.1006/geno.2002.6745

Huntington, K., Hunter, A. G. W., & Chan, K. L. (1997). A prospective study to assess the frequency of familial clustering of congenital bicuspid aortic valve. *Journal of the American College of Cardiology*, *30*(7), 1809–1812. http://doi.org/10.1016/S0735-1097(97)00372-0

Isselbacher, E. M. (2005). Thoracic and abdominal aortic aneurysms. *Circulation*. http://doi.org/10.1161/01.CIR.0000154569.08857.7A

Jao, L.-E., Wente, S. R., & Chen, W. (2013). Efficient multiplex biallelic zebrafish genome editing using a CRISPR nuclease system. *Proceedings of the National Academy of Sciences of the United States of America*, *110*(34), 13904–9. http://doi.org/10.1073/pnas.1308335110

Jaskula-Ranga, V., & Zack, D. J. (2016). grID: A CRISPR-Cas9 guide RNA Database and Resource for Genome-Editing. *bioRxiv*. Retrieved from

http://biorxiv.org/content/early/2016/12/30/097352.abstract

Jones, C. a, London, N. R., Chen, H., Park, K. W., Sauvaget, D., Stockton, R. a, … Li, D. Y. (2008). Robo4 stabilizes the vascular network by inhibiting pathologic angiogenesis and endothelial hyperpermeability. *Nature Medicine*, *14*(4), 448–453. http://doi.org/10.1038/nm1742

Kang, B. J., Park, J., Kim, J., Kim, H. H., Lee, C., Hwang, J. Y., … Juergensen, L. (2014). High-frequency dual mode pulsed wave Doppler imaging for monitoring the functional regeneration of adult zebrafish hearts. *Interface*, 1154. http://doi.org/10.1371/journal.pone.0122665

Koch, A. W., Mathivet, T., Larrivée, B., Tong, R. K., Kowalski, J., Pibouin-Fragner, L., … Eichmann, A. (2011). Robo4 Maintains Vessel Integrity and Inhibits Angiogenesis by Interacting with UNC5B. *Developmental Cell*, *20*(1), 33–46. http://doi.org/10.1016/j.devcel.2010.12.001

Kopp, R., Schwerte, T., & Pelster, B. (2005). Cardiac performance in the zebrafish breakdance mutant. *The Journal of Experimental Biology*, *208*(Pt 11), 2123–2134. http://doi.org/10.1242/jeb.01620

Kostina, A. S., Uspensky, V. E., Irtyuga, O. B., Ignatieva, E. V., Freylikhman, O., Gavriliuk, N. D., … Malashicheva, A. B. (2016). Notch-dependent EMT is attenuated in patients with aortic aneurysm and bicuspid aortic valve. *Biochimica et Biophysica Acta - Molecular Basis of Disease*, *1862*(4), 733–740. http://doi.org/10.1016/j.bbadis.2016.02.006

Laforest, B., Andelfinger, G., & Nemer, M. (2011). Loss of Gata5 in mice leads to bicuspid aortic valve. *Journal of Clinical Investigation*, *121*(7), 2876–2887. http://doi.org/10.1172/JCI44555

Langheinrich, U., Vacun, G., & Wagner, T. (2003). Zebrafish embryos express an orthologue of HERG and are sensitive toward a range of QT-prolonging drugs inducing severe arrhythmia. *Toxicology and Applied Pharmacology*, *193*(3), 370–382. http://doi.org/10.1016/j.taap.2003.07.012

Larson, E. W., & Edwards, W. D. (1984). Risk factors for aortic dissection: A necropsy study of 161 cases. *The American Journal of Cardiology*, *53*(6), 849–855. http://doi.org/10.1016/0002-9149(84)90418-1

Lee, J., Cao, H., Kang, B. J., Jen, N., Yu, F., Lee, C.-A., … Hsiai, T. K. (2014). Hemodynamics and ventricular function in a zebrafish model of injury and repair. *Zebrafish*, *11*(5), 447–54. http://doi.org/10.1089/zeb.2014.1016

Lee, L., Genge, C. E., Cua, M., Sheng, X., Rayani, K., Beg, M. F., … Tibbits, G. F. (2016). Functional assessment of cardiac responses of adult zebrafish (danio rerio) to acute and chronic temperature change using high-resolution echocardiography. *PLoS ONE*, *11*(1). http://doi.org/10.1371/journal.pone.0145163

Lee, M. P., Ravenel, J. D., Hu, R. J., Lustig, L. R., Tomaselli, G., Berger, R. D., … Feinberg, A. P. (2000). Targeted disruption of the Kvlqt1 gene causes deafness and gastric hyperplasia in mice. *Journal of Clinical Investigation*, *106*(12), 1447–1455. http://doi.org/10.1172/JCI10897

Lee, T. C., Zhao, Y. D., Courtman, D. W., & Stewart, D. J. (2000). Abnormal aortic valve development in mice lacking endothelial nitric oxide synthase. *Circulation*, *101*(20), 2345–2348. http://doi.org/10.1161/01.CIR.101.20.2345

Leong, I. U. S., Skinner, J. R., Shelling, A. N., & Love, D. R. (2010). Identification and expression analysis of kcnh2 genes in the zebrafish. *Biochemical and Biophysical Research Communications*, *396*(4), 817–824. http://doi.org/10.1016/j.bbrc.2010.04.157

Leong, I. U. S., Skinner, J. R., Shelling, A. N., & Love, D. R. (2010). Zebrafish as a model for long QT syndrome: The evidence and the means of manipulating zebrafish gene expression. *Acta Physiologica*. http://doi.org/10.1111/j.1748-1716.2010.02111.x

Li, H., & Durbin, R. (2009). Fast and accurate short read alignment with Burrows-Wheeler transform. *Bioinformatics*, *25*(14), 1754–1760. http://doi.org/10.1093/bioinformatics/btp324

Li, H., Handsaker, B., Wysoker, A., Fennell, T., Ruan, J., Homer, N., … Subgroup, 1000 Genome Project Data Processing. (2009). The Sequence Alignment / Map format and SAMtools. *Bioinformatics*, *25*(16), 2078–2079. http://doi.org/10.1093/bioinformatics/btp352

Liang, C.-C. C., Park, A. Y., & Guan, J.-L. L. (2007). In vitro scratch assay: a convenient and inexpensive method for analysis of cell migration in vitro. *Nature Protocols*, *2*(2), 329–333. http://doi.org/10.1038/nprot.2007.30

Loeys, B. L., Schwarze, U., Holm, T., Callewaert, B. L., Thomas, G. H., Pannu, H., … Dietz, H. C. (2006). Aneurysm syndromes caused by mutations in the TGF-beta receptor. *The New England Journal of Medicine*, *355*(8), 788–798. http://doi.org/10.1056/NEJMoa055695

Loscalzo, M. L., Goh, D. L. M., Loeys, B., Kent, K. C., Spevak, P. J., & Dietz, H. C. (2007). Familial thoracic aortic dilation and bicommissural aortic valve: A prospective analysis of natural history and inheritance. *American Journal of Medical Genetics, Part A*, *143*(17), 1960–1967. http://doi.org/10.1002/ajmg.a.31872

Mack, G., & Silberbach, M. (2000). Aortic and pulmonary stenosis. *Pediatrics in Review / American Academy of Pediatrics*, *21*(3), 79–85. http://doi.org/10.1542/pir.21-3-79

Maleki, S., Kjellqvist, S., Paloschi, V., Magné, J., Branca, R. M. M., Du, L., … Björck, H. M. (2016). Mesenchymal state of intimal cells may explain higher propensity to ascending aortic aneurysm in bicuspid aortic valves. *Scientific Reports*, *6*(October), 35712. http://doi.org/10.1038/srep35712

Martin, L. J., Ramachandran, V., Cripe, L. H., Hinton, R. B., Andelfinger, G., Tabangin, M., … Benson, D. W. (2007). Evidence in favor of linkage to human chromosomal regions 18q, 5q and 13q for bicuspid aortic valve and associated cardiovascular malformations. *Human Genetics*, *121*(2), 275–284. http://doi.org/10.1007/s00439-006-0316-9

McKellar, S. H., Tester, D. J., Yagubyan, M., Majumdar, R., Ackerman, M. J., & Sundt, T. M. (2007). Novel NOTCH1 mutations in patients with bicuspid aortic valve

disease and thoracic aortic aneurysms. *The Journal of Thoracic and Cardiovascular Surgery*, *134*(2), 290–6. http://doi.org/10.1016/j.jtcvs.2007.02.041

McKenna, A., Hanna, M., Banks, E., Sivachenko, A., Cibulskis, K., Kernytsky, A., … DePristo, M. A. (2010). The genome analysis toolkit: A MapReduce framework for analyzing next-generation DNA sequencing data. *Genome Research*, *20*(9), 1297–1303. http://doi.org/10.1101/gr.107524.110

Mckusick, V. A., Logue, R. B., & Bahnson, H. T. (1957). Association of Aortic Valvular Disease and Cystic Medial Necrosis of the Ascending Aorta. *Circulation*, *16*, 188–194. http://doi.org/10.1161/01.CIR.16.2.188

Meder, B., Scholz, E. P., Hassel, D., Wolff, C., Just, S., Berger, I. M., … Rottbauer, W. (2011). Reconstitution of defective protein trafficking rescues Long-QT syndrome in zebrafish. *Biochemical and Biophysical Research Communications*, *408*(2), 218–224. http://doi.org/10.1016/j.bbrc.2011.03.121

Milan, D. J., Jones, I. L., Ellinor, P. T., & Macrae, C. A. (2006). In vivo recording of adult zebrafish electrocardiogram and assessment of drug-induced QT prolongation. *American Journal of Physiology. Heart and Circulatory Physiology*, *291*(1), H269-73. http://doi.org/10.1152/ajpheart.00960.2005

Mommersteeg, M. T. M., Yeh, M. L., Parnavelas, J. G., & Andrews, W. D. (2015). Disrupted Slit-Robo signalling results in membranous ventricular septum defects and bicuspid aortic valves. *Cardiovascular Research*, *106*(1), 55–66. http://doi.org/10.1093/cvr/cvv040

Nerbonne, J. M. (2004). Studying cardiac arrhythmias in the mouse - A reasonable model for probing mechanisms? *Trends in Cardiovascular Medicine*. http://doi.org/10.1016/j.tcm.2003.12.006

Park, K. W., Morrison, C. M., Sorensen, L. K., Jones, C. A., Rao, Y., Chien, C. Bin, … Li, D. Y. (2003). Robo4 is a vascular-specific receptor that inhibits endothelial migration. *Developmental Biology*, *261*(1), 251–267. http://doi.org/10.1016/S0012-1606(03)00258-6

Pelster, B., & Burggren, W. W. (1996). Disruption of hemoglobin oxygen transport does not impact oxygen-dependent physiological processes in developing embryos of zebrafish (Danio rerio). *Circulation Research*, *79*, 358–362. http://doi.org/10.1161/01.RES.79.2.358

Pereira, L., Andrikopoulos, K., Tian, J., Lee, S. Y., Keene, D. R., Ono, R., … Ramirez, F. (1997). Targetting of the gene encoding fibrillin-1 recapitulates the vascular aspect of Marfan syndrome. *Nat Genet*, *17*(2), 218–222. http://doi.org/10.1038/ng1097-218

Pettersen, M. D., Du, W., Skeens, M. E., & Humes, R. A. (2008). Regression Equations for Calculation of Z Scores of Cardiac Structures in a Large Cohort of Healthy Infants, Children, and Adolescents: An Echocardiographic Study. *Journal of the American Society of Echocardiography*, *21*(8), 922–934. http://doi.org/10.1016/j.echo.2008.02.006

Ran, F. A., Hsu, P. D., Wright, J., Agarwala, V., Scott, D. A., & Zhang, F. (2013). Genome engineering using the CRISPR-Cas9 system. *Nat. Protocols*, *8*(11), 2281–

2308. http://doi.org/10.1038/nprot.2013.143\rhttp://www.nature.com/nprot/journal/v8/n11/abs/nprot.2013.143.html#supplementary-information

Robinson, J. T., Thorvaldsdóttir, H., Winckler, W., Guttman, M., Lander, E. S., Getz, G., & Mesirov, J. P. (2011). Integrative genomics viewer. *Nature Biotechnology*, *29*(1), 24–26. http://doi.org/10.1038/nbt.1754

Roman, M. J., Devereux, R. B., Kramer-Fox, R., & O'Loughlin, J. (1989). Two-dimensional echocardiographic aortic root dimensions in normal children and adults. *The American Journal of Cardiology*, *64*(8), 507–512. http://doi.org/0002-9149(89)90430-X (pii)

Salama, G., & London, B. (2007). Mouse models of long QT syndrome. *The Journal of Physiology*, *578*(Pt 1), 43–53. http://doi.org/10.1113/jphysiol.2006.118745

Sander, J. D., Maeder, M. L., Reyon, D., Voytas, D. F., Joung, J. K., & Dobbs, D. (2010). ZiFiT (Zinc Finger Targeter): An updated zinc finger engineering tool. *Nucleic Acids Research*, *38*(SUPPL. 2), W462–W468. http://doi.org/10.1093/nar/gkq319

Sander, J. D., Zaback, P., Joung, J. K., Voytas, D. F., & Dobbs, D. (2007). Zinc Finger Targeter (ZiFiT): An engineered zinc finger/target site design tool. *Nucleic Acids Research*, *35*(SUPPL.2), W599–W605. http://doi.org/10.1093/nar/gkm349

Scheid, L.-M., Mosqueira, M., Hein, S., Kossack, M., Juergensen, L., Mueller, M., … Hassel, D. (2016). Essential light chain S195 phosphorylation is required for cardiac adaptation under physical stress. *Cardiovascular Research*. http://doi.org/10.1093/cvr/cvw066

Sedmera, D., Reckova, M., deAlmeida, A., Sedmerova, M., Biermann, M., Volejnik, J., … Thompson, R. P. (2003). Functional and morphological evidence for a ventricular conduction system in zebrafish and Xenopus hearts. *American Journal of Physiology. Heart and Circulatory Physiology*, *284*(November 2002), H1152–H1160. http://doi.org/10.1152/ajpheart.00070.2002

Sehnert, A. J., & Stainier, D. Y. R. (2002). A window to the heart: Can zebrafish mutants help us understand heart disease in humans? *Trends in Genetics*. http://doi.org/10.1016/S0168-9525(02)02766-X

Sluysmans, T. (2005). Theoretical and empirical derivation of cardiovascular allometric relationships in children. *Journal of Applied Physiology*, *99*(2), 445–457. http://doi.org/10.1152/japplphysiol.01144.2004

Splawski, I., Shen, J., Timothy, K. W., Lehmann, M. H., Priori, S., Robinson, J. L., … Keating, M. T. (2000). Spectrum of mutations in long-QT syndrome genes. KVLQT1, HERG, SCN5A, KCNE1, and KCNE2. *Circulation*, *102*(10), 1178–1185. http://doi.org/10.1161/01.CIR.102.10.1178

Stainier, D. Y., & Fishman, M. C. (1994). The zebrafish as a model system to study cardiovascular development. *Trends in Cardiovascular Medicine*, *4*(5), 207–12. http://doi.org/10.1016/1050-1738(94)90036-1

Stainier, D. Y., Fouquet, B., Chen, J. N., Warren, K. S., Weinstein, B. M., Meiler, S. E., … Fishman, M. C. (1996). Mutations affecting the formation and function of the

cardiovascular system in the zebrafish embryo. *Development (Cambridge, England)*, *123*, 285–92. Retrieved from http://www.ncbi.nlm.nih.gov/sites/entrez?Db=pubmed&DbFrom=pubmed&Cmd=Link&LinkName=pubmed_pubmed&LinkReadableName=Related Articles&IdsFromResult=9007248&ordinalpos=3&itool=EntrezSystem2.PEntrez.Pubmed.Pubmed_ResultsPanel.Pubmed_RVDocSum%5Cnhttp://www.ncbi

Sun, L., Lien, C.-L., Xu, X., Shung, K. K., Aristizabal, O., Christopher, D. A., … Shung, K. K. (2008). In vivo cardiac imaging of adult zebrafish using high frequency ultrasound (45-75 MHz). *Ultrasound in Medicine & Biology*, *34*(1), 31–9. http://doi.org/10.1016/j.ultrasmedbio.2007.07.002

Sun, L., Lien, C. L., Xu, X., & Shung, K. K. (2008). In Vivo Cardiac Imaging of Adult Zebrafish Using High Frequency Ultrasound (45-75 MHz). *Ultrasound in Medicine and Biology*, *34*(1), 31–39. http://doi.org/10.1016/j.ultrasmedbio.2007.07.002

Sun, Y., Fang, Y., Xu, X., Lu, G., & Chen, Z. (2015). Evidence of an Association between Age-Related Functional Modifications and Pathophysiological Changes in Zebrafish Heart. *Gerontology*, *61*(5), 435–447. http://doi.org/10.1159/000369094

Tadros, T. M., Klein, M. D., & Shapira, O. M. (2009). Ascending aortic dilatation associated with bicuspid aortic valve. Pathophysiology, molecular biology, and clinical implications. *Circulation*. http://doi.org/10.1161/CIRCULATIONAHA.108.795401

Tan, H. L., Glen, E., Töpf, A., Hall, D., O'Sullivan, J. J., Sneddon, L., … Keavney, B. D. (2012). Nonsynonymous variants in the SMAD6 gene predispose to congenital cardiovascular malformation. *Human Mutation*, *33*(4), 720–727. http://doi.org/10.1002/humu.22030

van de Laar, I. M. B. H., van der Linde, D., Oei, E. H. G., Bos, P. K., Bessems, J. H., Bierma-Zeinstra, S. M., … Wessels, M. W. (2012). Phenotypic spectrum of the SMAD3-related aneurysms-osteoarthritis syndrome. *Journal of Medical Genetics*, *49*(1), 47–57. http://doi.org/10.1136/jmedgenet-2011-100382

Van Hemelrijk, C., Renard, M., & Loeys, B. (2010). The Loeys-Dietz syndrome: an update for the clinician. *Current Opinion in Cardiology*, *25*(6), 546–551. http://doi.org/10.1097/HCO.0b013e32833f0220

Wang, K., Li, M., & Hakonarson, H. (2010). ANNOVAR: functional annotation of genetic variants from high-throughput sequencing data. *Nucleic Acids Research*, *38*(16), e164. http://doi.org/10.1093/nar/gkq603

Wang, L., Guo, D. C., Cao, J., Gong, L., Kamm, K. E., Regalado, E., … Milewicz, D. M. (2010). Mutations in myosin light chain kinase cause familial aortic dissections. *American Journal of Human Genetics*, *87*(5), 701–707. http://doi.org/10.1016/j.ajhg.2010.10.006

Wang, L. W., Huttner, I. G., Santiago, C. F., Kesteven, S. H., Yu, Z.-Y., Feneley, M. P., & Fatkin, D. (2017). Standardized echocardiographic assessment of cardiac function in normal adult zebrafish and heart disease models. *Disease Models & Mechanisms*, *10*(1), 63–76. http://doi.org/10.1242/dmm.026989

Ward, C. (2000). Clinical significance of the bicuspid aortic valve. *Heart*, *83*(1), 81–85. http://doi.org/10.1136/heart.83.1.81

Warren, K. S., Wu, J. C., Pinet, F., & Fishman, M. C. (2000). The genetic basis of cardiac function: dissection by zebrafish (Danio rerio) screens. *Philosophical Transactions of the Royal Society of London. Series B, Biological Sciences*, *355*(1399), 939–44. http://doi.org/10.1098/rstb.2000.0629

Westerfield, M. (2007). The Zebrafish Book. A Guide for the Laboratory Use of Zebrafish (Danio rerio), 5th Edition. *University of Oregon Press, Eugene (Book)*.

Williams, J. A., Loeys, B. L., Nwakanma, L. U., Dietz, H. C., Spevak, P. J., Patel, N. D., … Cameron, D. E. (2007). Early Surgical Experience With Loeys-Dietz: A New Syndrome of Aggressive Thoracic Aortic Aneurysm Disease. *Annals of Thoracic Surgery*, *83*(2). http://doi.org/10.1016/j.athoracsur.2006.10.091

Yu, J., Zhang, X., Kuzontkoski, P. M., Jiang, S., Zhu, W., Li, D. Y., & Groopman, J. E. (2014). Slit2N and Robo4 regulate lymphangiogenesis through the VEGF-C/VEGFR-3 pathway. *Cell Communication and Signaling*, *12*(1), 25. http://doi.org/10.1186/1478-811X-12-25

Zhu, L., Vranckx, R., Khau Van Kien, P., Lalande, A., Boisset, N., Mathieu, F., … Jeunemaitre, X. (2006). Mutations in myosin heavy chain 11 cause a syndrome associating thoracic aortic aneurysm/aortic dissection and patent ductus arteriosus. *Nature Genetics*, *38*(3), 343–349. http://doi.org/10.1038/ng1721

Curriculum vitae

Courtney E. Woods
(210) 324-3768
cwoods12@cmc.edu

EDUCATION

2012-Present Johns Hopkins University School of Medicine, Baltimore, MD
Ph.D. in Human Genetics, Expected Graduation: May 2017
Thesis work: Using genome-editing technologies in zebrafish to provide a rapid screen of the biological relevance of candidate genes implicated in patients with cardiovascular disorders via whole exome sequencing.
Advisor: Andrew McCallion, Ph.D.

2008-2012 Claremont McKenna College, Claremont, CA
B.A. in Biology and Literature
Studied abroad for a semester at King's College of London (Spring 2011)

CLINICAL EXPERIENCE

2014-Present Shadowing Hans Bjornsson, M.D., Ph.D., Johns Hopkins McKusick-Nathans Epigenetics and Chromatin Clinic
Assisting with patient visits, preparing presentations on genetic testing results and differential diagnoses, managing the clinic's social media (Monthly)

2015-Present Volunteer, Mercy Medical Center, Baltimore, MD
Teaching adult in-patients how to use the electronic medical education system that explains individual medications and conditions (Weekly)

2016 Shadowed Julie Hoover-Fong, M.D., Ph.D., Johns Hopkins Greenberg Center for Skeletal Dysplasias
Supported in pediatric patient visits with skeletal disorders, prepared differential diagnoses and patient management plans, presented a specific patient to physicians and trainees

2015 Shadowed Jennifer Prado-Habashi, M.D., Johns Hopkins Comprehensive Marfan Center
Aided in visits with pediatric and adult patients with connective tissue disorders

2015 Shadowed Hilary Vernon, M.D., Ph.D., Kennedy Krieger Institute Metabolism Clinic
Interacted with pediatric patients with metabolic and mitochondrial diseases

2015 Shadowed David Valle, M.D., Johns Hopkins Hospital Medical Genetics Clinic
Assisted in a visit with a pediatric patient with a rare Mendelian disorder

RESEARCH EXPERIENCE

2011-2012 Senior Thesis Research, W. M. Keck Science Department of Claremont McKenna College
Thesis title: "*Optimizing chromatin immunoprecipitations of CHD1 from salivary glands*." Advisor: Jennifer Armstrong, Ph.D.

2009-2011 Individual Research, W. M. Keck Science Department of Claremont McKenna College
Investigations into chromatin structure and the chromatin remodeler, CHD1, in *D. melanogaster.*
Advisor: Jennifer Armstrong, Ph.D.

2009-2011 Laboratory Assistant, Organic Chemistry and General Chemistry
Prepared all class lab experiments, solutions, and laboratory materials
Advisor: Jennifer Luft, Ph.D.

PUBLICATIONS/PRESENTATIONS

C.E. Woods, "Phenotyping pipeline for bicuspid aortic valve with/without ascending aortic aneurysm highlights pathological relevance of *ROBO4* to cardiovascular function." (PgmNr 214). 66th Annual Meeting of The American Society of Human Genetics (Vancouver, Canada, October 2016)

C. E. Woods, "Phenotyping pipeline for bicuspid aortic valve with/without ascending aortic aneurysm highlights pathological relevance of *ROBO4* to cardiovascular function." APS/ASHG Joint Symposium: Attaching Physiology to the Genome: Spotlight on Cardiovascular Genetics (Vancouver, Canada, October 2016)

C. E. Woods, "Developing a pipeline for functional analysis of BAV/AscAA candidate genes in zebrafish." Mechanistic Investigation into Bicuspid Aortic Valve and Aneurysm Biannual Meeting. Leducq Fondation Consortium (Lubeck, Germany, December 2015)

H. E. Edelman, **C. Woods**, J. E. Hoover-Fong, A. S. McCallion, "*cbx3* and its role in craniofacial development: Zebrafish as a model system for testing dysmorphology candidate genes." (PrgNr 121). 65th Annual Meeting of The American Society of Human Genetics (Baltimore, MD, October 2015)

J. Jurgens, **C. Woods**, P. W. Hook, N. Sobreira, J. E. Hoover-Fong, A. S. McCallion, D. Valle, "Strategy for generating and characterizing a zebrafish model of spondylometaphyseal dysplasia with cone-rod dystrophy." (PrgNr 2814). 65th Annual Meeting of The American Society of Human Genetics (Baltimore, MD, October 2015)

R. A. Gould, H. Aziz, A. Kumar, C. Preuss, **C. Woods**, N. Sobreira, H. Ling, S. A. Mohamed, A. Franco-Cereceda, G. Andelfinger, A. S. McCallion, P. Eriksson, L. V.

Laer, B. L. Loeys, H. C. Dietz, "*ROBO-SLIT* mutations predispose individuals to bicuspid aortic valve with ascending aortic aneurysm." (PrgNr 156). 65th Annual Meeting of The American Society of Human Genetics (Baltimore, MD, October 2015)

C. E. Woods, "Developing a pipeline for functional analysis of BAV/AscAA candidate genes in zebrafish." Mechanistic Investigation into Bicuspid Aortic Valve and Aneurysm Biannual Meeting. Leducq Fondation Consortium (Antwerp, Belgium, May 2015)

C. E. Woods, "Developing a pipeline for functional analysis of BAV/AscAA candidate genes in zebrafish." Mechanistic Investigation into Bicuspid Aortic Valve and Aneurysm Biannual Meeting. Leducq Fondation Consortium (Toronto, Canada, January 2015)

C. E. Woods, Journal Club for the McKusick-Nathans Institute of Genetic Medicine. Johns Hopkins University School of Medicine (Baltimore, MD, November 2014)

C. E. Woods, "The location of CHD1 on the *fkh* gene in *Drosophila melanogaster*." W. M. Keck Science Department of Claremont McKenna Poster Presentation (Claremont, CA, December 2011)

C. E. Woods, "The location of CHD1 on the *fkh* gene in *Drosophila melanogaster*." W. M. Keck Science Department of Claremont McKenna College Summer Research Symposium (Claremont, CA, August 2011)

TEACHING EXPERIENCE

Fall 2014	Teaching Assistant for Human Genetics Program course, Evolution of Ideas in Human Genetics Supervised students to help them understand the required reading and prepare presentations

LEADERSHIP AND SERVICE

2015-Present	Contributing Writer, Online Mendelian Inheritance in Man (OMIM) Writing entries on genes and genetic phenotypes monthly
2013-Present	Organizing Committee Member, "Journeys of Women in Genetics" Seminar Series Orchestrating lunch forums four times a year with female trainees and faculty members to discuss solutions to challenges faced by women in the workplace and life/work balance strategies
Fall 2015	Course Organizer, Johns Hopkins University School of Medicine Developed the course, "Understanding Genetic Disease," to provide Ph.D. students the opportunity to engage with patients of genetic diseases in the clinic to further their understanding of the diseases
Fall 2015	Educator, Smithsonian National Museum of Natural History "Genome Geeks Day"

	Science outreach with the general public on using zebrafish as a model organism for genetics
2014-2015	Organizing Committee Member, East Coast Kabuki Syndrome Conference Planned the largest conference to date for Kabuki Syndrome with over 200 patient families
Spring 2014	Volunteer, Medical Education Resources Initiative for Teens (MERIT) Taught life-skills to low income, under-privileged high school students from Baltimore, who are dedicated to becoming biomedical professionals
Summer 2013	Trainee, 54th Annual Short Course on Medical and Experimental Mammalian Genetics, Jackson Laboratories, Bar Harbor, ME Attended a two-week course on heredity, disease, and genetics
2008-2012	Member, Women in Science Club at the Claremont Colleges Participated in lunch seminars regarding gender issues in science
Summer 2010	Sophomore Leadership Experience, Claremont McKenna College Attended a four-day program to develop leadership skills and increase self-awareness
2009-2010	Tutor, Uncommon Good Taught high school Chemistry and English to a student from a low-income family in the Southern California area
2009-2010	Instructor, Physical Education at Claremont McKenna College Taught three semesters of aerobics to college students
2008-2009	Tutor, Middle School English and Science Participated in a college-sponsored volunteer group to help tutor community students

AWARDS/HONORS

Fall 2016	Semifinalist for the 2016 American Society of Human Genetics/Charles J. Epstein Trainee Award for Excellence in Human Genetics